

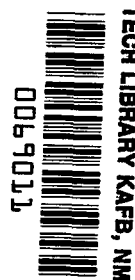
**NASA TECHNICAL  
TRANSLATION**

NASA TT F-547



**NASA TT F-547**

C.1



**LOAN COPY: RETURN TO**  
AFWL (WLIL-2)  
KIRTLAND AFB, N MEX

# **INVESTIGATION OF VIBRATION AND STABILITY OF AIRCRAFT ENGINE COMPONENTS**

*G. S. Skubachevskiy, Editor*

*Transactions of the Moscow Aviation Institute, No. 172*

*"Mashinostroyeniye" Press, Moscow, 1967*



INVESTIGATION OF VIBRATION AND STABILITY  
OF AIRCRAFT ENGINE COMPONENTS

G. S. Skubachevskiy, Editor

Translation of "Issledovaniye Vibratsii i Prochnosti Detaley Aviadvigateley"  
Transactions of the Moscow Aviation Institute, No. 172. "Mashinostroyeniye"  
Press, Moscow, 1967

NATIONAL AERONAUTICS AND SPACE ADMINISTRATION

---

For sale by the Clearinghouse for Federal Scientific and Technical Information  
Springfield, Virginia 22151 - CFSTI price \$3.00



### Annotation

This collection consists of articles devoted to vibrations, vibration strength of aircraft engine components and the stability of three-layer shells. These papers deal with vibrations of turbomachine rotors and methods for determining optimal parameters of hydraulic damping mounts, the vibrations of systems with friction and determination of their dynamic compliance, as well as self-induced vibrations of compressor blades. A design method taking into account the vibration of variable-thickness disks and an analysis of the operation of a hydrostatic bearing as a source of shaft vibrations are presented. These papers are intended for scientific workers and engineers of the aircraft engine industry, as well as of the power and transportation industries. It may be useful to instructors and students of senior courses in these specializations.



# TABLE OF CONTENTS

Annotation.....	iii
Foreword.....	vi
Abstracts.....	vii
The Shape of the Elastic Curve of a Weightless Rotating Shaft Carrying Eccentrically Located Point Masses or Disks.....	1
The Optimum Hydraulic Damping Mount for a Turbine Rotor.....	20
Dynamic Compliances in a System with Friction.....	48
Forced Vibrations of a Free Shaft with Friction.....	53
Self-Induced Vibrations of Axial-Compressor Blades.....	71
Computation of Vibrations of Variable-Thickness Disks by the Ritz Method.....	83
The Hydrostatic Bearing as a Source of Vibrations.....	89
Stability of Three-Layer Cylindrical Shells Beyond the Elastic Limit.....	93
The Application of Conformal Mapping to Problems of the Theory of Elasticity.....	105
Stability of Three-Layer Cylindrical Shells in the Elastic and Inelastic Regions.....	111

## FOREWORD

Over several years the Moscow Aviation Institute has conducted studies on vibration, strength and stability of aircraft engine components. The present collection contains a brief description of some of these studies.

/3\*

The first four articles - by Docent A. N. Ogurechnikov, Docent Candidate of Technical Sciences K. A. Kryukov, engineers V. M. Balepin and Ye. A. Artemov - are devoted to the problem of critical rpm of gas turbine rotors. They describe the shape of the elastic curve of a weightless shaft carrying eccentric point masses and obliquely seated disks and prove the validity of Wiedler's postulate for systems executing flexural oscillations; they also present methods for determining the optimal parameters of turbomachinery rotor mounts and the compliance of a system with friction. In addition, they analyze forced vibrations of a free shaft with friction and give an overall method for calculating them. These articles are continuations of the papers previously published in Transactions of the Moscow Aviation Institute (Issues No. 74, 1956; No. 100, 1959 and No. 136, 1961).

The article of Candidate of Technical Sciences I. M. Movshovich is devoted to the study of self-induced vibrations in axial compressors, a phenomenon encountered in modern machinery. Here, blade assemblies of the same design and manufacture start to vibrate at different initial air stream pressures. Movshovich shows what must be done to tune the blade assembly to the highest initial air stream pressure.

The remaining articles deal with the vibrations in certain aircraft engine components and the determination of their stability. Thus, engineer A. V. Karpov presents a variational method for calculating the vibrations of variable-thickness disks. Candidate of Technical Sciences G. A. Ivanov is concerned with the hydrostatic bearing as a source of rotor vibrations and points out a method for eliminating them. Candidate of Technical Sciences V. V. Serdyukov gives a method for calculating the stability of a three-layer shell beyond the elastic limit. Candidate of Technical Sciences V. B. Gorlov considers the use of conformal mapping in problems of the theory of elasticity. Candidate of Technical Sciences I. A. Yefimov examines the stability of three-layer cylindrical shells in the elastic and nonelastic regions, and presents a method for determining critical loads in the case of combined action of an axial force and lateral pressure on such a shell with a longitudinal and transverse corrugated filler.

/4

G. Skubachevskiy

## ABSTRACTS

THE SHAPE OF THE ELASTIC CURVE OF A WEIGHTLESS ROTATING SHAFT CARRYING ECCENTRICALLY LOCATED POINT MASSES OR DISKS, Docent A.N. Ogurechnikov .....	1
--	---

Proves the validity of Wiedler's postulate for the following systems which execute flexural vibrations: 1) a shaft with two eccentrically located point masses; 2) a shaft carrying an eccentrically coupled point mass and an obliquely seated ideal thin disk.

THE OPTIMUM HYDRAULIC DAMPING MOUNT FOR A TURBINE ROTOR, Candidate of Technical Sciences, K.A. Kryukov .....	20
--	----

Derives and analyzes the expressions for the critical shaft rpm of gas-turbine rotors in the presence of deformation in the direction of the frictional force and taking into account the dynamic intensification factor, deflection, angle of displacement, unbalance forces, and stresses. Also discusses the operation of hydraulic damping mounts for these turbines.

DYNAMIC COMPLIANCES IN A SYSTEM WITH FRICTION, Engineer V.M. Balepin .....	48
---	----

Derives (subject to several constraints) the equations for the dynamic compliance of flexing systems with several degrees of freedom in the presence of different types of friction.

FORCED VIBRATIONS OF A FREE SHAFT WITH FRICTION, Engineer Ye.A. Artemov .....	53
--	----

Presents an integral method for computing the vibrations of a free shaft in the presence of viscous friction. The resulting equations give the frequency - amplitude characteristic of a rotating, disk-loaded shaft in the presence of damping.

SELF-INDUCED VIBRATIONS OF AXIAL-COMPRESSOR BLADES, Candidate of Technical Sciences, I.M. Movshovich.....	71
--	----

Discusses self-induced vibrations of axial compressor systems in terms of a profile which exhibits the reduced mass of an entire blade and the aerodynamic characteristics of its peripheral cross section, and describes optimum turning of the blade assembly.

COMPUTATIONS OF VIBRATIONS OF VARIABLE-THICKNESS DISKS BY THE RITZ METHOD, Engineer A.V. Karpov.....	83
---	----

Presents a technique for vibration design of intricately-shaped rotating disks, using functions approximating the actual thicknesses of these disks.

THE HYDROSTATIC BEARING AS A SOURCE OF VIBRATIONS, Candidate of Technical Sciences, G.A. Ivanov .....	89
--	----

Discusses techniques for eliminating rotor vibrations due to hydrostatic bearings.

STABILITY OF THREE-LAYER CYLINDRICAL SHELLS BEYOND THE ELASTIC LIMIT, Candidate of Technical Sciences, V.V. Serdyukov .....	93
---	----

Examines the stability of cylindrical shells consisting of two layers connected by a filler and subject to normal pressure and axial force such that the stresses generated exceed the elastic limit.

THE APPLICATION OF CONFORMAL MAPPING TO PROBLEMS OF THE THEORY OF ELASTICITY, Candidate of Technical Sciences, V.B. Gorlov .....	105
--	-----

Describes the derivation of conformal mapping functions for computing stresses and stress concentration factors in machine parts with complex shapes.

STABILITY OF THREE-LAYER CYLINDRICAL SHELLS IN THE ELASTIC AND INELASTIC REGIONS, Candidate of Technical Sciences, I.A. Yefimov .....	111
---	-----

Discusses the "small-scale" stability of three-layer (filled), corrugated cylindrical shells under several combined loads, assuming elastic behavior of the filler and a plastic condition in the bearing layers at instant of buckling.

# THE SHAPE OF THE ELASTIC CURVE OF A WEIGHTLESS ROTATING SHAFT CARRYING ECCENTRICALLY LOCATED POINT MASSES OR DISKS

Docent A. N. Ogurechnikov

The study of the shape of the elastic curve of a rotating shaft which precesses as it undergoes resonance vibrations is of no particular practical significance, since the theoretical basis in calculating the vibration frequency is Wiedler postulate, in which the elastic curve is regarded as plane, and its shape during resonance is assumed to be similar to that of the elastic curve in unrestrained oscillation. However, it is quite frequently claimed that the elastic curve of a vibrating shaft, by virtue of the different directions of eccentricities of its associated masses, is actually a space curve. This assertion, which is entirely correct for forced vibrations of a shaft, becomes invalid when extended to the case of resonance vibrations.

/5

The elastic curve of a shaft undergoing precession during resonance vibrations must be a plane curve, since the shaft vibrates in all axial planes with the same frequency; thus, all the projections of the outline of the elastic curve onto these planes should be similar, which can occur only if the elastic curve is a planar one.

Academician B. S. Stechkin has rigorously proven the validity of Wiedler's postulate for systems executing torsional vibrations. We shall prove the validity of this postulate for systems which execute flexural vibrations, namely:

- 1) for a shaft with two eccentrically located point masses;
- 2) for a shaft carrying an eccentrically coupled point mass and an obliquely seated ideal thin disk.

Without detriment to the generality of proof, we shall consider the case of direct synchronous precession, where the eccentricities and the torque transmitted to the shaft by the drive are the sources of the vibrations.

## A PERFECTLY ELASTIC WEIGHTLESS SHAFT WITH TWO ECCENTRICALLY COUPLED POINT MASSES

/6

A schematic of the shaft system is shown in Fig. 1. The axis of the system at rest is denoted by point  $O$ . We use the notation:  $e_1$  and  $e_2$  - eccentricities of the coupled point masses;  $2\tau$  - angle between the direction of above eccentricities;  $m_1$  and  $m_2$  - point masses coupled to the system;  $O_1$  and  $O_2$  - points of the elastic curve of the bent shaft at the sections passing through the sites of coupling of the point masses;

---

\*Numbers in the margin indicate pagination in the foreign text.

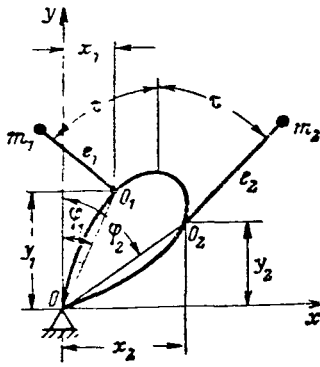


Figure 1. The Projection of the Elastic Curve of a Shaft with Two Point Masses onto a Plane Perpendicular to its Axis.

$\underline{y}$  and  $\underline{x}$  - coordinate axes; here  $\underline{y}$  is the axis parallel to the bisector of angle  $2\tau$ ;  $\varphi_1$  and  $\varphi_2$  - direction angles of the shaft deflections.

When the shaft rotates with velocity  $\omega$  lower than the critical one, a direct synchronous precession ensues. Due to the eccentricities  $\underline{e}_1$  and  $\underline{e}_2$  of the coupled masses  $\underline{m}_1$  and  $\underline{m}_2$  the shaft axis will be deflected and thus become a spatial curve; the shaft sections, to which these masses are connected, will occupy positions  $\underline{O}_1$  and  $\underline{O}_2$ .

Since

$$\omega \neq \omega_{cr}$$

the shaft deflections are described by

$$\begin{aligned} y_1 &= (y_1 + e_1 \cos \tau) m_1 \omega^2 \delta_{11} + (y_2 + e_2 \cos \tau) m_2 \omega^2 \delta_{21}; \\ y_2 &= (y_1 + e_1 \cos \tau) m_1 \omega^2 \delta_{12} + (y_2 + e_2 \cos \tau) m_2 \omega^2 \delta_{22}; \\ x_1 &= (x_1 - e_1 \sin \tau) m_1 \omega^2 \delta_{11} + (x_2 + e_2 \sin \tau) m_2 \omega^2 \delta_{21}; \\ x_2 &= (x_1 - e_1 \sin \tau) m_1 \omega^2 \delta_{12} + (x_2 + e_2 \sin \tau) m_2 \omega^2 \delta_{22}, \end{aligned}$$

where  $\delta_{11}$ ,  $\delta_{12}$ ,  $\delta_{21}$ ,  $\delta_{22}$  are the compliances of the shaft. If we denote

$$\begin{aligned} e_1 \cos \tau &= \vartheta_1; & e_2 \cos \tau &= \vartheta_2; \\ e_1 \sin \tau &= \theta_1; & e_2 \sin \tau &= \theta_2; \\ m_1 \omega^2 \delta_{11} &= n_{11}; & m_1 \omega^2 \delta_{12} &= n_{12}; \\ m_2 \omega^2 \delta_{22} &= n_{22}; & m_2 \omega^2 \delta_{21} &= n_{21}, \end{aligned}$$

then this system of equations can be written as

$$\begin{aligned} y_1(n_{11} - 1) + n_{21}y_2 &= -\vartheta_1 n_{11} - \vartheta_2 n_{21}; \\ y_1 n_{12} + y_2(n_{22} - 1) &= -\vartheta_1 n_{12} - \vartheta_2 n_{22}; \\ x_1(n_{11} - 1) + x_2 n_{21} &= \theta_1 n_{11} - \theta_2 n_{21}; \\ x_1 n_{12} + x_2(n_{22} - 1) &= \theta_1 n_{12} - \theta_2 n_{22}. \end{aligned}$$

As can be seen, this system of equations contains two parts: the first two equations contain only  $y_1$  and  $y_2$ , while the last two contain only  $x_1$  and  $x_2$ .

/7

The determinant composed of coefficients of the unknown  $y_1$  and  $y_2$  (of the first two equations) is

$$D_y = (n_{11} - 1)(n_{22} - 1) - n_{12}n_{21}.$$

The value of  $y_1$  is the fraction

$$g_1 = \frac{\Delta y_1}{D_y},$$

where  $\Delta y_1$  is a determinant which is obtained from the system's determinant by replacing the first column by the column of free terms

$$\Delta y_1 = -(\vartheta_1 n_{11} + \vartheta_2 n_{21})(n_{22} - 1) + (\vartheta_1 n_{12} + \vartheta_2 n_{22})n_{21},$$

and, consequently,

$$y_1 = \frac{-(\vartheta_1 n_{11} + \vartheta_2 n_{21})(n_{22} - 1) + (\vartheta_1 n_{12} + \vartheta_2 n_{22})n_{21}}{(n_{11} - 1)(n_{22} - 1) - n_{12}n_{21}}.$$

Similarly,

$$\Delta y_2 = -(n_{11} - 1)(\vartheta_1 n_{12} + \vartheta_2 n_{22}) + n_{12}(\vartheta_1 n_{11} + \vartheta_2 n_{21})$$

and

$$y_2 = \frac{-(\vartheta_1 n_{12} + \vartheta_2 n_{22})(n_{11} - 1) + (\vartheta_1 n_{11} + \vartheta_2 n_{21})n_{12}}{(n_{11} - 1)(n_{22} - 1) - n_{12}n_{21}}.$$

The determinant composed of coefficients of unknown  $x_1$  and  $x_2$  (of the two last equations) is

$$D_x = (n_{11} - 1)(n_{22} - 1) - n_{12}n_{21} = D_y;$$

$$\Delta x_1 = (\theta_1 n_{11} - \theta_2 n_{21})(n_{22} - 1) - (\theta_1 n_{12} - \theta_2 n_{22})n_{21},$$

hence we find in the same manner as above

$$x_1 = \frac{(\theta_1 n_{11} - \theta_2 n_{21})(n_{22} - 1) - (\theta_1 n_{12} - \theta_2 n_{22})n_{21}}{(n_{11} - 1)(n_{22} - 1) - n_{12}n_{21}}$$

and, using the expression

$$\Delta x_2 = (n_{11} - 1)(\theta_1 n_{12} - \theta_2 n_{22}) - (\theta_1 n_{11} - \theta_2 n_{21})n_{12},$$

we get

$$x_2 = \frac{(\theta_1 n_{12} - \theta_2 n_{22})(n_{11} - 1) - (\theta_1 n_{11} - \theta_2 n_{21}) n_{12}}{(n_{22} - 1)(n_{11} - 1) - n_{12} n_{21}}.$$

/7

From the deflection coordinates thus found we can obtain the deflections themselves

/8

$$Q_1 = \sqrt{x_1^2 + y_1^2} \text{ and } Q_2 = \sqrt{x_2^2 + y_2^2},$$

as well as the angles between the direction of deflections and the y axis

$$\tan \varphi_1 = \frac{x_1}{y_1} \text{ and } \tan \varphi_2 = \frac{x_2}{y_2}.$$

Let us now ask two questions: 1) is the elastic curve of the shaft planar? 2) How do angles  $\varphi_1$  and  $\varphi_2$  vary with changes in the rpm?

If the elastic curve of the shaft is to be planar, then angles  $\varphi_1$  and  $\varphi_2$  must be equal, i.e., the ratios

$$\frac{x_1}{y_1} \text{ and } \frac{x_2}{y_2},$$

must be equal; representing this in terms of previously found values of x and y

$$\frac{x_1}{y_1} = \frac{(\theta_1 n_{11} - \theta_2 n_{21})(n_{22} - 1) - (\theta_1 n_{12} - \theta_2 n_{22}) n_{21}}{-(\theta_1 n_{11} + \theta_2 n_{21})(n_{22} - 1) + (\theta_1 n_{12} + \theta_2 n_{22}) n_{21}}$$

and

$$\frac{x_2}{y_2} = \frac{(\theta_1 n_{12} - \theta_2 n_{22})(n_{11} - 1) - (\theta_1 n_{11} - \theta_2 n_{21}) n_{12}}{-(\theta_1 n_{12} + \theta_2 n_{22})(n_{11} - 1) + (\theta_1 n_{11} + \theta_2 n_{21}) n_{12}}.$$

We first consider two cases: 1) if  $2\tau = 0$  and consequently  $\tau = 0$ , i.e., if the eccentricities are codirectional away from the shaft, then

$$\theta_1 = e_1 \text{ and } \theta_2 = e_2,$$

and

$$\theta_1 = 0 \text{ and } \theta_2 = 0.$$

It can be seen from the expressions for  $\underline{x}_1$  and  $\underline{x}_2$  that the numerators become zero so that  $\varphi_1 = 0$  and  $\varphi_2 = 0$ , since the denominators then are not zero. Then also  $y_1 \neq 0$ , and  $y_2 \neq 0$ , since  $\mathfrak{g}_1 \neq 0$  and  $\mathfrak{g}_2 \neq 0$ . As far as  $D_x = D_y \neq 0$  is concerned, the expressions for these terms are finite when  $\omega \neq \omega_{cr}$ .

When  $\omega = \omega_{cr}$ ,  $\underline{D} = \frac{\underline{D}}{\underline{x}} = \frac{\underline{D}}{y} = 0$ , or

$$\begin{aligned} D &= (\bar{n}_{11} - 1)(\bar{n}_{22} - 1) - \bar{n}_{12}\bar{n}_{21} = \\ &= (m_1\omega_{cr}^2\delta_{11} - 1)(m_2\omega_{cr}^2\delta_{22} - 1) - m_1\omega_{cr}^2\delta_{12}m_2\omega_{cr}^2\delta_{21} = \\ &= \omega_{cr}^4 m_1 m_2 (\delta_{11}\delta_{22} - \delta_{12}\delta_{21}) - \omega_{cr}^2 (m_1\delta_{11} + m_2\delta_{22}) + 1 = 0, \end{aligned}$$

since the last expression is a periodic equation when written in the standard form.

In analyzing the first case we see that when the eccentricities are directed in the same direction, the elastic curve of the shaft will be planar if

$$\omega \neq \omega_{cr} \text{ and } \varphi_1 = \varphi_2 = 0.$$

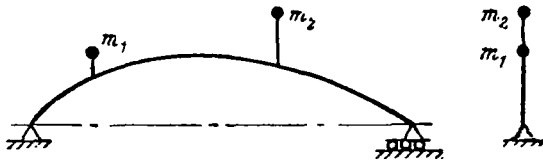


Figure 2. The Shape of the Elastic Curve of a Shaft Rotating at Subcritical Speed.

Since  $\underline{D} \rightarrow 1$  as  $\omega \rightarrow 0$  and remains greater than zero for all the  $\omega < \omega_{cr}$ , then the critical angular velocity  $\omega_{cr}$  is smaller than the partial angular velocity  $\omega_{part}$ . Since

$$\omega_{1part} = \sqrt{\frac{1}{m_1\delta_{11}}}; \quad \omega_{2part} = \sqrt{\frac{1}{m_2\delta_{22}}}$$

and further  $0 < \underline{n}_{22} < 1$  and  $0 < \underline{n}_{11} < 1$  when  $n_{12} > 0$  and  $n_{21} > 0$ ,

then

$$y_1 > 0 \text{ and } y_2 > 0.$$

/9

Consequently, at  $\omega < \omega_{cr}$ , the elastic curve has a deflection in the direction of the initial eccentricities (Fig. 2).

When the speed is raised by an infinitesimal increment above the critical, the sign of the determinant will change to minus and therefore the deflections  $y_1$  and  $y_2$  will become negative (Fig. 3).

When  $\omega \rightarrow \infty - e_1$  and  $y_2 \rightarrow -e_2$  (Fig. 4), since

$$y_2 = \frac{-e_1 n_{11} n_{12} - e_2 n_{11} n_{22} + e_1 n_{11} n_{12} + e_2 n_{21} n_{12}}{n_{11} n_{22} - n_{12} n_{21}} = -e_2$$

and

$$y_1 = \frac{-e_1 n_{11} n_{22} - e_2 n_{22} n_{21} + e_1 n_{12} n_{21} + e_2 n_{22} n_{21}}{n_{11} n_{22} - n_{12} n_{21}} = -e_1.$$

2) If the eccentricities are oppositely directed, so that

$$2\tau = \pi; \quad \tau = \pi/2,$$

from which

$$\vartheta_1 = 0 \text{ and } \vartheta_2 = 0, \text{ and } \theta_1 = e_1 \text{ and } \theta_2 = e_2,$$

then, when  $\omega \neq \omega_{cr}$ , one obtains

$$x_1 \neq 0; \quad y_1 = 0; \quad x_2 \neq 0; \quad y_2 = 0$$

/10

and

$$|\tan \varphi_1| = |\tan \varphi_2| = |\infty|.$$

Under these conditions the elastic curve will lie in the plane of the x axis.

When  $\omega \rightarrow \infty$

$$x_1 = \frac{e_1 n_{11} n_{22} - e_2 n_{22} n_{21} - e_1 n_{12} n_{21} + e_2 n_{22} n_{21}}{n_{11} n_{22} - n_{12} n_{21}} = e_1,$$

$$x_2 = \frac{e_1 n_{11} n_{12} - e_2 n_{22} n_{11} - e_1 n_{11} n_{12} + e_2 n_{21} n_{12}}{n_{11} n_{22} - n_{12} n_{21}} = -e_2.$$

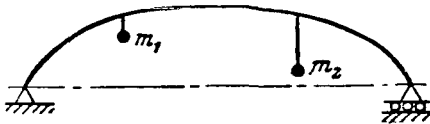


Figure 3. The Shape of the Elastic Curve of a Shaft Rotating at Supercritical Speed.

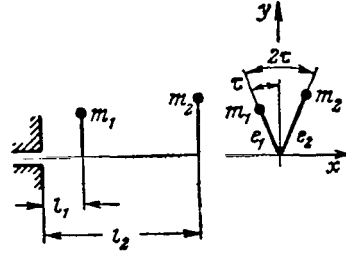


Figure 4. Schematic of a Cantilevered Weightless Elastic Shaft Carrying Two Point Masses.

For small  $\omega$  (as compared with  $\omega_{cr}$  and  $\omega_{part}$ )  $D > 0$ ,  $n_{11}n_{22} > n_{12}n_{21}$  and the sign of  $\underline{x}_1$  will depend on the sign of the expression

$$\theta_1 n_{11} n_{22} - \theta_2 n_{22} n_{21} - \theta_1 n_{11} + \theta_2 n_{21} - \theta_1 n_{21} n_{12} + \theta_2 n_{22} n_{21}$$

in which, by collecting terms with  $\theta_1$  and factoring out  $\theta_1$ , we get

$$\begin{aligned} & \theta_1 (n_{11} n_{22} - n_{11} - n_{12} n_{21}) + \theta_2 n_{21} = \\ & = e_1 (m_1 \omega^2 \delta_{11} m_2 \omega^2 \delta_{22} - m_1 \omega^2 \delta_{11} - m_1 \omega^2 \delta_{12} m_2 \omega^2 \delta_{21}) + e_2 m_2 \omega^2 \delta_{21} = \\ & = e_1 [\omega^4 m_1 m_2 (\delta_{11} \delta_{22} - \delta_{12} \delta_{21})] + e_2 m_2 \omega^2 \delta_{21} - e_1 m_1 \omega^2 \delta_{11}. \end{aligned}$$

Analysis of this expression shows that if we neglect  $\omega^4$  and divide the expression by  $\omega^2$ , we will find that the sign of  $\underline{x}_1$  depends on the sign of the expression  $e_2 m_2 \delta_{21} - e_1 m_1 \delta_{11}$ .

Proceeding in the same manner, the sign of  $\underline{x}_2$  will depend on the sign of

$$e_2 m_2 \delta_{22} - e_1 m_1 \delta_{12}.$$

If  $\omega \rightarrow 0$ , then

$$\tan \varphi_1(0) = \frac{-\theta_1 n_{11} + \theta_2 n_{21}}{\delta_1 n_{11} + \delta_2 n_{21}} \quad \text{and} \quad \tan \varphi_2(0) = \frac{-\theta_1 n_{12} + \theta_2 n_{22}}{\delta_1 n_{12} + \delta_2 n_{22}}.$$

/11

Returning to the initial notation, we get

$$\tan \varphi_1(0) = \tan \tau \frac{e_2 m_2 \delta_{21} - e_1 m_1 \delta_{11}}{e_1 m_1 \delta_{11} + e_2 m_2 \delta_{21}}$$

$$\tan \varphi_2(0) = \tan \tau \frac{e_2 m_2 \delta_{22} - e_1 m_1 \delta_{12}}{e_1 m_1 \delta_{12} + e_2 m_2 \delta_{22}}$$

We now find angles  $\varphi_1$  and  $\varphi_2$  for  $\omega \gg \omega_{cr}$  and for any angle  $2\tau$

$$\begin{aligned} \tan \varphi_1 &= \frac{\theta_1 n_{11} n_{22} - \theta_2 n_{22} n_{21} - \theta_1 n_{12} n_{21} + \theta_2 n_{22} n_{21}}{-\vartheta_1 n_{11} n_{22} - \vartheta_2 n_{22} n_{21} + \vartheta_1 n_{12} n_{21} + \vartheta_2 n_{22} n_{21}} = \\ &= \frac{\theta_1 (n_{11} n_{22} - n_{12} n_{21})}{-\vartheta_1 (n_{11} n_{22} - n_{12} n_{21})} = -\frac{\theta_1}{\vartheta_1} = -\frac{e_1 \sin \tau}{e_1 \cos \tau} = -\tan \tau. \end{aligned}$$

Consequently,

$$\begin{aligned} \varphi_1 &= -\tau, \\ \tan \varphi_2 &= \frac{\theta_1 n_{11} n_{12} - \theta_2 n_{11} n_{22} - \theta_1 n_{11} n_{12} + \theta_2 n_{21} n_{12}}{-\vartheta_1 n_{11} n_{12} - \vartheta_2 n_{11} n_{22} + \vartheta_1 n_{11} n_{12} + \vartheta_2 n_{21} n_{12}} = \\ &= \frac{-\theta_2 (n_{11} n_{22} - n_{21} n_{12})}{-\vartheta_2 (n_{11} n_{22} - n_{21} n_{12})} = \frac{\theta_2}{\vartheta_2} = \frac{e_2 \sin \tau}{e_2 \cos \tau} = \tan \tau, \end{aligned}$$

from which

$$\varphi_2 = \tau.$$

Comparing the expressions just obtained with those for  $\tan \varphi_1$  and  $\tan \varphi_2$  derived at low rpm, we see that the multiplier of  $\tan \varphi$  in the latter equation contains fractions not equal to unity. Consequently, angles  $\varphi_1$  and  $\varphi_2$  depend on the shaft rpm.

We shall now consider a system in resonance. If it is assumed that the shaft resonance amplitude is limited by frictional forces and that the resonance vibrations become steady if the system is operating in vacuum, and, furthermore, assuming perfect (i.e., frictionless) bearings we will have to assume that the amplitude will have to be limited by the friction between the fibers of the shaft.

As is known from literature and as can be seen from one case of angle  $2\tau = 0$ , when the system passes through the critical velocity, the directions of eccentricities relative to the elastic curve of the shaft shift

by the amount  $\pi$ . It is also known that at the critical velocity, the phase shift is  $\pi/2$  in the direction of the rotation; i.e., at the instant when the system goes into resonance, the shaft is twisted about the axis of the elastic curve. This also should happen in a system with any value of  $2\tau$ . In this case, since even at resonance the angle between the directions of eccentricities should remain  $2\tau$  (we shall neglect the torsional deformations of the shaft), the shaft of our system will be twisted so that the directions of the eccentricities will form angles  $\tau$  with the  $y$  axis.

From the expressions derived above for  $\varphi_1$  and  $\varphi_2$ , we can write equations for  $\omega = \omega_{cr}$

/12

$$\begin{aligned}
 n_{ik} &= \bar{n}_{ik}; \\
 \tan \bar{\varphi}_1 &= \left( \frac{x_1}{y_1} \right)_{cr} = \frac{(\theta_1 \bar{n}_{11} - \theta_2 \bar{n}_{21})(\bar{n}_{22} - 1) - (\theta_1 \bar{n}_{12} - \theta_2 \bar{n}_{22}) \bar{n}_{21}}{-(\theta_1 \bar{n}_{11} + \theta_2 \bar{n}_{21})(\bar{n}_{22} - 1) + (\theta_1 \bar{n}_{12} + \theta_2 \bar{n}_{22}) \bar{n}_{21}} = \\
 &= \frac{\theta_1 (\bar{n}_{11} \bar{n}_{22} - \bar{n}_{12} \bar{n}_{21}) - \theta_2 (\bar{n}_{22} \bar{n}_{21} - \bar{n}_{22} \bar{n}_{21}) - \theta_1 \bar{n}_{11} + \theta_2 \bar{n}_{21}}{-\theta_1 (\bar{n}_{11} \bar{n}_{22} - \bar{n}_{12} \bar{n}_{21}) + \theta_2 (\bar{n}_{22} \bar{n}_{21} - \bar{n}_{22} \bar{n}_{21}) + \theta_1 \bar{n}_{11} + \theta_2 \bar{n}_{21}} = \\
 &= \frac{\theta_1 (\bar{n}_{11} \bar{n}_{22} - \bar{n}_{12} \bar{n}_{21}) - \theta_1 \bar{n}_{11} + \theta_2 \bar{n}_{21}}{-\theta_1 (\bar{n}_{11} \bar{n}_{22} - \bar{n}_{12} \bar{n}_{21}) + \theta_1 \bar{n}_{11} + \theta_2 \bar{n}_{21}}
 \end{aligned}$$

We collect some terms of the numerator and denominator in parentheses, and reduce the expressions in parentheses to the form

$$\begin{aligned}
 D_{cr} &= (\bar{n}_{11} - 1)(\bar{n}_{22} - 1) - \bar{n}_{12} \bar{n}_{21} = \bar{n}_{11} \bar{n}_{22} - \bar{n}_{12} \bar{n}_{21} - \bar{n}_{11} - \bar{n}_{22} + 1 = 0; \\
 \tan \bar{\varphi}_1 &= \frac{\theta_1 (\bar{n}_{11} + \bar{n}_{22} - 1) - \theta_1 \bar{n}_{11} + \theta_2 \bar{n}_{21}}{-\theta_1 (\bar{n}_{11} + \bar{n}_{22} - 1) + \theta_1 \bar{n}_{11} + \theta_2 \bar{n}_{21}} = \\
 &= \frac{\theta_1 (\bar{n}_{22} - 1) + \theta_2 \bar{n}_{21}}{-\theta_1 (\bar{n}_{22} - 1) + \theta_2 \bar{n}_{21}} = \tan \tau \frac{e_1 (\bar{n}_{22} - 1) + e_2 \bar{n}_{21}}{-e_1 (\bar{n}_{22} - 1) + e_2 \bar{n}_{21}}
 \end{aligned}$$

or

$$\begin{aligned}
 \tan \varphi_{1cr} &= -\tan \tau \frac{e_1 (\bar{n}_{22} - 1) + e_2 \bar{n}_{21}}{e_1 (\bar{n}_{22} - 1) - e_2 \bar{n}_{21}}; \\
 \tan \varphi_{2cr} &= \left( \frac{x_2}{y_2} \right)_{cr} = \frac{\theta_1 \bar{n}_{11} \bar{n}_{12} - \theta_2 \bar{n}_{11} \bar{n}_{22} - \theta_1 \bar{n}_{12} + \theta_2 \bar{n}_{22} - \theta_1 \bar{n}_{11} \bar{n}_{12} + \theta_2 \bar{n}_{12} \bar{n}_{21}}{-\theta_1 \bar{n}_{11} \bar{n}_{12} - \theta_2 \bar{n}_{11} \bar{n}_{22} + \theta_1 \bar{n}_{12} + \theta_2 \bar{n}_{22} + \theta_1 \bar{n}_{11} \bar{n}_{12} + \theta_2 \bar{n}_{12} \bar{n}_{21}} = \\
 &= \frac{-\theta_2 (\bar{n}_{11} \bar{n}_{22} - \bar{n}_{12} \bar{n}_{21}) - \theta_1 \bar{n}_{12} + \theta_2 \bar{n}_{22}}{-\theta_2 (\bar{n}_{11} \bar{n}_{22} - \bar{n}_{12} \bar{n}_{21}) + \theta_1 \bar{n}_{12} + \theta_2 \bar{n}_{22}} =
 \end{aligned}$$

$$= \frac{-\vartheta_2(\bar{n}_{11} + \bar{n}_{22} - 1) - \vartheta_1\bar{n}_{12} + \vartheta_2\bar{n}_{22}}{-\vartheta_2(\bar{n}_{11} + \bar{n}_{22} - 1) + \vartheta_1\bar{n}_{12} + \vartheta_2\bar{n}_{22}} = \frac{-\vartheta_2(\bar{n}_{11} - 1) - \vartheta_1\bar{n}_{12}}{-\vartheta_2(\bar{n}_{11} - 1) + \vartheta_1\bar{n}_{12}};$$

$$\tan \varphi_{2\text{ cr}} = \tan \tau \frac{e_2(\bar{n}_{11} - 1) + e_1\bar{n}_{12}}{e_2(\bar{n}_{11} - 1) - e_1\bar{n}_{12}}.$$

We find the ratio

/13

$$\begin{aligned} \left( \frac{y_1}{y_2} \right)_{\text{cr}} &= \frac{-\vartheta_1(\bar{n}_{11}\bar{n}_{22} - \bar{n}_{12}\bar{n}_{21}) + \vartheta_1\bar{n}_{11} + \vartheta_2\bar{n}_{21}}{-\vartheta_2(\bar{n}_{11}\bar{n}_{22} - \bar{n}_{12}\bar{n}_{21}) + \vartheta_1\bar{n}_{12} + \vartheta_2\bar{n}_{22}} = \\ &= \frac{-\vartheta_1(\bar{n}_{11} + \bar{n}_{22} - 1) + \vartheta_1\bar{n}_{11} + \vartheta_2\bar{n}_{21}}{-\vartheta_2(\bar{n}_{11} + \bar{n}_{22} - 1) + \vartheta_2\bar{n}_{22} + \vartheta_1\bar{n}_{12}} = \frac{-\vartheta_1(\bar{n}_{22} - 1) + \vartheta_2\bar{n}_{21}}{-\vartheta_2(\bar{n}_{11} - 1) + \vartheta_1\bar{n}_{12}} = \\ &= \frac{e_1(\bar{n}_{22} - 1) - e_2\bar{n}_{21}}{e_2(\bar{n}_{11} - 1) - e_1\bar{n}_{12}}. \end{aligned}$$

Similarly,

$$\left( \frac{x_1}{x_2} \right)_{\text{cr}} = \frac{\vartheta_1(\bar{n}_{22} - 1) + \vartheta_2\bar{n}_{21}}{-\vartheta_2(\bar{n}_{11} - 1) - \vartheta_1\bar{n}_{12}} = \frac{e_1(\bar{n}_{22} - 1) + e_2\bar{n}_{21}}{e_2(\bar{n}_{11} - 1) + e_1\bar{n}_{12}}.$$

When  $\omega \rightarrow 0$  and  $\underline{n} \rightarrow 0$ , and neglecting the product  $(\underline{n}_{ik} \cdot \underline{n}_{ps})$ , we find

$$\begin{aligned} \left( \frac{x_1}{x_2} \right)_0 &= \frac{-\vartheta_1\bar{n}_{11} + \vartheta_2\bar{n}_{21}}{-\vartheta_1\bar{n}_{12} + \vartheta_2\bar{n}_{22}} = \frac{e_1m_1\delta_{11} - e_2m_2\delta_{21}}{e_1m_1\delta_{12} - e_2m_2\delta_{22}}, \\ \left( \frac{y_1}{y_2} \right)_0 &= \frac{\vartheta_1\bar{n}_{11} + \vartheta_2\bar{n}_{21}}{\vartheta_1\bar{n}_{12} + \vartheta_2\bar{n}_{22}} = \frac{e_1m_1\delta_{11} + e_2m_2\delta_{21}}{e_1m_1\delta_{12} + e_2m_2\delta_{22}} \end{aligned}$$

We shall now prove that the elastic curve of a shaft rotating at critical speed is a planar curve. This is equivalent to the condition

that

$$\tan \varphi_{1\text{ cr}} = \tan \varphi_{2\text{ cr}}$$

or, if we use the previously obtained expressions for the tangents, to

$$\frac{e_1(\bar{n}_{22} - 1) + e_2\bar{n}_{21}}{-e_1(\bar{n}_{22} - 1) + e_2\bar{n}_{21}} = \frac{e_2(\bar{n}_{11} - 1) + e_1\bar{n}_{12}}{e_2(\bar{n}_{11} - 1) - e_1\bar{n}_{12}}$$

We shall show that this equality really holds

$$[e_1(\bar{n}_{22}-1)+e_2\bar{n}_{21}][e_2(\bar{n}_{11}-1)-e_1\bar{n}_{12}] = \\ = [-e_1(\bar{n}_{22}-1)+e_2\bar{n}_{21}][e_2(\bar{n}_{11}-1)+e_1\bar{n}_{12}].$$

We remove the parentheses

$$e_1e_2\bar{n}_{11}\bar{n}_{22}-e_1e_2\bar{n}_{11}+e_2^2\bar{n}_{11}\bar{n}_{21}-e_1e_2\bar{n}_{22}+e_1e_2- \\ -e_2^2\bar{n}_{21}-e_1^2\bar{n}_{22}\bar{n}_{12}+e_1^2\bar{n}_{12}-e_1e_2\bar{n}_{12}\bar{n}_{21} = -e_1e_2\bar{n}_{11}\bar{n}_{22}+ \\ +e_1e_2\bar{n}_{11}+e_2^2\bar{n}_{11}\bar{n}_{21}+e_1e_2\bar{n}_{22}-e_1e_2-e_2^2\bar{n}_{21}- \\ -e_1^2\bar{n}_{22}\bar{n}_{12}+e_1^2\bar{n}_{12}+e_1e_2\bar{n}_{12}\bar{n}_{21}.$$

Canceling out identical terms [of opposite sign], factoring out and dividing through by  $\underline{e}_1\underline{e}_2$ , we satisfy ourselves that the remaining terms add up to  $D = 0$ , and hence the difference in sign does not disprove the identity of the expressions.

It is thus proven that the elastic curve of a shaft carrying two eccentrically coupled point masses with differently directed eccentricities and rotating at critical speed is a planar curve.

#### A PERFECTLY ELASTIC WEIGHTLESS SHAFT CARRYING AN ECCENTRICALLY COUPLED POINT MASS AND AN OBLIQUELY SEATED PERFECT THIN DISK

/14

Let there be a weightless, elastic cantilevered shaft carrying a point mass and an obliquely seated disk (Fig. 5). The directions of the eccentricity and of the obliqueness form an angle  $2\tau$ .

The coordinate axes  $\underline{y}$  and  $\underline{x}$  are associated with the shaft, but in such a manner that on rotation the  $\underline{y}$  axis divides angle  $2\tau$  into two equal parts; i.e., the axis is parallel to the bisector of this angle.

We introduce the notation:  $\underline{m}_1$  - the point mass;  $\underline{e}_1$  - the eccentricity of this mass;  $\alpha$  - the angle of skewness of the disk (a small quantity);  $\theta_2$  - the equatorial moment of inertia of the disk mass.

If the skewness of the disk is expressed in terms of its shift (from vertical) at radius  $\underline{r}$ , then

$$\tan \alpha = \frac{a}{r}$$

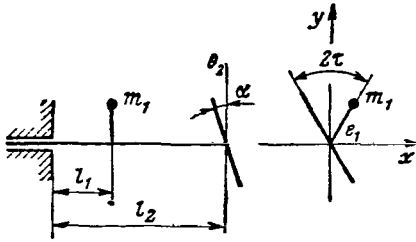


Figure 5. Schematic of a Cantilevered Weightless, Elastic Shaft Carrying a Point Mass and an Obliquely Seated Disk.

Making use of the fact that the skewness is small, we write

$$\alpha = \frac{a}{r}.$$

The angles made by the skew disk with axes  $\underline{y}$  and  $\underline{x}$  are

$$\tan \alpha_y = \frac{a \cos \tau}{r} = \tan \alpha \cos \tau;$$

$$\text{and } \alpha_x = \frac{a \sin \tau}{r} = \tan \alpha \sin \tau$$

or

$$\alpha_y = \alpha \cos \tau \text{ and } \alpha_x = \alpha \sin \tau.$$

We now write the equation of shaft deformations when the shaft rotates at any  $\omega \neq \omega_{cr}$

/15

$$y_1 = (y_1 m_1 \omega^2 + \omega^2 e m_1 \cos \tau) \delta_{11} + \theta_2 (\alpha_y - \varphi_2) \omega^2 \delta_{21}; \quad (1)$$

$$y_3 = (y_1 m_1 \omega^2 + \omega^2 e m_1 \cos \tau) \delta_{13} + \theta_2 (\alpha_y - \varphi_2) \omega^2 \delta_{23}; \quad (2)$$

$$\varphi_2 = (y_1 m_1 \omega^2 + \omega^2 e m_1 \cos \tau) \delta_{12} + \theta_2 (\alpha_y - \varphi_2) \omega^2 \delta_{22}. \quad (3)$$

We introduce the notation

$$\begin{aligned} m_1 \omega^2 \delta_{11} &= n_{11}; & m_1 \omega^2 \delta_{12} &= n_{12}; & e \sin \tau &= \theta_1; \\ \theta_2 \omega^2 \delta_{22} &= n_{22}; & \theta_2 \omega^2 \delta_{21} &= n_{21}; & e \cos \tau &= \vartheta_1. \end{aligned}$$

Then, Eqs. (1) and (3) form an independent system

$$\begin{aligned} y_1 (n_{11} - 1) - \varphi_2 n_{21} &= -\vartheta_1 n_{11} - \alpha_y n_{21}; \\ y_1 n_{12} - \varphi_2 (n_{22} + 1) &= -\vartheta_1 n_{12} - \alpha_y n_{22}, \end{aligned}$$

whose determinants are

$$\begin{aligned}
D &= -(n_{11}-1)(n_{22}+1) + n_{12}n_{21} = -n_{11}n_{22} + n_{12}n_{21} - n_{11} + n_{22} + 1; \\
\Delta y_1 &= (n_{22}+1)(\vartheta_1 n_{11} + \alpha_y n_{21}) - n_{21}(\vartheta_1 n_{12} + \alpha_y n_{22}) = \\
&= \vartheta_1 (n_{11}n_{22} - n_{12}n_{21} + n_{11}) + \alpha_y (n_{22}n_{21} - n_{22}n_{21} + n_{21}) = \\
&= \vartheta_1 (n_{11}n_{22} - n_{12}n_{21} + n_{11}) + \alpha_y n_{21}
\end{aligned} \tag{15}$$

and

$$\begin{aligned}
\Delta \varphi_2 &= (n_{11}-1)(-\vartheta_1 n_{12} - \alpha_y n_{22}) + n_{12}(\vartheta_1 n_{11} + \alpha_y n_{21}) = \\
&= \vartheta_1 n_{12} + \alpha_y (n_{22} + n_{12}n_{21} - n_{11}n_{22}).
\end{aligned}$$

Consequently,

$$y_1 = \frac{\Delta y_1}{D} \text{ and } \varphi_2 = \frac{\Delta \varphi_2}{D}.$$

The coordinate  $y_3$  of the second equation is written in terms of  $y_1$  and  $\varphi_2$  in the form

$$y_3 = y_1 n_{13} + \vartheta_1 n_{13} + \alpha_y n_{23} - \varphi_2 n_{23}.$$

Setting up the equations of deformations in the  $\underline{x}$  direction, we get

$$\begin{aligned}
x_1 &= (x_1 - \vartheta_1) n_{11} + (\alpha_x - \Psi_2) n_{21}; \\
\Psi_2 &= (x_1 - \vartheta_1) n_{12} + (\alpha_x - \Psi_2) n_{22}; \\
x_3 &= (x_1 - \vartheta_1) n_{13} + (\alpha_x - \Psi_2) n_{23}.
\end{aligned}$$

The first two of these equations form the system

$$\begin{aligned}
x_1 (n_{11}-1) - \Psi_2 n_{21} &= \vartheta_1 n_{11} - \alpha_x n_{21}; \\
x_1 n_{12} - \Psi_2 (n_{22}+1) &= \vartheta_1 n_{12} - \alpha_x n_{22},
\end{aligned}$$

the determinant of which is

$$D = -(n_{11}-1)(n_{22}+1) + n_{12}n_{21} = -n_{11}n_{22} + n_{12}n_{21} - n_{11} + n_{22} + 1.$$

The determinant, as should have been expected, proves to be the same as for the system of equations for deformations  $(y_1, \varphi)$

$$\begin{aligned}
\Delta x_1 &= -\vartheta_1 (n_{11}n_{22} - n_{12}n_{21} + n_{11}) + \alpha_x n_{21}; \\
\Delta \Psi_2 &= -\alpha_x (n_{11}n_{22} - n_{12}n_{21} - n_{22}) - \vartheta_1 n_{12}; \\
x_1 &= \frac{\Delta x_1}{D} \text{ and } \Psi_2 = \frac{\Delta \Psi_2}{D},
\end{aligned} \tag{16}$$

and

$$x_3 = x_1 n_{13} - \Psi_2 n_{23} - \vartheta_1 n_{13} + \alpha_x n_{23}.$$

We now seek the tangents of the angles of deflection of the shaft sections as  $\omega \rightarrow 0$

/16

$$\begin{aligned}\tan \varphi_1(0) &= \left( \frac{x_1}{y_1} \right)_0 \cong \frac{-\theta_1 n_{11} + \alpha_x n_{21}}{\vartheta_1 n_{11} + \alpha_y n_{21}} = \\ &= \frac{-e \sin \tau \cdot m_1 \delta_{11} + \alpha \theta_2 \sin \tau \cdot \delta_{21}}{m_1 e \cos \tau \cdot \delta_{11} + \theta_2 \alpha \cos \tau \cdot \delta_{21}} = -\tan \tau \frac{m_1 e \delta_{11} - \theta_2 \alpha \delta_{21}}{m_1 e \delta_{11} + \theta_2 \alpha \delta_{21}}, \\ \tan \varphi_3(0) &\cong \left( \frac{x_3}{y_3} \right) = \frac{-e \sin \tau \cdot m_1 \delta_{13} + \theta_2 \alpha \sin \tau \cdot \delta_{23}}{e \cos \tau \cdot m_1 \delta_{13} + \theta_2 \alpha \cos \tau \cdot \delta_{23}} = \\ &= -\tan \tau \frac{e m_1 \delta_{13} - \theta_2 \alpha \delta_{23}}{e m_1 \delta_{13} + \theta_2 \alpha \delta_{23}}.\end{aligned}$$

We shall find the direction angles of the deflections of the elastic curve as  $\omega \rightarrow \infty$ ; here we shall drop all terms containing  $\omega$  raised to the lowest powers

$$\begin{aligned}\lim_{\omega \rightarrow \infty} D &= -n_{11} n_{22} + n_{12} n_{21}, \\ \lim_{\omega \rightarrow \infty} \Delta y_1 &= \vartheta_1 (n_{11} n_{22} - n_{12} n_{21}) + \alpha_y (n_{22} n_{21} - n_{22} n_{21}) = \\ &= \vartheta_1 (n_{11} n_{22} - n_{12} n_{21}); \\ \lim_{\omega \rightarrow \infty} \frac{\Delta y_1}{D} &= \frac{\Delta y_1}{D} = \frac{\vartheta_1 (n_{11} n_{22} - n_{12} n_{21})}{-(n_{11} n_{22} - n_{12} n_{21})} = -\vartheta_1 \\ y_1 &= -\vartheta_1 = -e \cos \tau, \\ \lim_{\omega \rightarrow \infty} \Delta x_1 &= -\theta_1 (n_{11} n_{22} - n_{12} n_{21}), \\ \lim_{\omega \rightarrow \infty} \frac{\Delta x_1}{D} &= \frac{\Delta x_1}{D} = \frac{-\theta_1 (n_{11} n_{22} - n_{12} n_{21})}{-(n_{11} n_{22} - n_{12} n_{21})} = \theta_1, \\ x_1 &= \theta_1 = e \sin \tau, \\ \tan \varphi_1(\infty) &= \frac{x_1}{y_1} = -\tan \tau; \\ \varphi_2(\infty) &= \frac{-\alpha_y (n_{11} n_{22} - n_{12} n_{21})}{-(n_{11} n_{22} - n_{12} n_{21})} = \alpha_y.\end{aligned}$$

Let us consider the state of the system when it rotates at critical velocity

/17

$$\begin{aligned}D &= -(n_{11} - 1)(n_{22} + 1) + n_{12} n_{21} = 0; \\ D &= -n_{11} n_{22} + n_{12} n_{21} - n_{11} + n_{22} + 1 = 0\end{aligned}$$

or

$$\tan \varphi_{1cr} = \frac{\Delta x_{1cr}}{\Delta y_{1cr}} = \frac{-\theta_1 (n_{11} n_{22} - n_{12} n_{21} + n_{11}) + \alpha_x n_{21}}{\vartheta_1 (n_{11} n_{22} - n_{12} n_{21} + n_{11}) + \alpha_y n_{21}}.$$

If in the parentheses of the numerator and denominator we reduce the terms to  $\underline{D}$ , then

/17

$$\tan \varphi_{1cr} = \frac{-\theta_1(n_{22} + 1) + a_x n_{21}}{\theta_1(n_{22} + 1) + a_y n_{21}},$$

$$\tan \varphi_{3cr} = \left( \frac{x_3}{y_3} \right)_{kp} = \frac{x_1 n_{13} - \Psi_2 n_{23} - \theta_1 n_{13} + a_x n_{23}}{y_1 n_{13} - \varphi_2 n_{23} + \theta_1 n_{13} + a_y n_{23}}.$$

Multiplying the numerator and denominator by  $\underline{D}_{cr} = 0$ , we get

$$\tan \varphi_{3cr} = \frac{\Delta x_1 n_{13} - \Delta \Psi_2 n_{23}}{\Delta y_1 n_{13} - \Delta \varphi_2 n_{23}}.$$

In this case, the third and fourth terms of the numerator and denominator become zero. Then

$$\tan \varphi_{3cr} = \frac{-\theta_1(n_{22} + 1)n_{13} + a_x n_{21} n_{13} - a_x(n_{11} - 1)n_{23} + \theta_1 n_{12} n_{23}}{\theta_1(n_{22} + 1)n_{13} + a_y n_{21} n_{13} - a_y(n_{11} - 1)n_{23} - \theta_1 n_{12} n_{23}}.$$

If it is assumed that the elastic curve of a shaft rotating at resonance speed is planar, then we must have

$$\tan \varphi_{1cr} = \tan \varphi_{3cr}.$$

However, this expression will hold only when it will be proven that the expressions in parentheses are proportional to the corresponding expressions outside of parentheses, which means that we must prove

$$\frac{-\theta_1(n_{22} + 1) + a_x n_{21}}{\theta_1(n_{22} + 1) + a_y n_{21}} = \frac{-a_x(n_{11} - 1) + \theta_1 n_{12}}{-a_y(n_{11} - 1) - \theta_1 n_{12}},$$

since

$$\frac{a}{b} = \frac{a + ka}{b + kb} = \frac{a(1 + k)}{b(1 + k)}$$

We change to a somewhat different expression

$$\frac{-e \sin \tau \cdot (n_{22} + 1) + a \sin \tau \cdot n_{21}}{e \cos \tau \cdot (n_{22} + 1) + a \cos \tau \cdot n_{21}} = \frac{-a \sin \tau \cdot (n_{11} - 1) + e \sin \tau \cdot n_{12}}{-a \cos \tau \cdot (n_{11} - 1) - e \cos \tau \cdot n_{12}}$$

Dividing through both sides of the expression by  $\tan \tau$  and, cross multiplying, we get

/18

$$[-e(n_{22} + 1) + an_{21}][-a(n_{11} - 1) - en_{12}] =$$

$$= [e(n_{22} + 1) + an_{21}][-a(n_{11} - 1) + en_{12}].$$

We remove the parentheses

$$\begin{aligned} & e\alpha(n_{22}+1)(n_{11}-1)+e^2(n_{22}+1)n_{12}-\alpha^2(n_{11}-1)n_{21}-\alpha en_{12}n_{21}= \\ & =e\alpha(n_{22}+1)(n_{11}-1)+e^2(n_{22}+1)n_{12}-\alpha^2(n_{11}-1)n_{21}+\alpha en_{12}n_{21}. \end{aligned}$$

Cancelling out identical terms with opposite sign and dividing through by  $\underline{e}$ , we get

$$\begin{aligned} & \alpha(n_{11}n_{21}+n_{11}-n_{22}-1)-\alpha n_{12}n_{21}= \\ & =-\alpha(n_{11}n_{22}+n_{11}-n_{22}-1)+\alpha n_{12}n_{21}. \end{aligned}$$

Then, factoring out  $\alpha$  and dividing through, we shall satisfy ourselves that the remaining expressions are equal to  $\underline{D} = 0$ , which proves that

$$\tan \varphi_{1cr} = \tan \varphi_{3cr}$$

as well as the assertion that when the system rotates at resonance rpm, the elastic curve of the shaft is a planar curve.

It is also possible to prove the validity of the Wiedler postulate for systems more complex than those presented above, but this would only involve more complicated calculations without changing the substance of the argument. Thus, Wiedler's postulate, stated as a theorem, has been proven.

In closing, we present two numerical examples which illustrate the fundamental tenets of this article.

Example 1 (see Fig. 4). Given an elastic, weightless bar, carrying two eccentrically coupled point masses  $\underline{m}_1$  and  $\underline{m}_2$  (with eccentricities  $\underline{e}_1$  and  $\underline{e}_2$ ) at an angle  $2\tau$  from one another, find the critical speeds  $\bar{\omega}_1$  and  $\bar{\omega}_2$ ,  $\varphi_1$  and  $\varphi_2$ , construct the elastic curve at critical rpm, as well as at  $\omega = 0$  and  $\omega = \infty$ . The system data listed above are tabulated below:

Quantity	$l_1$	$l_2$	$EJ$	$m_1$	$m_2$	$\tau$	$e_1$	$e_2$
Value	2	4	1	3	1	45°	2	4

The matrix of effect coefficients is

$$\begin{array}{|c|c|} \hline \delta_{11} & \delta_{12} \\ \hline \delta_{21} & \delta_{22} \\ \hline \end{array} = \begin{array}{|c|c|} \hline \frac{8}{3} & \frac{20}{3} \\ \hline \frac{20}{3} & \frac{64}{3} \\ \hline \end{array}$$

The equation of  $\Omega$ , the natural frequencies of the system, is

/19

$$\Omega^4 \cdot 3 \cdot 1 \left( \frac{8}{3} \cdot \frac{64}{3} - \frac{400}{9} \right) - \Omega^2 \left( 3 \cdot \frac{8}{3} + \frac{64}{3} \right) + 1 = 0$$

or

$$\Omega^4 - \frac{88}{112} \Omega^2 + \frac{3}{112} = 0,$$

from which

$$\Omega_1^2 = \frac{1}{28}; \quad \Omega_1 = 0.19$$

and

$$\Omega_2^2 = \frac{3}{4}; \quad \Omega_2 = 0.865.$$

When  $\omega \rightarrow 0$

$$\tan \varphi_1(0) = \frac{-\theta_1 n_{11} + \theta_2 n_{21}}{\theta_1 n_{11} + \theta_2 n_{21}}.$$

Dividing by  $\sin \tau = \cos \tau$  and by  $1/3$ , we find

$$\begin{aligned} \tan \varphi_1(0) &= \frac{-2 \cdot 3 \cdot 8 + 4 \cdot 1 \cdot 20}{2 \cdot 3 \cdot 8 + 4 \cdot 1 \cdot 20} = \frac{1}{4}; \\ \tan \varphi_2(0) &= \frac{-\theta_1 n_{12} + \theta_2 n_{22}}{\theta_1 n_{12} + \theta_2 n_{22}} = \frac{-2 \cdot 3 \cdot 20 + 4 \cdot 1 \cdot 64}{2 \cdot 3 \cdot 20 + 4 \cdot 1 \cdot 64} \approx 0.361; \\ \left( \frac{x_1}{x_2} \right)_{\omega \rightarrow 0} &= \frac{-\theta_1 n_{11} + \theta_2 n_{21}}{-\theta_1 n_{12} + \theta_2 n_{21}} = \frac{-2 \cdot 3 \cdot 8 + 4 \cdot 1 \cdot 20}{-2 \cdot 3 \cdot 20 + 4 \cdot 1 \cdot 64} \approx 0.235; \\ \left( \frac{y_1}{y_2} \right)_{\omega \rightarrow 0} &= \frac{\theta_1 n_{11} + \theta_2 n_{21}}{\theta_1 n_{12} + \theta_2 n_{22}} = \frac{48 + 80}{120 + 256} \approx 0.341. \end{aligned}$$

We now determine the angles of deflection of the shaft's sections at the first critical speed

$$\begin{aligned} \tan \varphi_{1cr} &= -\tan \tau \cdot \frac{e_1 (\bar{n}_{22} - 1) + e_2 \bar{n}_{21}}{e_1 (\bar{n}_{22} - 1) - e_2 \bar{n}_{21}} = \\ &= -1 \cdot \frac{2(0.762 - 1) + 4 \cdot 0.238}{2(0.762 - 1) - 4 \cdot 0.238} = \frac{1}{3}; \\ \bar{n}_{22} &= m_2 \theta_{22} \omega_{cr}^2 = 1 \cdot \frac{64}{3} \cdot \frac{1}{28} = 0.762; \\ \bar{n}_{21} &= m_2 \theta_{21} \omega_{cr}^2 = 1 \cdot \frac{20}{3} \cdot \frac{1}{28} \approx 0.238; \end{aligned}$$

$$\begin{aligned}\bar{n}_{11} &= m_1 \bar{e}_{11} \omega_{cr}^2 = 3 \cdot \frac{8}{3} \cdot \frac{1}{28} = 0.286; \\ \bar{n}_{12} &= m_1 \bar{e}_{12} \omega_{cr}^2 = 3 \cdot \frac{20}{3} \cdot \frac{1}{28} = 0.714; \\ \tan \varphi_{2cr} &= \tan \tau \frac{e_2 (\bar{n}_{11} - 1) + e_1 \bar{n}_{12}}{e_2 (\bar{n}_{11} - 1) - e_1 \bar{n}_{12}} = \\ &= \frac{4(0.286 - 1) + 2 \cdot 0.714}{4(0.286 - 1) - 2 \cdot 0.714} = \frac{1}{3}.\end{aligned}$$

From the fact that angles  $\varphi_1$  and  $\varphi_2$  are equal, we can conclude that the elastic curve of the shaft is planar

$$\begin{aligned}\left(\frac{y_1}{x_2}\right)_{cr} &= \frac{e_1 (\bar{n}_{22} - 1) - e_2 \bar{n}_{21}}{e_2 (\bar{n}_{11} - 1) - e_1 \bar{n}_{12}} = \frac{2(0.762 - 1) - 4 \cdot 0.238}{4(0.286 - 1) - 2 \cdot 0.714} = \frac{1}{3}; \\ \left(\frac{x_1}{x_2}\right)_{cr} &= -\frac{e_1 (\bar{n}_{22} - 1) + e_2 \bar{n}_{21}}{e_2 (\bar{n}_{11} - 1) + e_1 \bar{n}_{12}} = -\frac{2(0.762 - 1) + 4 \cdot 0.238}{4(0.286 - 1) + 2 \cdot 0.714} = \frac{1}{3}.\end{aligned}$$

We now find the projections of the shaft's deflections at  $\omega \rightarrow \infty$

$$\begin{aligned}y_{1\infty} &= \frac{-\vartheta_1 n_{11} n_{22} - \vartheta_2 n_{21} n_{22} + \vartheta_1 n_{12} n_{21} + \vartheta_2 n_{22} n_{21}}{n_{11} n_{22} - n_{12} n_{21}} = \\ &= -\vartheta_1 \frac{n_{11} n_{22} - n_{12} n_{21}}{n_{11} n_{22} - n_{12} n_{21}} = -\vartheta_1 = -e \cos \tau = -2 \frac{\sqrt{2}}{2} = -1.414; \\ x_{1\infty} &= \frac{\vartheta_1 n_{11} n_{22} - \vartheta_2 n_{22} n_{21} - \vartheta_1 n_{12} n_{21} + \vartheta_2 n_{22} n_{21}}{n_{11} n_{22} - n_{12} n_{21}} = \\ &= \vartheta_1 = e_1 \sin \tau = 1.414; \\ y_2 &= \frac{-\vartheta_1 n_{11} n_{12} - \vartheta_2 n_{11} n_{22} + \vartheta_1 n_{11} n_{12} + \vartheta_2 n_{12} n_{21}}{n_{11} n_{22} - n_{12} n_{21}} = -\vartheta_2 = \\ &= -e_2 \cos \tau = -2.828; \\ x_2 &= \frac{\vartheta_1 n_{11} n_{12} - \vartheta_2 n_{11} n_{22} - \vartheta_1 n_{11} n_{12} + \vartheta_2 n_{12} n_{21}}{n_{11} n_{22} - n_{12} n_{21}} = \\ &= -\vartheta_2 = -e_2 \sin \tau = -2.828.\end{aligned}$$

**Example 2** (see Fig. 5). Given an elastic weightless bar, carrying one eccentrically coupled point mass  $\underline{m}_1$  with eccentricity  $\underline{e}_1$  and one ideal disk with moment of inertia  $\theta_2$  and skewness angle  $\alpha$ , the angle between the direction of the eccentricity and the direction of skewness being  $2\alpha$ , find the critical speed and the coordinates of deflections for  $\omega_{cr}$ ,  $\omega = 0$  and  $\omega \rightarrow \infty$ .

Quantity	$l_1$	$l_2$	$EJ$	$m_1$	$\theta_2$	$2\tau$	$\alpha$	$e_1$
Value	2	4	1	2	3	90°	0.1	2

The matrix of effect coefficients is

/21

$$\begin{bmatrix} b_{11} & b_{12} \\ b_{21} & b_{22} \end{bmatrix} = \begin{bmatrix} 8/3 & 2 \\ 2 & 4 \end{bmatrix}$$

The equation for the frequency of direct synchronous precession is

$$-\Omega^4 \cdot 2 \cdot 3 \left( \frac{8}{3} \cdot 4 - 4 \right) - \Omega^2 \left( 2 \cdot \frac{8}{3} - 3 \cdot 4 \right) + 1 = 0$$

or

$$\Omega^4 - \frac{1}{6} \Omega^2 - \frac{1}{40} = 0;$$

$$\Omega^2 = \frac{1}{12} \pm \sqrt{\frac{1}{144} + \frac{1}{40}} = \frac{1 \pm 2.145}{12}$$

$$\Omega = 0.512.$$

When  $\omega \rightarrow 0$

$$\tan \varphi_1(0) = -\tan \tau \frac{m_1 e b_{11} - \theta_2 \alpha b_{21}}{m_1 e b_{11} + \theta_2 \alpha b_{21}} =$$

$$= -\frac{2 \cdot 2 \cdot \frac{8}{3} - 3 \cdot 0.1 \cdot 2}{2 \cdot 2 \cdot \frac{8}{3} + 3 \cdot 0.1 \cdot 2} = -0.895;$$

$$\tan \varphi_3(0) = -\tan \tau \frac{e m_1 b_{13} - \theta_2 \alpha b_{23}}{e m_1 b_{13} + \theta_2 \alpha b_{23}} = -\frac{2 \cdot 2 \cdot \frac{20}{3} - 3 \cdot 0.1 \cdot 8}{2 \cdot 2 \cdot \frac{20}{3} + 3 \cdot 0.1 \cdot 8} = -0.835.$$

The angle of deflection of the elastic curve when the shaft rotates at critical rpm is

$$\tan \varphi_{cr} = \frac{-\theta_1(n_{22}-1) + \alpha_x n_{21}}{\theta_1(n_{22}-1) + \alpha_y n_{21}} = -\tan \tau \frac{e(n_{22}-1) - \alpha n_{21}}{e(n_{22}-1) + \alpha n_{21}} =$$

$$= -\frac{2(3.14-1) - 0.1 \cdot 1.57}{2(3.14-1) + 0.1 \cdot 1.57} = -0.93;$$

$$n_{22} = \theta_2 \Omega^2 b_{22} = 3 \cdot 0.262 \cdot 4 = 3.14;$$

$$n_{21} = \theta_2 \Omega^2 b_{21} = 3 \cdot 0.262 \cdot 2 = 1.57.$$

The tangent of the angle of displacement of the second angle is not calculated, since the equality of these angles was proven in the general case.

## THE OPTIMUM HYDRAULIC DAMPING MOUNT FOR A TURBINE ROTOR

Candidate of Technical Sciences K. A. Kryukov

Modern turbine engines used in transportation evolve toward higher rpm and greater rpm range, as well as lower weight. The weight reductions usually result in lower rigidity which in turn increases the number of natural vibration modes which must be considered in the design. All this results in the fact that, very frequently, the proper selection of compliances of the elements of the system does not completely shift the resonance rpm beyond the range of the operating speeds. Under these conditions, safe operation at critical or near-critical rpm, as well as transition through these operating modes, is possible only with use of special damping devices [1, 6]. One of the most effective means for reducing the deflections of turbomachine shafts operating at critical rpm is employment of hydraulic damping mounts [5, 7].

/22

Reference [5] deals with forced vibrations of a single-wheel rotor with a damper, when both the perturbing force and the damper are located in the same section. In this case the elastic curve of the shaft will lie in a single plane. In our case, the points of application of the perturbing force and of the frictional force are not the same and, consequently, the elastic curve of the shaft will be a spatial curve. If we neglect the deformation of the shaft in the direction of the frictional force, then, by increasing the damping resistance factor in the expression for the deflection of the shaft to infinity, it is possible to reduce this deflection to zero. On the other hand, if one takes into account the shaft's deflection in two mutually perpendicular directions, it follows from the equation of the shaft's deflection that the smallest deflection will occur at some optimum damping resistance factor, but that in all the other cases the amplitude of the shaft's deflection will be larger.

We shall derive and analyze the expressions for the critical shaft rpm by taking into account the deformation in the direction of the frictional force, the dynamic intensification factor, the deflection, the angles of displacement of the deflections relative to the perturbing force, the unbalance force, the stresses in the shaft, and other parameters. We shall also discuss the operation of a hydraulic damping mount and shall give alternate methods for selecting optimum parameters when the oil temperature increases. Finally, we shall examine the conditions under which deformation in the direction of the frictional force can be neglected.

The magnitude of the required damping resistance factor can be established from the tolerable deflection and stresses in the shaft and the magnitude of the unbalance force.

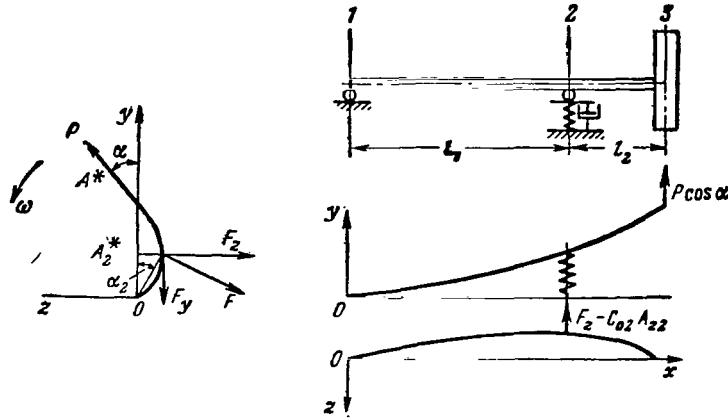


Figure 1. Computational Schematic.

considering steady-state motion. It is also assumed that at time  $t = 0$ , point 3 of the shaft is on  $Oy$ ; i.e., that  $A_z = 0$ .

We now determine the displacement of point 2 in the  $Oz$  direction. The equation of equilibrium for forces applied at point 2 requires that

$$F_z = (C_{02} + C_{22}) A_{z2}, \quad (1)$$

where  $C_{22} = \delta_{22}^{-1}$  is the transverse stiffness of the shaft at point 2.

It follows from Fig. 2 that

$$\delta_{22} = \overline{np} + (\overline{ok} - \overline{np}) \frac{l_2}{(l_1 + l_2)}, \quad (2)$$

where

$$\overline{ok} = \delta_1 Q_1 \text{ and } \overline{np} = \delta_2 Q_3. \quad (3)$$

Here,  $\delta_1$  and  $\delta_2$  are the displacements of points 1 and 3 of the shaft clamped at point 2, upon application of unit force at points 1 and 3, respectively.

Substituting Eq. (3) into Eq. (2) and making use of the fact that

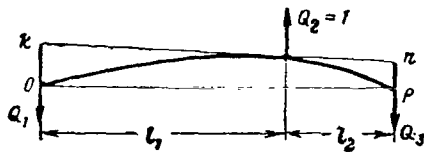
$$Q_1 = \frac{l_2}{l_1 + l_2} \text{ and } Q_3 = \frac{l_1}{l_1 + l_2},$$

we find

Figure 1 shows a cantilever system with one disk of mass  $m$ . The shaft is supported at point 2 by a hydraulic damping mount with a compliance of  $\delta_{02} = C_{02}^{-1}$ . The deflections at points 2 and 3 in the direction of axis  $Oy$  are denoted by  $A_2^*$  and  $A_2$ , respectively, while those in the  $Oz$  directions are denoted  $A_{z2}$  and  $A_z$ . We are

/23

/24



$$\delta_{22} = \frac{\bar{\delta}_1 l_2^2 + \delta_2 l_1^2}{(l_1 + l_2)^2} \quad (4)$$

/24

We now consider the case of viscous friction, when

$$F_y = \xi \omega A_{z2} \text{ and } F_z = \xi \omega A_{y2}^*, \quad (5)$$

Figure 2. Schematic for Determining the Compliance of the Shaft in the Qz direction.

where  $\omega$  is the angular velocity of the vector of perturbing force  $\underline{P}$  (which is identical to the angular velocity of the shaft provided that  $\underline{P}$  is produced by disk imbalance), and  $\xi$  is the viscous friction coefficient.

Substituting expressions (4) and (5) into Eq. (1), we find

$$\tan \alpha_2 = \frac{F_y}{F_z} = \frac{A_{z2}}{A_{y2}^*} = a_1 \bar{\delta} \omega, \quad (6)$$

where

$$\left. \begin{aligned} a_1 &= \frac{\xi \omega}{C_{02}}; \\ \bar{\delta} &= \frac{\delta_{22}}{\delta_{22} + \delta_{02}} = \frac{\delta'}{\delta}; \\ \delta' &= \bar{\delta}_1 \frac{l_2^2}{l_1^2} + \delta_2; \\ \delta &= \delta' + \left(1 + \frac{l_2}{l_1}\right)^2 \delta_{02}; \\ \bar{\omega} &= \frac{\omega}{\omega_1}; \quad \omega_1 = \frac{2}{\sqrt{m \delta}}. \end{aligned} \right\} \quad (7)$$

Here  $\underline{a}_1$  represents the ratio of the frictional force to the restoring force exerted by the mount at  $\omega = \omega_1$ ;  $\delta$  and  $\delta'$  are the compliances of the system at point 2, when supported by a compliant or a perfectly rigid mount, respectively, Eq. (14); and  $\omega_1$  is the natural frequency of the system at  $\xi = 0$ .

Using Eq. (7), we can write

/25

$$\bar{\delta} = \frac{1}{1 + (1 + \bar{l})^2 \bar{\delta}_{02}}, \quad (8)$$

where

$$\bar{\delta}_{02} = \frac{\delta_{02}}{\delta'}, \text{ and } \bar{l} = \frac{l_2}{l_1}$$

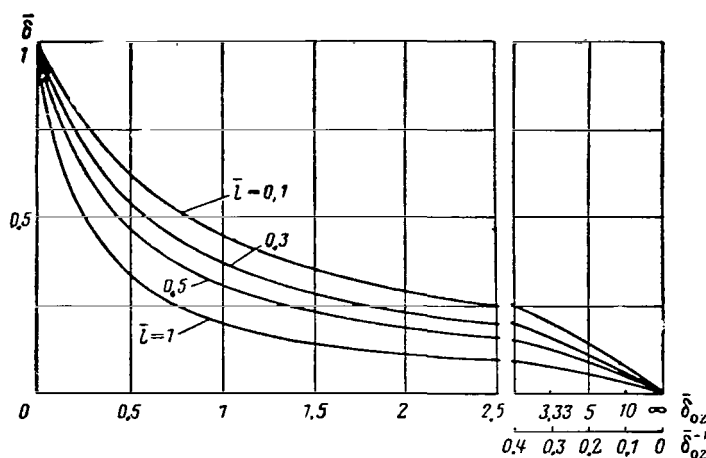


Figure 3. Parameter  $\bar{\delta}$  as Function of the Support Compliance and the Ratio  $\bar{l} = l_2/l_1$ .

Figure 3 shows curves of  $\bar{\delta} = \bar{\delta}(\bar{\delta}_{02})$  for different  $\bar{l}$ . It can be seen that  $\bar{\delta}$  varies from  $\bar{\delta} = 1$  at  $\bar{\delta}_{02} = 0$  to  $\bar{\delta} = 0$  at  $\bar{\delta}_{02} = \infty$ . For a shaft with constant cross section

$$\delta_1 = \frac{l_1^3}{3EJ}; \quad \delta_2 = \frac{l_2^3}{3EJ}; \quad \delta' = \frac{l_2(l_1 + l_2)}{3EJ};$$

$$\bar{\delta} = \frac{l_1^2 l_2^2}{l_1^2 l_2^2 + 3EJ(l_1 + l_2)\delta_{02}}.$$

As can be seen from this expression,  $\bar{\delta} = 0$  when  $l_1 = 0$  or  $l_2 = 0$ .

Examining Eq. (7) we find that the ratio of the natural frequencies with and without consideration of the mount compliance is

$$\bar{\omega}'_1 = \frac{\omega_1}{\omega'_1} = \sqrt{\bar{\delta}}, \quad (9)$$

where  $\omega'_1 = \frac{1}{\sqrt{m\delta'}}$  is the natural frequency of the system supported by a perfectly rigid mount.

The graph of function  $\bar{\omega}'$  is presented in Fig. 6 and holds for all values of  $\bar{\delta}_{02}$  and  $\bar{l}$  with the exception of the case when  $l_2 = 0$ . In that case, according to Eq. (7),  $\delta' = 0$  and

$$\omega_1 = \frac{1}{\sqrt{m\delta_{02}}}. \quad (10)$$

From Fig. 6 we note that a hydraulic mount sharply reduces the natural frequency of the system, particularly in the region of small  $\bar{\delta}$ .

Returning to Eq. (6) we note that ratio  $\underline{A}_{z2}/\underline{A}_2^*$  is proportional to quantities  $\xi$ ,  $\omega$  and  $\bar{\delta}$ . When the perturbing and frictional forces are applied at the same point ( $\underline{l}_2 = 0$ ,  $\bar{\delta} = 0$ ) there will be no deflection in the  $\underline{z}$  direction and the elastic curve of the shaft will lie in a single plane. In all the other cases ( $\bar{\delta} \neq 0$ ), the elastic curve will be a space curve.

Let us now determine the displacement  $\underline{A}^*$  of point 3 (see Fig. 1). The equation of force equilibrium in point 3 is

$$(C^* - m\omega^2) A^* = P \cos \alpha. \quad (11)$$

where  $\delta^* = C^*{}^{-1}$  is the compliance of the system at point 3, assuming existence of friction force  $\underline{F}_y$ .

When point 2 is deflected in the direction of the axis, there arise the restoring force  $\underline{C}_{02} \underline{A}_2^*$  and friction force  $\underline{F}_y$ , directed oppositely to displacement  $\underline{A}_2^*$ ; i.e.,

$$Q_2 = C_{02} A_2^* + F_y.$$

Using Eqs. (6) and (7) we write

$$Q_2 = C_{02} A_2^* (1 + a_1^2 \bar{\delta} \omega^2).$$

From this the compliance of the hydraulic damper system in the  $\underline{y}$  direction is

$$\bar{\delta}_{02}^* = \frac{A_2^*}{Q_2} = \frac{\bar{\delta}_{02}}{1 + a_1^2 \bar{\delta} \omega^2}. \quad (12)$$

Turning to the schematic shown in Fig. 4, we write

$$\bar{\delta}^* = \overline{Ob} + \overline{cd} + \overline{df} = \overline{Ob} + l_2 \tan \vartheta + \bar{\delta}_2.$$

Substituting in this expression the quantities

$$\begin{aligned} \tan \vartheta &= \frac{\overline{Oa} + \overline{Ob}}{l_1}; \\ \overline{Oa} &= \bar{\delta}_1 Q_1; \quad \overline{Ob} = \bar{\delta}_{02}^* Q_2; \\ Q_1 &= \frac{l_2}{l_1} \quad \text{and} \quad Q_2 = \frac{l_1 + l_2}{l_1} \end{aligned}$$



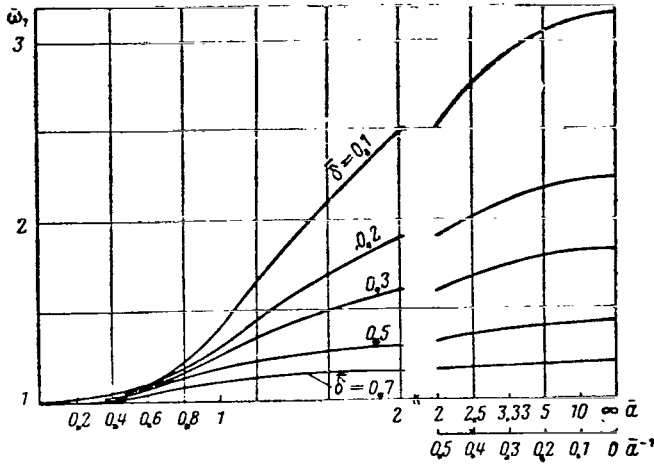


Figure 5. The Critical Speed as a Function of The Relative Damping Resistance Factor and of Parameter  $\delta$ .

We shall now clarify the effect of the damping resistance factor  $\bar{a}$  on  $\bar{\omega}_1$ . Figure 5 presents curves of  $\bar{\omega}_1 = \bar{\omega}_1(\bar{a})$  for some  $\delta$ . Values of  $\bar{\omega}_1$  vary from 1 when  $\bar{a} = 0$  ( $\xi = 0$ ), smoothly increasing with an increase in  $\bar{a}$  and asymptotically approaching the values

$$\bar{\omega}_1 = \bar{\omega}^{-1/2} (\omega_1^* = \omega_1') \text{ as } \bar{a} \rightarrow \infty.$$

The physical meaning of this is that when the damping resistance increases to infinity, the mount becomes immovable and the natural frequency of the system becomes equal to its natural frequency when placed on an uncompliant support. Note that  $\bar{\omega}_1$  increases with  $\bar{a}$  at a higher rate in the case of smaller  $\delta$ .

We now write an equation of moments about point  $O$  (see Fig. 1)

$$A_2^* F_z + A_{22} F_y = A_3 P \sin \alpha.$$

Using Eqs. (5) and (6), we write this as

$$\xi \omega \frac{A_2^{*2}}{A^2} (1 + a^2 \bar{\delta}^2 \omega^2) A^* = P \sin \alpha. \quad (20)$$

According to Fig. 4,

$$\frac{A_2^*}{A} = \frac{\bar{O}b}{\delta^*} = \frac{\bar{\omega}_{02}(1 + \bar{l})}{\delta^*}.$$

optimum value [as given Eqs. (36) and (38)].

Restricting ourselves to two terms of the binomial expansion of the radicand, we get an approximate expression for  $\bar{\omega}_1$ :

$$\omega_1 \approx 1 + 0.5 a_1^2 \bar{\delta}. \quad (19)$$

This yields values of  $\bar{\omega}_1$  which are somewhat high, but it is sufficiently accurate for determining these values at small  $\bar{a}_1$  and  $\delta$ .

Using Eqs. (12) and (14a), we write

/29

$$\frac{A_2^*}{A} = \frac{\delta_{02}(1+\bar{l})}{\delta(1+a_1^2\bar{\delta}^2\bar{\omega}^2)}. \quad (21)$$

Substituting the above into Eq. (20) and taking note of Eq. (7), we write

$$\frac{a_1(1-\bar{\delta})\bar{\omega}A^*}{\delta(1+a_1^2\bar{\delta}^2\bar{\omega}^2)^2} = P \sin \alpha. \quad (22)$$

Squaring Eqs. (22) and (11) and then adding them, we find

$$\left[ (C^* - m\omega^2)^2 + \frac{a_1^2(1-\bar{\delta})^2\bar{\omega}^2}{\delta^2(1+a_1^2\bar{\delta}^2\bar{\omega}^2)^2} \right] A^2 = P^2,$$

from which, using Eq. (14) and assuming that  $\underline{P} = \underline{m}\underline{e}\omega^2$ , we find

$$A^* = e\lambda^*, \quad (23)$$

where  $\underline{e}$  is the eccentricity or displacements of the center of mass of the disk relative to the centers of the bearings at  $\omega = 0$ , and

$$\lambda^* = \frac{(1+a_1^2\bar{\delta}^2\bar{\omega}^2)\bar{\omega}^2}{\sqrt{[1-\bar{\omega}^2+a_1^2\bar{\delta}\bar{\omega}^2(1-\bar{\delta}\bar{\omega}^2)]^2+a_1^2(1-\bar{\delta})^2\bar{\omega}^2}} \quad (24)$$

or

$$\lambda^* = \frac{(1+\bar{a}_0^2\bar{\delta}^2\bar{\omega}^2)\bar{\omega}^2}{\sqrt{[1-\bar{\omega}^2+\bar{a}_0^2\bar{\delta}\bar{\omega}^2(1-\bar{\delta}\bar{\omega}^2)]^2+\bar{a}_0^2(1-\bar{\delta})^2\bar{\omega}^2}}. \quad (24a)$$

For convenience in subsequent analysis, we now present the two above expressions as

$$\lambda^* = \frac{\frac{1}{\bar{\omega}^2} + \bar{a}_1^2\bar{\delta}^2}{\sqrt{\left[\frac{1}{\bar{\omega}^4} - \frac{1}{\bar{\omega}^2} + \bar{a}_1^2\bar{\delta}\left(\frac{1}{\bar{\omega}^2} - \bar{\delta}\right)\right]^2 + \frac{\bar{a}_1^2(1-\bar{\delta})^2}{\bar{\omega}^6}}}; \quad (25)$$

/30

$$\lambda^* = \frac{\left(\frac{1}{\bar{a}_1^2} + \bar{\delta}^2\bar{\omega}^2\right)\bar{\omega}^2}{\sqrt{\left[\frac{1-\bar{\omega}^2}{\bar{a}_1^2} + \bar{\delta}\bar{\omega}^2(1-\bar{\delta}\bar{\omega}^2)\right]^2 + \frac{(1-\bar{\delta})^2\bar{\omega}^2}{\bar{a}_1^2}}}. \quad (26)$$

When  $\omega = \omega_1^*$ , the expression in square brackets in the denominator of

Eq. (24) becomes zero according to Eq. (16), and then  $\lambda^*$  is

/30

$$\lambda_k^* = \frac{(1 - a_1^2 \bar{\delta}^2 \bar{\omega}_1^2) \bar{\omega}_1}{a_1(1 - \bar{\delta})} \quad (27)$$

or, according to Eq. (15)

$$\lambda_k^* = \frac{1 + a_1^2 \bar{\delta} \bar{\omega}_1^2}{(1 - \bar{\delta}) a_1 \bar{\omega}_1}. \quad (28)$$

It is more convenient to write the last expression as

$$\lambda_k^* = \frac{1 + \bar{a}^2 a_0^2 \bar{\delta} \bar{\omega}_1^2}{(1 - \bar{\delta}) \bar{a} a_0 \bar{\omega}_1}. \quad (29)$$

The quantity  $\lambda^*$  is the dynamic intensification factor, showing the number of times by which the shaft deflection at the point of disk location exceeds the eccentricity. As follows from Eqs. (24) and (25),  $\lambda^*$  varies from 0 at  $\bar{\omega} = 0$  to 1 at  $\bar{\omega} = \infty$ ; when  $\omega = \omega_1^*$ ,  $\lambda^*$  takes on the value  $\lambda_k^*$ .

Figure 8 shows graphs of  $\lambda^* = \lambda^*(\bar{\omega})$  for several values of  $\bar{a}$  at  $\delta = 0.23$  (see the example below). Turning to curves of Figs. 5 and 8, we note that the magnitudes of  $\lambda_k^*$  at small  $\bar{a}$  are virtually identical with the maximum dynamic load factor  $\lambda_m^*$ , while  $\omega_k \approx \omega_m \approx 1$  (see Fig. 5). For large  $\bar{a}$  the divergence between  $\lambda_k^*$  and  $\lambda_m^*$  (as well as between the  $\bar{\omega}_k$  and  $\bar{\omega}_m$  corresponding to them) becomes appreciable. For example, at  $\bar{a} = 1$  (Fig. 8)  $\lambda_m^* = 1.67$  for  $\bar{\omega}_m = 1.9$  and  $\lambda_k^* = 1.245$  when  $\bar{\omega}_k = 1.273$ .

When  $\bar{a} = 0$  ( $\xi = 0$ ), we get instead of Eq. (24)

/31

$$\left. \begin{aligned} \lambda_{\xi=0}^* &= \frac{\bar{\omega}^2}{1 - \bar{\omega}^2} & \text{for } \bar{\omega} < 1; \\ \lambda_{\xi=0}^* &= \frac{\bar{\omega}^2}{\bar{\omega}^2 - 1} & \text{for } \bar{\omega} > 1. \end{aligned} \right\} \quad (30)$$

When  $\bar{a} = \infty$  ( $\xi = \infty$ ), we find from Eq. (26)

$$\left. \begin{aligned} \lambda_{\xi=\infty} &= \frac{\bar{\delta} \bar{\omega}^2}{1 - \bar{\delta} \bar{\omega}^2} & \text{for } \bar{\omega} < \bar{\delta}^{-0.5}; \\ \lambda_{\xi=\infty} &= \frac{\bar{\delta} \bar{\omega}^2}{\bar{\delta} \bar{\omega}^2 - 1} & \text{for } \bar{\omega} > \bar{\delta}^{-0.5}. \end{aligned} \right\} \quad (31)$$

When  $l_2 = 0$ ,  $\delta = 0$  according to Eq. (7), and

$$\lambda_{i_2=0}^* = \sqrt{1 - \frac{\bar{\omega}^2}{(1 - \bar{\omega}^2)^2 + a_1^2 \bar{\omega}^2}},$$

while when  $\omega = \omega_1$  ( $\bar{\omega} = 1$ )

$$\lambda_k^* = a_1^{-1} = \frac{\xi_c}{2\xi},$$

where  $\xi_c = 2\sqrt{C_{02}m}$  — is the critical damping factor. When  $\xi > \xi_c$  the free vibrations become an aperiodic limiting motion [3].

Note that irrespective of the magnitude of the relative damping resistance  $\underline{a}$ , the curves of  $\lambda^*$  (Fig. 8) pass through a point with coordinates  $\bar{\omega}_{11}$  and  $\lambda_{11}^*$ . Equating Eqs. (30) and (31) and making use of the fact that  $1 < \bar{\omega}_{11} < \bar{\delta}^{-0.5}$ , we find

$$\bar{\omega}_{11} = \sqrt{\frac{1 - \bar{\delta}}{2\bar{\delta}}}. \quad (32)$$

Substituting this value into Eqs. (30) and (31), we get

$$\lambda_{11}^* = \frac{1 + \bar{\delta}}{1 - \bar{\delta}}. \quad (33)$$

It follows from curves of Eqs. (32) and (33) (Fig. 6) that, as  $\bar{\delta}$  is made smaller,  $\bar{\omega}_{11}$  increases infinitely while  $\lambda_{11}^*$  tends to unity.

It is easy to see from Eqs. (30) and (31) that  $\lambda^*$  goes to infinity when  $\bar{\omega} = 1$  and  $\bar{\omega} = \bar{\delta}^{-0.5}$ , respectively. Consequently, when  $\xi = 0$  and  $\xi = \infty$ , the damper in the mount does not operate. Indeed, the natural damping, which we have not taken into account, and which always exists in the engine system, causes large, although finite, shaft deflections. For example, rotors supported on rolling-contact bearings exhibit load factors on resonance which may range from 30 to 100 [6]. Operation at resonance rpm can, at worst, result in destruction of the rotor or the bearings, and in complete failure of the engine.

We shall now determine the value of parameter  $\underline{a}_1 = \underline{a}_0$ , for which  $\lambda_k^*$  will be at minimum. Taking the derivative in Eq. (28) with respect to  $\underline{a}$  and equating the expression thus obtained to zero, we get

$$\left( a_1 \frac{d\bar{\omega}_1}{d\bar{a}_1} - \bar{\omega}_1 \right) \frac{(a_1^2 \bar{\omega}_1^2 \bar{\delta} - 1)}{(1 - \bar{\delta}) a_1^2 \bar{\omega}_1^2} = 0. \quad (34)$$

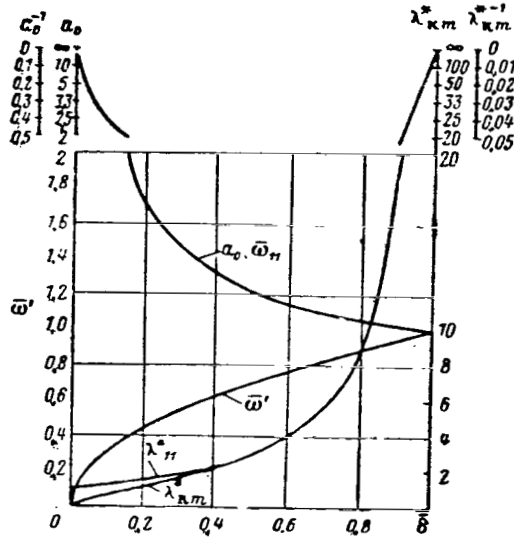


Figure 6. Quantities  $\underline{a}$ ,  $\bar{\omega}_1$ ,  $\bar{\omega}_{11}$ ,  $\lambda_{11}^*$  and  $\lambda_{k0}^*$  As a Function of  $\bar{\delta}$ .

which quantity will, by means of Eq. (17), be written as

$$a_0 = \sqrt{\frac{1 + \bar{\delta}}{2\bar{\delta}}} \quad (36)$$

or, using Eqs. (7) and (8), as

$$a_0 = \sqrt{1 + 0.5 \left(1 + \frac{l_2}{l_1}\right) \frac{\bar{\delta} \omega_2}{\bar{\delta}'}} \quad (37)$$

The optimum damper resistance, according to Eq. (7), is

$$\xi_0 = \frac{a_0}{\bar{\delta} \omega_1} \quad (38)$$

Substituting Eq. (36) into Eq. (28), we get

$$\lambda_{k0}^* = \frac{2\sqrt{\bar{\delta}}}{1 - \bar{\delta}} = \frac{2\sqrt{1 + (1 + l)^2 \bar{\delta} \omega_2}}{(1 + l) \bar{\delta} \omega_2} \quad (39)$$

Figure 6 shows graphs of  $\underline{a}_0$  and  $\lambda_{k0}^*$  as a function of  $\bar{\delta}$ . It follows from these graphs that at small  $\bar{\delta}$ ,  $\lambda_{k0}^*$  and  $\lambda_{11}^*$  are small. When  $\bar{\delta}$  increases ( $\bar{\delta} > 0.7$ ), the values of  $\lambda_{k0}^*$  and  $\lambda_{11}^*$  increase sharply; i.e., the

Differentiating Eq. (16) and performing the necessary transformations, we get

$$\frac{d\bar{\omega}_1}{da_1} = \frac{\bar{\delta} a_1 \bar{\omega}_1 (1 - \bar{\delta} \bar{\omega}_1^2)}{1 - \bar{\delta} a_1^2 (2\bar{\omega}_1^2 - 1)}$$

After substituting this expression into Eq. (34), we obtain

$$\frac{(1 + a_1^2 \bar{\delta}^2 \bar{\omega}_1^2)(a_1^2 \bar{\delta} \bar{\omega}_1^2 - 1)}{(1 - \bar{\delta}) a_1^2 \bar{\omega}_1^2 [1 + \bar{\delta} a_1^2 (2\bar{\omega}_1^2 - 1)]} = 0.$$

The real root of this equation is

$$a_1 = a_0 = \bar{\omega}_0^{-1} \bar{\delta}^{-0.5} \quad (35)$$

damper's operation becomes ineffective. The values of  $\lambda_{11}^*$  differ from those of  $\lambda_{k0}^*$  only at small  $\bar{\delta}$ ; for  $\bar{\delta} > 0.4$ , the values of  $\lambda_{11}^*$  and  $\lambda_{k0}^*$  virtually coincide.

/33

The deflection at the point where the disk is located corresponding to that given by Eq. (39) is, according to expression (23),

$$A_{k0}^* = e\lambda_{k0}^* = \frac{2e\sqrt{\bar{\delta}}}{1-\bar{\delta}}. \quad (40)$$

Upon dividing Eq. (29) by Eq. (39) and using Eq. (35), we find that

$$\Lambda = \frac{\lambda_k^*}{\lambda_{k0}^*} = \frac{1 + \bar{a}^2 \bar{\omega}_1^2}{2\bar{a} \bar{\omega}_1}, \quad (41)$$

where

$$\bar{a} = \frac{a_1}{a_0} = \frac{\xi}{\xi_0} \quad \text{and} \quad \bar{\omega}_1 = \frac{\omega_1}{\omega_0} = \frac{\omega_1^*}{\omega_1}.$$

There,  $\Lambda$  shows by how many times the shaft deflection  $A_k^*$  at the point of disk location is larger than  $A_{k0}^*$  when  $\bar{a} \neq 1$ . Equation (41) is plotted in Fig. 7 for some values of  $\bar{\delta}$ . Note that for small  $\bar{\delta}$ ,  $\Lambda$  is more sensitive to changes in the relative damping resistance factor  $\bar{a}$ . When  $\bar{a}$  deviates from unity,  $\Lambda$  increases (more so at small  $\bar{a}$ ).

/34

Above, we have derived expressions for the deflections at points 2 and 3, taking into account the deformation in the  $z$  direction. If this deformation is neglected, Eqs. (23) and (24) simplify to

$$A_3 = e\lambda, \quad (42)$$

where

$$\lambda = \frac{\bar{\omega}^2}{\sqrt{(1 - \bar{\omega}^2)^2 + a_1^2(1 - \bar{\delta})^2 \bar{\omega}^2}}.$$

If

$$\omega = \omega_1 \quad (43)$$

$$\lambda_k = \frac{1}{a_1(1 - \bar{\delta})} = \frac{C_{02}}{\xi \omega_1(1 - \bar{\delta})}.$$

The quantity

$$\bar{A} = \frac{A_k^*}{A_k} = \frac{\lambda_k^*}{\lambda_k} = \frac{1 + \bar{a}^2 \bar{\omega}_1^2}{\bar{\omega}_1}, \quad (44)$$

shows how many times  $\frac{A_k^*}{A_k}$  of Eq. (28) (where deflection in the  $z$  direction was taken into account) is greater than  $\frac{A_k}{A_k}$  (deflection neglected). It allows us to estimate the error which is introduced by neglecting this deflection. As follows from Eq. (44) and curves of Fig. 7, at small values of  $\underline{a}$  this error is not appreciable and, conversely, when  $\underline{a}$  is large ( $\underline{a} > 1$ ), the error is very large, particularly at small  $\delta$ .

/34

The deformation of the hydraulic damping mount (point 2 of Fig. 1) in the  $y$  direction is found from Eqs. (7) and (21)

$$A_2^* = \frac{(1+i)\delta_0 A^*}{i(1+a_1^2 \bar{\omega}^2)} = \frac{(1-\bar{\delta})e\lambda^*}{(1+i)(1+a_1^2 \bar{\omega}^2)}.$$

With reference to Eqs. (24) and (25), we write

$$A_2^* = \frac{e(1-\bar{\delta})\bar{\omega}^2}{(1+i)\sqrt{[1-\bar{\omega}^2+a_1^2 \bar{\omega}^2(1-\bar{\delta}\bar{\omega}^2)]^2+a_1^2(1-\bar{\delta})^2\bar{\omega}^2}}$$

The total deformation at point 2, according to Eqs. (6) and (24), is

/36

$$r_2 = \sqrt{A_{21}^{*2} + A_{22}^{*2}} = A_2^* \sqrt{1 + a_1^2 \bar{\omega}^2} = e\lambda_2^*, \quad (45)$$

where

$$\begin{aligned} \lambda_2^* &= \frac{(1-\bar{\delta})\lambda^*}{(1+i)\sqrt{1+a_1^2 \bar{\omega}^2}} \\ &= \frac{(1-\bar{\delta})\bar{\omega}^2 \sqrt{1+a_1^2 \bar{\omega}^2}}{(1+i)\sqrt{[1-\bar{\omega}^2+a_1^2 \bar{\omega}^2(1-\bar{\delta}\bar{\omega}^2)]^2+a_1^2(1-\bar{\delta})^2\bar{\omega}^2}} \end{aligned} \quad (45a)$$

or

$$\lambda_2^* = \frac{(1-\bar{\delta})\bar{\omega}^2 \sqrt{1+a_0^2 \bar{\omega}^2}}{(1+i)\sqrt{[1-\bar{\omega}^2+a_0^2 \bar{\omega}^2(1-\bar{\delta}\bar{\omega}^2)]^2+a_0^2(1-\bar{\delta})^2\bar{\omega}^2}}. \quad (46)$$

Equation (45a) can also be written as

$$\lambda_2^* = \frac{(1-\bar{\delta})\sqrt{\frac{1}{a_1^4} + \frac{\bar{\delta}^2 \bar{\omega}^2}{a_1^2}}}{(1+i)\sqrt{\left[\frac{1+\bar{\omega}^2}{a_1^2} + \bar{\delta}\bar{\omega}^2(1-\bar{\delta}\bar{\omega}^2)\right]^2 + \frac{(1-\bar{\delta})^2 \bar{\omega}^2}{a_1^2}}}. \quad (47)$$

when

$$\omega = \omega_k^* (\bar{\omega} = \bar{\omega}_1) \quad (48) \quad /36$$

$$\lambda_{k2}^* = \frac{\bar{\omega}_1 \sqrt{1 + a_1^2 \bar{\delta}^2 \bar{\omega}^2}}{(1 + \bar{l}) a_1} = \frac{\bar{\omega}_1 \sqrt{\frac{1}{a_1^2} + \bar{\delta}^2 \bar{\omega}^2}}{1 + \bar{l}}$$

If  $\xi \rightarrow \infty$  ( $\underline{a}_1 \rightarrow \infty$ ), then, according to Eq. (47)  $\lambda_k^* \rightarrow 0$  for all  $\bar{\omega}$ , except for  $\bar{\omega} = \bar{\omega}_1 = \bar{\delta} - 0.5$ . In this last case, according to Eq. (48), we have

$$\lambda_{k2}^* = \frac{1}{1 + \bar{l}}. \quad (49)$$

This value applies to all curves  $\lambda_2^* = \lambda_2^* (\bar{\omega})$  irrespective of the value of parameter  $\bar{a}$ ; this is easy to see by substituting  $\bar{\omega} = \bar{\delta} - 0.5$  into Eq. (46).

Graphs of Eq. (46) are presented in Fig. 9 for some values of  $\bar{a}$  for  $\bar{\delta} = 0.23$ . It can be seen that deflection of the elastic damper support (Fig. 9) are appreciably smaller than deflections at the point of the disk location (Fig. 8). When  $\bar{a} > 1$ ,  $\lambda_2^*$  increases, going to infinity as  $\bar{a} \rightarrow \infty$ . This does not happen to  $\lambda_2^*$ . When  $\bar{a}$  increases ( $\bar{a} > 1$ ), the value of  $\lambda_2^*$  decreases further. At  $\bar{a} = 0$ , the values of  $\lambda_2^*$  do not exceed the limits of the curve of Eq. (46); in this case, this equation becomes

$$\lambda_k^* = \frac{(1 - \bar{\delta}) \bar{\omega}^2}{(1 + \bar{l}) |1 - \bar{\omega}^2|}. \quad /38$$

The total frictional force, according to Eqs. (5), (44) and (46), is

$$F = \xi \omega r_2 = e \bar{a} a_0 C_{O_2} \bar{\omega} \lambda_2^* = \quad (50)$$

$$= \frac{e \bar{a} a_0 C_{O_2} (1 - \bar{\delta}) \bar{\omega}^3 \sqrt{1 + \bar{a}^2 a_0^2 \bar{\delta}^2 \bar{\omega}^2}}{(1 + \bar{l}) \sqrt{[1 - \bar{\omega}^2 + \bar{a}^2 a_0^2 \bar{\delta} \bar{\omega}^2 (1 - \bar{\delta} \bar{\omega}^2)]^2 + \bar{a}^2 a_0^2 (1 - \bar{\delta})^2 \bar{\omega}^2}}.$$

The unbalance force which is transmitted to the aircraft structure and which produces vibrations in the latter, can be expressed as

$$R = \sqrt{r_2^2 C_{O_2}^2 + F^2} = e C_{O_2} \lambda_2^* \sqrt{1 + \bar{a}^2 a_0^2 \bar{\omega}^2}. \quad (51)$$

or, using the dimensionless form of Eq. (45a)

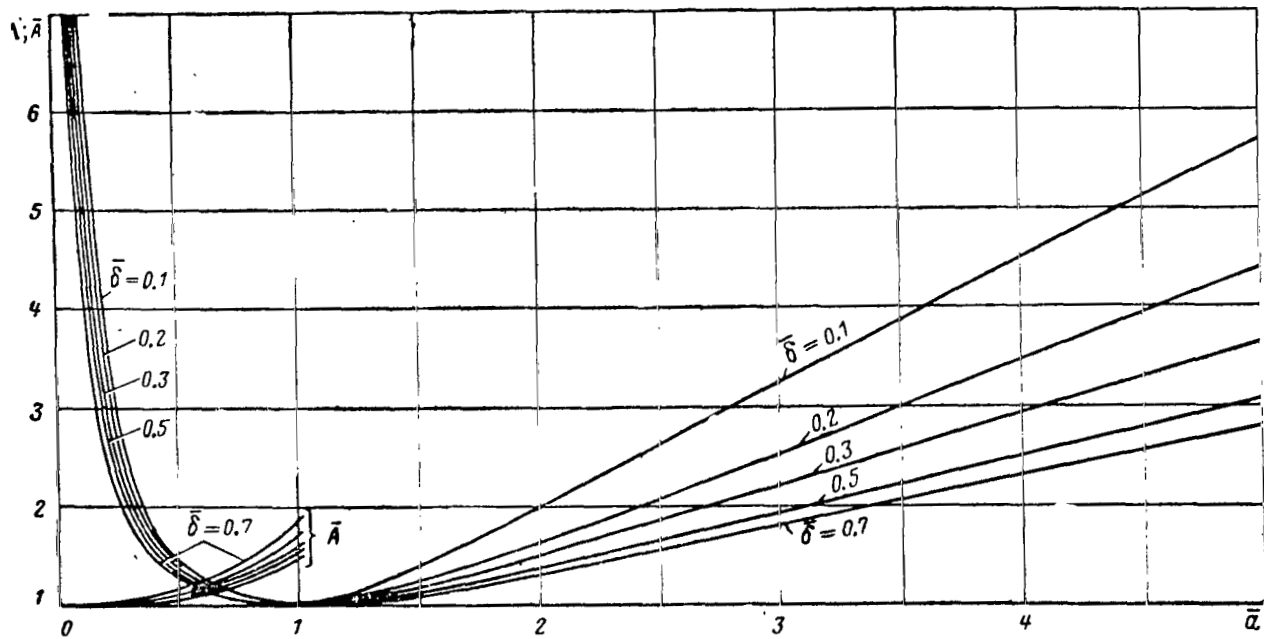


Figure 7. Curves of  $\Lambda$  and  $\bar{A}$  as Functions of the Damper Resistance and Parameter  $\bar{\delta}$ .

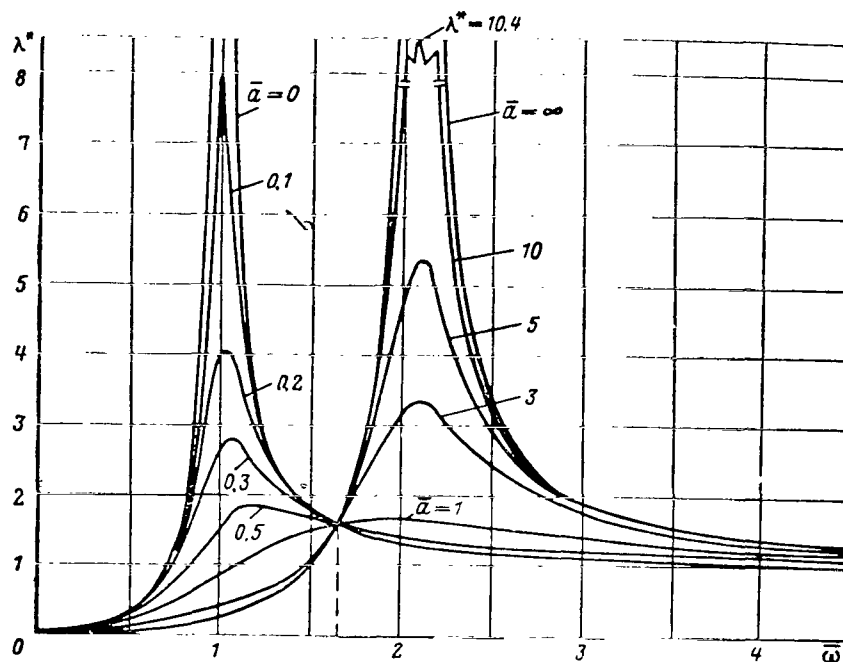


Figure 8. The Dynamic Intensification Factor of Shaft Deflection at the Point of Location of the Disk as a Function of the Frequency and Magnitude of the Damper Resistance.

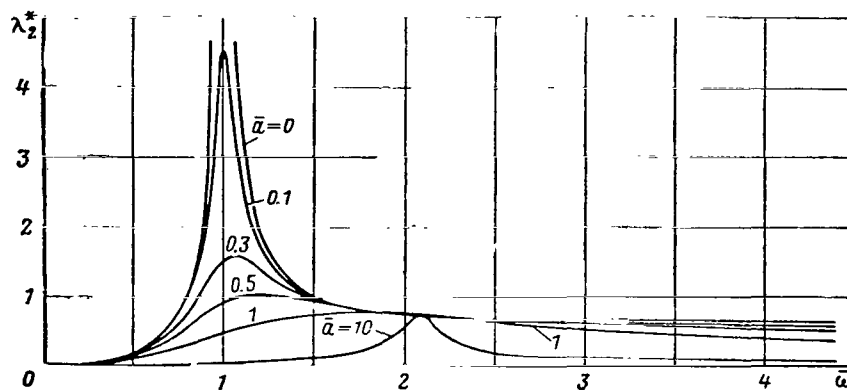


Figure 9. The Dynamic Intensification of the Support Deflection, as a Function of the Frequency and Magnitude of the Damper Resistance.

$$\begin{aligned} \bar{R} &= \frac{R(1+\bar{i})}{eC_{O2}(1-\bar{\delta})} = \\ &= \frac{\bar{\omega}^2 \sqrt{(1+\bar{a}^2 a_0^2 \bar{\delta}^2 \bar{\omega}^2)(1+\bar{a}^2 a_0^2 \bar{\omega}^2)}}{\sqrt{[1-\bar{\omega}^2 + \bar{a}^2 a_0^2 \bar{\delta} \bar{\omega}^2 (1-\bar{\delta} \bar{\omega}^2)]^2 + \bar{a}^2 a_0^2 (1-\bar{\delta})^2 \bar{\omega}^2}}. \end{aligned} \quad (52) \quad \underline{/38}$$

We write this expression as

$$\bar{R} = \frac{\bar{\omega}^2 \sqrt{\left(\frac{1}{\bar{a}^2} + a_0^2 \bar{\delta}^2 \bar{\omega}^2\right) \left(\frac{1}{\bar{a}^2} + a_0^2 \bar{\omega}^2\right)}}{\sqrt{\left[\frac{1-\bar{\omega}^2}{\bar{a}^2} + a_0^2 \bar{\delta} \bar{\omega}^2 (1-\bar{\delta} \bar{\omega}^2)\right]^2 + a_0^2 (1-\bar{\delta})^2 \bar{\omega}^2}}. \quad (53)$$

The flexural stress in the transverse section of the shaft above the elastic damping support is given by

$$\sigma = \frac{e\lambda^* l_2}{\bar{\delta}^* W}, \quad (54)$$

where

$$W = \frac{\pi D^3}{32} \left(1 - \frac{d^4}{D^4}\right), \text{ and}$$

$\underline{D}$  and  $\underline{d}$  are the outside and inside diameters of the shaft.

With reference to Eqs. (14a) and (24a), we write Eq. (54) in the following dimensionless form

$$\bar{\sigma} = \frac{\sigma \bar{\delta} W}{e l_2} = \frac{\bar{\omega}^2 (1 + \bar{a}^2 a_0^2 \bar{\delta} \bar{\omega}^2)}{\sqrt{[1 - \bar{\omega}^2 + \bar{a}^2 a_0^2 \bar{\delta} \bar{\omega}^2 (1 - \bar{\delta} \bar{\omega}^2)]^2 + \bar{a}^2 a_0^2 (1 - \bar{\delta})^2 \bar{\omega}^2}}. \quad (55)$$

or

$$\bar{\sigma} = \frac{\bar{\omega}^2 \left(\frac{1}{\bar{a}^2} + a_0^2 \bar{\delta} \bar{\omega}^2\right)}{\sqrt{\left[\frac{1-\bar{\omega}^2}{\bar{a}^2} + a_0^2 \bar{\delta} \bar{\omega}^2 (1-\bar{\delta} \bar{\omega}^2)\right]^2 + a_0^2 (1-\bar{\delta})^2 \bar{\omega}^2}}. \quad (56)$$

Setting  $\bar{a} = 0$  in Eqs. (53) and (55), and  $\bar{a} = \infty$  in Eqs. (53) and (56), and with reference to Eqs. (30) and (31), we can write

$$\left. \begin{aligned} \bar{R}_{\bar{\xi}=0} &= \bar{\sigma}_{\bar{\xi}=0} = \lambda_{\bar{\xi}=0}^*; \\ \bar{R}_{\bar{\xi}=\infty} &= \bar{\sigma}_{\bar{\xi}=\infty} = \frac{\lambda_{\bar{\xi}=\infty}^*}{\bar{\delta}}. \end{aligned} \right\} \quad (57)$$

Figures 10 and 11 are curves of  $\bar{R}$  and  $\bar{\sigma}$  as a function of  $\bar{\omega}$  for several values of  $\bar{a}$  at  $\bar{\delta} = 0.23$  (see example). All the curves of  $\bar{R} = \bar{R}(\bar{\omega})$ ,

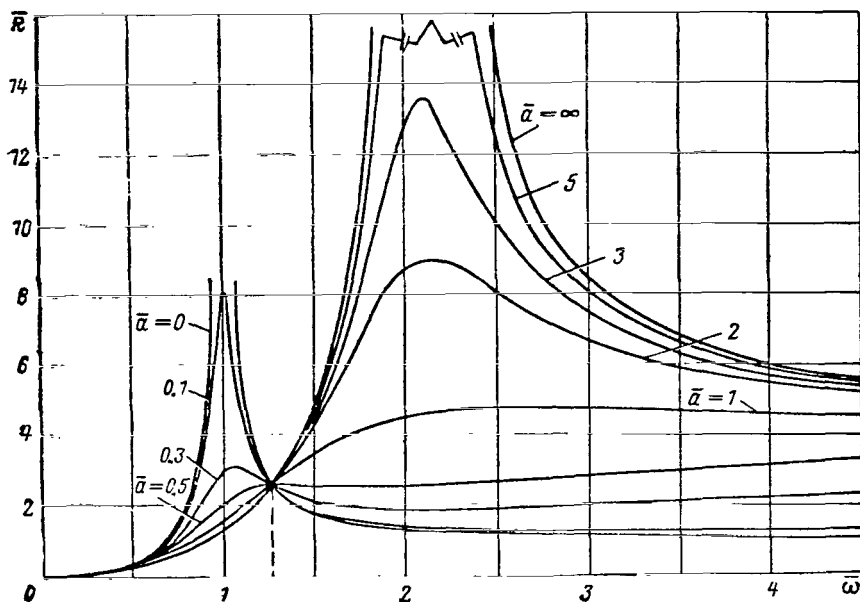


Figure 10. The Unbalance Force as a Function of the Frequency and Magnitude of the Damping Resistance.

irrespective of the value of  $\bar{\alpha}$ , intersect in one point, the coordinates of which are

/40

$$\left. \begin{aligned} \bar{\omega}_{12} &= \sqrt{\frac{2}{1+\bar{\delta}}} \\ \bar{R}_{12} &= \frac{2}{1-\bar{\delta}} \end{aligned} \right\} \quad (58)$$

It is not difficult to show that at  $\omega$  increasing infinitely,  $\bar{R}$  and  $\bar{\sigma}$  tend (irrespective of the value of  $\bar{\alpha}$ ) in the limit to

$$\bar{R}_{\bar{\alpha} \rightarrow 0} = \bar{\sigma}_{\bar{\alpha} \rightarrow 0} = \bar{\delta}^{-1},$$

with the exception of the case where  $\bar{\alpha} = 0$ . In this last case, when  $\bar{\omega} \rightarrow \infty$ , we will have

$$\bar{R}_{\bar{\alpha}=0} = \bar{\sigma}_{\bar{\alpha}=0} = 1.$$

Turning to curves of Fig. 11, it can be seen that in the region of  $\omega$  ranging from zero to  $\bar{\omega} = \bar{\omega}_{12}$ , the friction in the mount has a favorable effect on the magnitude of the unbalance force and of the stress in the shaft by appreciably reducing them. On the other hand, in the region of angular velocities larger than  $\bar{\omega}_{12}$ , the friction in the mount is an

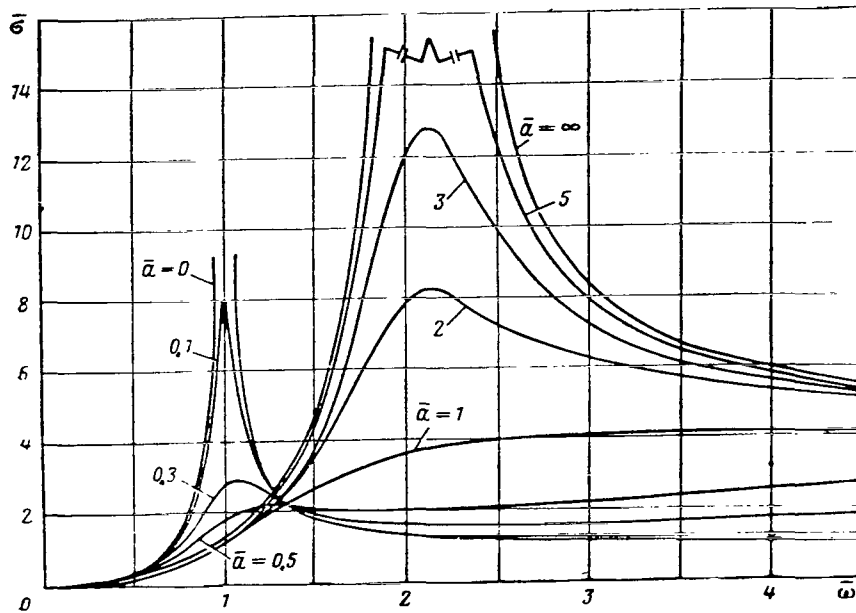


Figure 11. The Stress in the Shaft as a Function of the Frequency and the Magnitude of the Damping Resistance.

unfavorable factor, since it increases the unbalance force which is transmitted to the aircraft structure, as well as the stress in the shaft.

It follows from Eqs. (51) and (54), as well as from graphs of Figs. 10 and 11 that the use of a hydraulic damper reduces the unbalance force and stresses in the shaft, both because it increases the compliance  $\delta$ , and because it affords the possibility of shifting the critical speed past the limits of the operating rpm.

Dividing Eq. (22) by Eq. (11) and using Eq. (14a), we get an expression for angle  $\alpha$  (see Fig. 1)

$$\left. \begin{aligned} \tan \alpha &= \frac{a_1 (1 - \bar{\delta}) \bar{\omega}}{1 - \bar{\omega}^2 + a_1^2 \bar{\delta} \bar{\omega}^2 (1 - \bar{\delta} \bar{\omega})} \\ \tan \alpha &= \frac{\bar{a} a_0 (1 - \bar{\delta}) \bar{\omega}}{1 - \bar{\omega}^2 + \bar{a}^2 a_0^2 \bar{\delta} \bar{\omega}^2 (1 - \bar{\delta} \bar{\omega})} \end{aligned} \right\} \quad (59)$$

or

Equation (59) can also be written as

$$\tan \alpha = \frac{a_1 (1 - \bar{\delta})}{\frac{1}{\bar{\omega}} - \bar{\omega} + a_1^2 \bar{\delta} \bar{\omega}^2 (1 - \bar{\delta} \bar{\omega}^2)}.$$

It follows that angle  $\alpha$  varies from 0 to  $\pi$  when  $\omega$  goes from 0 to  $\infty$ . At the critical angular speed ( $\omega = \omega^*$ ),  $\alpha = \pi/2$ . For a system without

damping ( $\bar{a} = 0$ )  $\alpha = 0$ ; the vector of the perturbing force has the same direction as the displacement (see Fig. 1). Figure 12 presents graphs of  $\alpha = \alpha(\omega)$  for different values of  $\bar{a}$  at  $\delta = 0.23$ .

The following are the decisive factors which need to be considered in estimating the danger to a turbine operating at or near critical rpm: shaft deflection, stresses in the shaft, and the magnitude of the unbalance force. In each specific case, one or another of these factors can dominate. Let us consider them in detail.

The maximum permissible shaft deflection should be less than the operating clearance between the rotor and the housing (in order to eliminate the possibility of bumping and breaking of blades, labyrinth seals, etc). The possibility of failure in this case can be eliminated by increasing the radial clearance. However, this step, as is well known, would reduce the turbine efficiency. The tolerable increase in the shaft deflection available in this case is limited by the strength of the shaft, and is governed by the flexural stress produced when operating at critical rpm. This stress, combined with other stresses in the shaft, can exceed the yield strength and even the ultimate strength of the material, which would result in a residual strain of the shaft and to failure of the entire structure.

Great difficulties in aircraft and automotive gas turbine power plants are frequently brought about by excessive vibrations of the structural elements of these vehicles, which are due to unbalance forces or moments in the engine. Excessive vibrations can result in fatigue failure of aircraft parts, as well as cause premature tiredness of the crew and disturb the operation of aircraft instruments.

The reliability of aircraft and automotive gas turbine power plants is frequently rated in terms of the so-called vibration overload factor, which is the ratio of the maximum acceleration of a specific point of the engine housing (in case of vibrations) to the acceleration of gravity. Some values of the permissible vibration overload for various gas turbine engines are presented in [2].

The vibration overload factor, as well as the load on the bearings increases with the unbalance force. The vibration overload of an operating engine is determined by means of special instruments [1].

As follows from Eqs. (24), (51) and (54), all the factors which determine the reliability of a turbomachine are proportional to the eccentricity of the wheel. In a broader sense of the word, the term eccentricity should be understood to denote not only a displacement of the center of mass of the wheel to correspond with the imbalance not eliminated by dynamic balancing of the rotor, but also the increase in eccentricity brought about by design and production factors.

Depending on the precision with which the wheel, the shaft, the bearings, the housing, etc., have been manufactured and installed, as

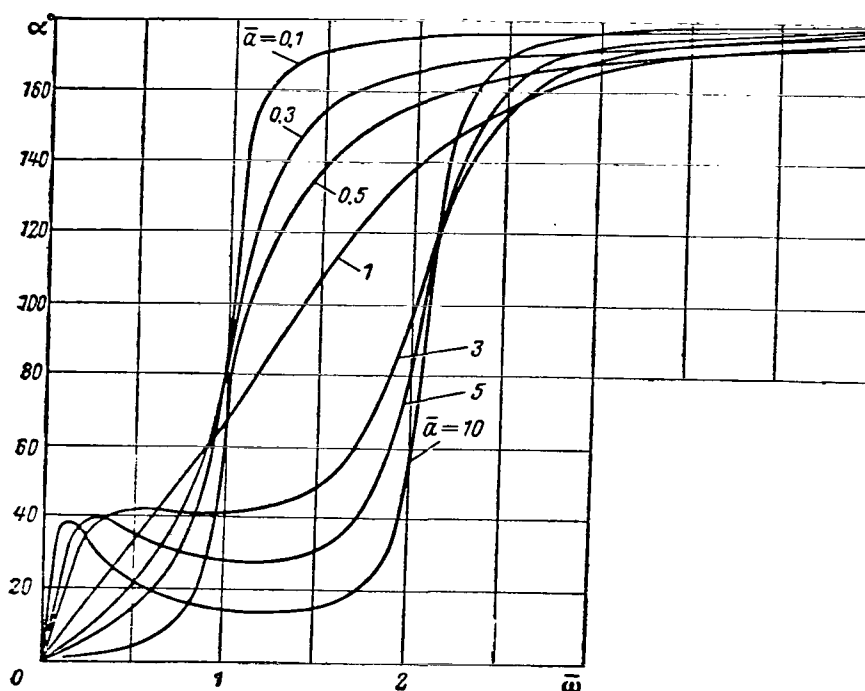


Figure 12. Phase Shift between the Force and Displacement as a Factor of the Frequency and of the Magnitude of Damping Resistance.

as well as depending on the size of clearances in the bearings, the eccentricity may vary over a wide range; i.e., from several thousandths to tenths of a millimeter and even to 1 millimeter (as, for example, in units for tensile testing of disks [6]). The eccentricity in some cases can also increase appreciably with time during operation due to, for example, nonuniform creep of gas turbine wheels and blades and, in particular, on partial or complete rupture of blades. It follows from the above that the eccentricity can be estimated only approximately.

It also follows from the above that the vibrational stability of turbomachines depends to a large extent on the quality of manufacture and that in some, but by far not all, cases tightening the production specifications and assembly precision can eliminate the above defects.

In those cases when the critical speed is in the range of operating rpm and when the system itself does not provide sufficient damping to eliminate dangerous deflections of the shaft, the vibration of the power plant and the possibility of engine failure, it must be equipped with a damper. As was shown by our analysis, the use of a hydraulic damper eliminates danger at critical rpm. This can be achieved by shifting the critical speed beyond the operating range, as well as by reducing the deflections, stresses, and the unbalance force to safe limits.

As was pointed out above, shifting the critical speed and reduction of the deflections depends to a great extent on parameter  $\bar{\delta}$  and the more so, the smaller the  $\bar{\delta}$  (see Fig. 6). In automotive and aircraft engines, however, if  $\bar{\delta}$  is small; i.e., the system has large compliance. There is the danger that the rotor will rub against the stator. This happens in aircraft engines at overloads which arise during acrobatics or on landing, and in automotive engines when riding on bumpy roads.

/43

The excessive deflections of hydraulic dampers of a shaft and bumping of the rotor against the housing, which are possible under those circumstances, can be eliminated by installing rigid supports which limit the rotor displacement. The presence of friction in this case will have a favorable effect, softening the bumping into the limiters and aiding in rapid damping of the free vibrations. In this case, the damping characteristic of the system will not be linear. At some deflections the elastic element of the damper will be compressed up to the stops. Then the stiffness of the system will increase and will be equal to the stiffness of a shaft supported by uncompliant supports; the natural frequency of the system increases, the resonance conditions change; the resonance deflection of the shaft will be smaller than in the case of a system with linear characteristic. A detailed study of the operation of nonlinear dampers is presented in [1].

/44

As follows from Eqs. (7) and (8) and from the graph of Fig. 3,  $\bar{\delta}$  depends on the geometric and damping properties of the system, which are governed by  $\underline{l}_1$ ,  $\underline{l}_2$ ,  $\delta'$  and  $\delta_{02}$ . The first three of these quantities are selected from strength and design considerations. For example, in gas turbine engines dimension  $\underline{l}_1$  is determined by the type and length of the combustion chamber and of the compressor, the location of supports, etc. Dimension  $\underline{l}_2$  is determined by the thickness of the wheel, the manner in which it is seated on the shaft, type of bearing, gas and oil lubricated seals, etc. From strength considerations it is desirable that dimension  $\underline{l}_2$  be as small as possible. Changing of shaft diameters and lengths involves quite complicated and expensive modifications, which may increase its weight. All this requires that one forego varying  $\underline{l}_1$ ,  $\underline{l}_2$  and  $\delta'$ , and obtain the required  $\bar{\delta}$  by providing the necessary mount compliance  $\delta_{02}$ . The latter quantity can be easily changed by introducing an elastic element into the mount, and can be accomplished without extensive redesigning.

It should be noted that for systems with many wheels, unlike the system with one degree of freedom which was considered here, the compliance of the hydraulic damping mount should be selected so that not only the first, but also the second, third, etc., critical speeds be sufficiently removed from the operating rpm range [8]. However, this cannot always be achieved. Then dangerous shaft deflections under critical speed conditions can be eliminated by appropriate selection of the damping resistance factor, the magnitude of which should be established

separately for each case.

In those cases when the critical speed is in the range of operating rpm and the predominant factor in safe operation of the given machine is minimum shaft deflection, it is necessary to select an optimum damping resistance factor ( $\xi = \xi_0$  and  $\bar{a} = 1$ ). However, these conditions frequently cannot be maintained since the viscosity of the oil drops sharply as the temperature increases [6].

The most suitable damping substances are silicone fluids, the viscosity of which varies little with temperature. However, these fluids are not too suitable as lubricants, which makes it necessary to maintain two separate systems, one for bearing lubrication and the other for supplying the damper. This complicates the design, so that usually one employs the simplest solution whereby damping is produced by the same oil as that used for bearing lubrication. In this case, however, the damping resistance factor can change appreciably due to change in viscosity as the oil heats up during operation. Turning to curves of Fig. 7, we note that this shortcoming can be appreciably alleviated by proper selection of  $\bar{a}$ , the relative damping factor.

In fact, if we select a value of  $\bar{a} = \bar{a}_2$  slightly larger than unity at conditions corresponding to the minimum oil temperature possible with a given machine, then on subsequent heating of the oil and reduction in the damping resistance; i.e., on moving to the left of the selected point  $\bar{a}$ , the dynamic intensification factor will change, first decreasing to  $\Lambda = 1$  at  $\bar{a} = 1$  and then increasing at  $\bar{a} < 1$ . By proper selection of  $\bar{a}_2$

$> 1$ , it is possible to obtain a situation whereby the change in the intensification factor, accompanying the heating of the oil will be minimum.

We shall clarify this by means of the following example. Examining the curve for  $\delta = 0.3$  (Fig. 7), we note that when, for example, the damping resistance factor is reduced by a factor of four as the oil heats up, one can use the following values of  $\bar{a}_2 \Lambda_2$  and obtain values of  $\bar{a}_1$  and  $\Lambda_1$  corresponding to them.

Parameters	Versions	
	1	2
$\bar{a}_2$	1	2
$\Lambda_2$	1	1.49
$\bar{a}_1$	0.25	0.5
$\Lambda_1$	2.65	1.38

It follows from this table that if one chooses  $\bar{a}_2 = 1$ , then, as the oil is heated up, the dynamic intensification factor increases by a factor of 2.65 (version 1) and, if, for example,  $\bar{a}_2 = 2$ , then the load factor

changes to a much lesser degree with changes in temperature (version 2). Obviously, the second version is more favorable from the point of view of minimizing deflection. However, this  $\bar{a}$  will not give the minimum unbalance force stresses in the shaft (see Figs. 10 and 11 at  $\bar{\omega} > \bar{\omega}_{12}$ ).

/45

In fact, from the point of view of obtaining minimum values of  $\underline{R}$  and  $\sigma$ , one should stop at  $\bar{a} < 1$ .

We have previously considered a case in which the critical speed is in the operating range. When, by proper selection of the mount compliance it is possible to shift the critical speed beyond operating range, so that  $\omega_{\min} > \bar{\omega}_{12}$  (see Figs. 10 and 11),  $\bar{a}$  should be smaller than 1 from the following considerations. As was pointed out above, the unbalance force of the engine is frequently a source of undesirable vibrations of the structural elements of the aircraft. In order to reduce this force, it is advantageous to use  $\bar{a}$  less than unity. Indeed, turning to the graphs of Fig. 10 it is easy to see that over wide range of frequencies (at  $\bar{\omega} > \bar{\omega}_{12}$ ) the unbalance force at  $\bar{a} = 0.1-0.3$  is approximately 2.5-3 times smaller than at  $\bar{a} = 1$ . Thus, selecting a value of  $\bar{a}$  ranging from 0.1 to 0.3, instead of  $\bar{a} = 1$ , one can appreciably reduce the aircraft vibrations.

/46

In this case above we have given approximate values of  $\bar{a}$ . Note that  $\bar{a}$  can be selected more rigorously when one knows the vibrational characteristics of the aircraft in which the engine or turbine is to be installed.

In choosing  $\bar{a} < 1$ , one must keep in mind that this will increase the deflection, the unbalance force, and the stresses at the critical rpm when  $\bar{\omega}$  is near unity (see Figs. 8, 10 and 11); however, in one case the critical rpm is below the lowest operating rpm. When the shaft speed increases and passes rapidly through the critical one ( $\bar{\omega} \neq \text{const}$ ) the deflection, the unbalance force and stresses in the shaft will be appreciably smaller than those obtained by us in considering steady-state operating conditions ( $\bar{\omega} = \text{const}$ ), [4]. For this reason, as well as due to the short time of passage through the critical speed, the slight increase in deflection, stresses, and unbalance force above those obtained at  $\bar{a} = 1$  will not harm the unit.

In order to illustrate the above, we now present a numerical example.

#### Example

1. Estimate the reliability, under vibrational conditions, of a gas turbine engine, the design of which is shown in Fig. 1, and which is described by the following data:

$$m = 30.6 \text{ kg}, \quad l_1 = 24.5 \text{ cm}, \quad l_2 = 9 \text{ cm}, \quad D = 5.5 \text{ cm}, \\ d = 2.5 \text{ cm}, \quad E = 2 \cdot 10^5 \text{ N} \cdot 10^6 / \text{m}^2; \quad J = 43 \text{ cm}^4;$$

$$W = 15.7 \text{ cm}^3, \quad \bar{v}_1 = 57.1 \cdot 10^{-9} \text{ m/n}; \quad \bar{v}_2 = 1.83 \cdot 10^{-9} \text{ m/n}.$$

The operating rpm range is  $\omega_{\min} = 1250 \text{ sec}^{-1}$  and  $\omega_{\max} = 2500 \text{ sec}^{-1}$ , and the eccentricity  $\underline{e} = 0.001 \text{ cm}$ .

2. Select the parameters of a hydraulic mount which would provide for safe and reliable operation of this system. /47

The compliance of the shaft on perfectly rigid supports is, from Eq. (7)

$$\delta' = 9.5 \cdot 10^{-9} \text{ m/n};$$

The critical speed on perfectly rigid supports is, from Eq. (9)

$$\omega_1' = 1852 \text{ sec}^{-1}.$$

We shall assume that in our case the rotor is mounted on rolling-contact bearings; then at  $\omega = \omega_1'$ , the dynamic intensification factor with the engine operating at the critical speed lies between 30 and 100 [6]. Then from Eqs. (23), (31), (52), (54) and (57) we find that

$$\begin{aligned} A^* &= 0.3 - 1.0 \text{ mm.} \\ R &= \frac{e C_{O2} (1 - \bar{\delta}) \lambda_{\xi=\infty}^*}{(1 + \bar{I}) \bar{\delta}} = 4340 - 14450 \text{ N;} \\ \sigma &= \frac{e l_2 \lambda_{\xi=\infty}^*}{\delta' W} = 181 - 603 \text{ N} \cdot 10^6 / \text{m}^2. \end{aligned} \quad \left. \vphantom{\begin{aligned} R \\ \sigma \end{aligned}} \right\} \quad (60)$$

The results show that the deflections of the shaft, the load on the bearing, the unbalance force and the stresses in the shaft at a critical speed lying in the operating range will be high. Operation of the engine under these conditions can produce dangerous vibrations in the turbine and in the aircraft, or bumping of the rotor against the housing, with subsequent failure of the power plant.

To reduce deflection, unbalance force and stress and to provide for safe and smooth power plant operation, it is necessary to provide the engine with a hydraulic damping mount.

We select the mount compliance at point 2

$$\delta_{O2} = 17 \cdot 10^{-9} \text{ m/n}.$$

According to Eq. (7), this value corresponds to

$$\delta = 41.33 \cdot 10^{-9} \text{ m/n}; \quad \bar{\delta} = 0.23 \text{ and } \omega_1 = 889 \text{ sec}^{-1}.$$

The optimum  $\underline{a}_1 = \underline{a}_0$  [Eq. (36)] and damping resistance factor [Eq. (38)]

are

$$a_0 = 1.63 \text{ and } \xi_0 = 1079 \text{ N/cm}^{-1} \text{ sec.}$$

/47

Figures 8 and 9 show values of  $\lambda^*$  and  $\lambda_2^*$  as functions of the relative angular velocity  $\bar{\omega}$ . Multiplying the ordinates of these curves by the eccentricity  $\underline{e} = 0.001 \text{ mm}$ , we determine the deflection of the shaft at points 2 and 3 (see Fig. 1).

Figures 10 and 11 show graphs of  $\bar{R}$  and  $\bar{\sigma}$  as functions of  $\bar{\omega}$ . The values of  $\bar{R}$  and  $\bar{\sigma}$  are then determined from

$$\left. \begin{aligned} R &= \frac{e C_{02} (1 - \bar{\delta}) \bar{R}}{1 + \bar{I}} = 332 \bar{R} \text{ N;} \\ \sigma &= \frac{e l_2 \bar{\sigma}}{\delta W} = 1.385 \bar{\sigma} \cdot 10^6 / \text{m}^2. \end{aligned} \right\} \quad (61)$$

The operating range of angular velocities lies between

/48

$$\bar{\omega}_{\min} = 1.4 \text{ and } \bar{\omega}_{\max} = 2.8. \quad (62)$$

It can be noted from Figs. 8, 10 and 11 that employment of hydraulic damping mount shifts the critical speed beyond the operating range. Passing the critical speed at  $\bar{\omega}$  close to unity is accompanied by increasing  $\underline{A}^*$ ,  $\bar{R}$  and  $\sigma$ . Selecting  $\bar{a} = 0.5$  from Figs. 8, 10 and 11, and using Eqs. (61) we find, at  $\bar{\omega} \approx 1.2$

$$\underline{A}^* = 0.0187 \text{ mm}; R = 830 \text{ N}; \sigma = 3 \cdot 10^6 / \text{m}^2. \quad (63)$$

These quantities are many times smaller than those given by Eq. (60) for a system without hydraulic damping.

If we assume that the viscosity drop accompanying the temperature rise produces a fivefold reduction in the damping resistance factor, then (at  $\bar{a} = 0.1$ ), the magnitudes of  $\underline{A}^*$ ,  $\bar{R}$  and  $\sigma$  for  $\bar{\omega} = 1$  will be

$$\underline{A}^* = 0.0795 \text{ mm}, R = 2680 \text{ N and } \sigma = 11.1 \cdot 10^6 / \text{m}^2 \quad (64)$$

These quantities are somewhat higher than those obtained from Eq. (63), but still appreciably lower than those given by Eq. (60). Here it should be remembered that in a system lacking a damper, the deflection, the unbalance force and the stress, may become quite high [Eq. (60)] in the operating rpm range on extended operation with relative angular speed  $\bar{\omega}_1' = 2.08$ , while the values of  $\underline{A}^*$ ,  $\bar{R}$  and  $\sigma$  at  $\bar{\omega} \approx 1$  will actually be appreciably lower than those calculated from Eq. (64) as a result of rapid passage through the critical rpm when picking up speed. It is not difficult to notice that, upon selecting an  $\bar{a} = 1$  it would have been possible to reduce to an even greater extent the level of  $\underline{A}^*$ ,  $\bar{R}$  and  $\sigma$  when passing through the critical speed. However, this is not necessary.

In addition, in examining the operation of the damping mount in the range of operating rpm [Eq. (62)], it is not difficult to notice (see Figs. 8, 10 and 11) that the values of  $\underline{A}^*$ ,  $\underline{R}$  and  $\sigma$  in this region at  $\underline{a} < 1$  are appreciably lower than at  $\underline{a} = 1$ . For example, if  $\bar{\omega} = 2.08$ , then for

$$\begin{aligned}\bar{a} = 0.1, \quad A^* &= 0.013 \text{ mm}, \quad R = 460 \text{ N and } \sigma = 1.8 \text{ N} \cdot 10^6 / \text{m}^2, \\ \bar{a} = 1.0, \quad A^* &= 0.0165 \text{ mm}, \quad R = 1530 \text{ N and } \sigma = 5.1 \text{ N} \cdot 10^6 / \text{m}^2.\end{aligned}$$

As these numbers show, the levels of  $\underline{A}^*$ ,  $\underline{R}$  and  $\sigma$  at  $\bar{a} = 0.1$  and at  $\bar{a} = 1$  are not too high compared with the values given by Eq. (60), and that the operation of the engine at these values of deflection, unbalance force and stress is safe. But in considering separately the effect of the unbalance force and remembering that it frequently causes dangerous vibrations, consideration should be given to a possible reduction in  $\bar{a}$  in order to reduce the vibration of the structural elements and to improve the vibrational damping of the engine. For example, if  $\bar{a} = 0.1$ , the unbalance force (and consequently also the vibration of the structural elements) will be approximately three times smaller than for  $\bar{a} = 1$  (by a factor of 3.3 when  $\bar{\omega} = 2.08$ ) over much of the operating range.

The study presented above and the cited example show that safe and reliable power plant operation can be achieved by using a hydraulic damping mount. This can be achieved by shifting the critical speeds beyond operating range, as well as by reducing the deflection, unbalance force and stresses in the shaft to safe levels when the critical speeds lie in the range of operating rpm.

#### REFERENCES

1. Grigor'yev, N.V. Nelineynyye kolebaniya elementov mashin i sooruzheniy [Nonlinear Vibrations of Machine and Structural Elements]. Mashgiz Press, 1961.
2. Gurov, A.F. Sovmestnyye kolebaniya v gazoturbinnnykh dvigatelyakh [Combined Vibrations in Gasturbine Engines]. Trudy MAI, Issue 122. Oborongiz Press, 1962.
3. Den Hartog. Mechanical Vibrations. McGraw-Hill Book Company, 3rd ed., 1947.
4. Dimentberg, F.M. Izgibnyye kolebaniya vrashchayushchikhsya valov [Flexural Vibrations of Rotating Shafts]. USSR Acad. Sci. Press, 1959.
5. Pichugin, D.F. Analysis of the Operation of a Dry-Friction Damping Mount for Reducing Shaft Vibrations on Passage Through Critical Speeds. Izvestiya Vuzov, Aviatsionnaya Tekhnika, No. 1, 1958.
6. Sergeyev, S.I. Dempfirovaniya mekhanicheskikh kolebaniy [Damping of Mechanical Vibrations]. Fizmatgiz. 1959.
7. Stolyarov, V.F. Kolebaniya nesbalansirovannogo rotora na uprugodempfernykh oporakh [Vibrations of an Unbalanced Rotor on Hydraulic Damping Mounts]. Trudy MAI, Issue 136. Oborongiz Press, 1961.

8. Kryukov, K.A. Vliyaniye konstruktivnykh parametrov na kriticheskiye skorosti rotor-korpus-podveska aviatsionnogo GTD [Effect of Design Parameters on the Critical Speeds of Rotor-Housing-Mount of an Aircraft Gas Turbine Engine]. Trudy MAI, Issue 136. Oborongiz Press, 1961.

# DYNAMIC COMPLIANCES IN A SYSTEM WITH FRICTION

Engineer V. M. Balepin

Dynamic stiffness (or compliance) methods are extensively used in the study of vibrations, as well as in practical calculations.

/50

Recently, extensive work was done on the effect of various types of friction on vibration. In this connection we would like to discuss the problem of the dynamic compliance of a system in which friction accompanies the flexural vibrations. F. M. Dimentberg [1, 2] has discussed a similar problem in its application to catenary systems.

The problem is formulated as follows. Determine the dynamic compliance of a system with two degrees of freedom undergoing flexural vibrations, assuming presence of internal friction forces. We shall consider a nonrotating beam (Fig. 1) of constant cross section with a moment of inertia  $J$ . The beam is hinged at the ends and carries two weights with masses  $m_1$  and  $m_2$ .

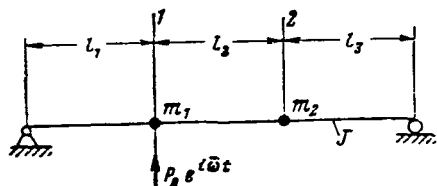
First we make some simplifying assumptions:

1. The internal friction forces are assumed applied over the design cross sections (at points of action of the masses).
2. There is no friction in the supporting hinges.
3. The moments due to rotation of the weights are small and may be neglected.
4. The frictional forces induced in the beam by these moments are also neglected.
5. The mass of the beam is neglected.

A perturbing force  $P$  is applied over the design section 1; it is defined as

/51

$$P = P_0 e^{i\bar{\omega}t} = P_0 e^{i(\omega + i\alpha)t}, \quad (1)$$



where  $P_0$  is the real amplitude of the force;  $e$  is the natural base of logarithms;  $\bar{\omega} = \omega + i\alpha$  is the complex frequency;  $\omega$  is the natural frequency of the beam;  $\alpha$  is the damping factor.

$$i = \sqrt{-1}.$$

Figure 1. Computational Schematic of a Shaft with Two Masses Acting between Supports.

It is assumed that the internal friction force is proportional to the complex displacement [3]; i.e.,

$$F_n = -(C_{nn}y_n + C_{nj}y_j)v_n. \quad (2) \quad /51$$

Here  $C_{nn}$  is a force producing a unit displacement at point of application  $n$ ;  $y_n$  is the complex displacement of section  $n$ ;  $\gamma$  is an internal friction coefficient, which is assumed to be constant

$$v_n = \frac{\gamma_n}{1 + \frac{\gamma_n^2}{4}}.$$

The equations of masses  $m_1$  and  $m_2$  will be

$$\left. \begin{aligned} y_1 &= -\delta_{11}m_1\ddot{y}_1 - \delta_{12}m_2\ddot{y}_2 - \delta_{11}(C_{11}y_1 + C_{12}y_2)iv_1 - \\ &\quad - \delta_{22}(C_{21}y_1 + C_{22}y_2)iv_2 + \delta_{11}P_0e^{i\omega t}; \\ y_2 &= -\delta_{21}m_1\ddot{y}_1 - \delta_{22}m_2\ddot{y}_2 - \delta_{21}(C_{11}y_1 + C_{12}y_2)iv_1 - \\ &\quad - \delta_{22}(C_{21}y_1 + C_{22}y_2)iv_2 + \delta_{21}P_0e^{i\omega t}, \end{aligned} \right\} \quad (3)$$

where  $\delta_{nj}$  is the displacement of the  $n$ th section produced by a unit force applied in the  $j$ th section

In the first equation of system (3), the first two terms of the right-hand side define displacements of section 1, produced by inertia forces of masses  $m_1$  and  $m_2$ , while the two following terms are displacements due to internal friction forces, and the last term defines the displacement due to the perturbing force. Terms in the right-hand side of the 2nd equation define the same quantities as in the 1st, except that these are applicable to section 2.

The stiffness factors are expressed in terms of action coefficients

$$C_{11} = \frac{\delta_{22}}{\delta_{11}\delta_{22} - \delta_{12}^2}; \quad C_{22} = \frac{\delta_{11}}{\delta_{11}\delta_{22} - \delta_{12}^2}; \quad C_{12} = C_{21} = -\frac{\delta_{21}}{\delta_{11}\delta_{22} - \delta_{12}^2}. \quad (4) \quad /52$$

It should be noted that:

1) taking into account the moment due to rotation of the masses will add two more equations to the system of equations (3). These equations would define the angles of rotation of the design sections. In addition, terms which take into account the displacements produced by these moments and by friction forces due to these moments would also be added.

2) inclusion of one external resistance force in the system would result in adding one term to Eqs. (3);

3) the method about to be presented makes it possible to set up equations for displacements [motion] of a system with any number of

degrees of freedom, as well as any perturbations and frictional forces.

Since we are considering induced vibrations of the shaft, it is sufficient to discuss only the particular solutions of inhomogeneous equations (3)

$$y_1 = y_{10} e^{i\bar{\omega}t}; \quad y_2 = y_{20} e^{i\bar{\omega}t}. \quad (5) \quad \underline{/52}$$

Substituting corresponding values of displacements and their derivatives into Eqs. (3) and transforming, we get

$$\left. \begin{aligned} (\delta_{11} m_1 \bar{\omega}^2 - 1 - i\delta_{11} C_{11} v_1 - i\delta_{12} C_{21} v_2) y_{10} + (\delta_{12} m_2 \bar{\omega}^2 - \\ - i\delta_{11} C_{12} v_1 - i\delta_{12} C_{22} v_2) y_{20} = -\delta_{11} P_0; \\ (\delta_{21} m_1 \bar{\omega}^2 - i\delta_{21} C_{11} v_1 - i\delta_{22} C_{21} v_2) y_{10} + (\delta_{22} m_2 \bar{\omega}^2 - 1 - \\ - i\delta_{21} C_{12} v_1 - i\delta_{22} C_{22} v_2) y_{20} = -\delta_{21} P_0. \end{aligned} \right\} \quad (6)$$

The expressions for dynamic compliances will be

$$\bar{e}_{11} = \frac{D_1}{P_0 D}; \quad \bar{e}_{21} = \frac{D_2}{P_0 D}, \quad (7)$$

where

$$\begin{aligned} D = & (\delta_{11} m_1 \bar{\omega}^2 - 1 - i\delta_{11} C_{11} v_1 - i\delta_{12} C_{21} v_2) (\delta_{22} m_2 \bar{\omega}^2 - 1 - \\ & - i\delta_{21} C_{12} v_1 - i\delta_{22} C_{22} v_2) - (\delta_{21} m_1 \bar{\omega}^2 - i\delta_{21} C_{11} v_1 - i\delta_{22} C_{21} v_2) \times \\ & \times (\delta_{12} m_2 \bar{\omega}^2 - i\delta_{11} C_{12} v_1 - i\delta_{12} C_{22} v_2); \end{aligned} \quad (8)$$

$$\begin{aligned} D_1 = & (\delta_{12} m_2 \bar{\omega}^2 - i\delta_{11} C_{12} v_1 - i\delta_{12} C_{22} v_2) \delta_{21} - \\ & - (\delta_{22} m_2 \bar{\omega}^2 - 1 - i\delta_{21} C_{12} v_1 - i\delta_{22} C_{22} v_2) \delta_{11}; \end{aligned} \quad (9)$$

$$D_2 = \delta_{21} + iC_{21} v_2 (\delta_{21} \delta_{12} - \delta_{11} \delta_{22}). \quad (10)$$

We now separate the real from the imaginary parts in expressions (7). Thus we substitute into determinants (8), (9) and (10) the expression

$$\bar{\omega} = \omega + i\alpha.$$

Without presenting the derivation, we write the final result

$$\bar{e}_{11} = M + iN; \quad \bar{e}_{21} = M_1 + iN_1; \quad (11)$$

$$|\bar{e}_{11}| = \sqrt{M^2 + N^2}; \quad |\bar{e}_{21}| = \sqrt{M_1^2 + N_1^2}; \quad (12)$$

$$M = \frac{AC + BK}{C^2 + K^2}; \quad M_1 = \frac{A_1 C + B_1 K}{C^2 + K^2};$$

$$N = \frac{BC - AK}{C^2 + K^2}; \quad N_1 = \frac{B_1 C - A_1 K}{C^2 + K^2},$$

where

/53

$$\begin{aligned}
A &= m_1^2 (\omega^2 - \alpha^2) (\delta_{21} \delta_{12} - \delta_{11} \delta_{22}) + \delta_{11}; \\
B &= (\delta_{21} \delta_{12} - \delta_{11} \delta_{22}) (2\alpha m_2 \omega - v_2 C_{22}); \\
C &= m_1 m_2 (\omega^2 - \alpha^2) (\delta_{11} \delta_{22} - \delta_{21} \delta_{12}) - (\delta_{11} m_1 - \delta_{22} m_2) (\omega^2 - \alpha^2) - \\
&\quad - 4m_1 m_2 \alpha^2 \delta_{11} \delta_{22} \omega^2 + 2v_1 \alpha \omega (m_2 c_{11} \delta_{11} \delta_{22} + m_1 c_{12} \delta_{21} \delta_{11}) + \\
&\quad + 2v_2 \alpha \omega (m_2 c_{21} \delta_{12} \delta_{22} + m_1 c_{22} \delta_{11} \delta_{22}) - v_1^2 c_{12} c_{11} \delta_{21} \delta_{11} - \\
&\quad - v_2^2 c_{21} c_{22} \delta_{22} + (2\delta_{21} m_1 \alpha \omega - v_1 c_{11} \delta_{21} - v_2 c_{21} \delta_{22}) \times \\
&\quad \times (2\delta_{12} m_2 \alpha \omega - v_1 c_{12} \delta_{11} - v_2 c_{22} \delta_{12}) + 1; \\
K &= (\omega^2 - \alpha^2) [\delta_{21} m_1 (v_1 c_{12} \delta_{11} + v_2 c_{22} \delta_{12} - 2\delta_{21} m_1 \alpha \omega) - \\
&\quad - \delta_{12} m_2 (2\delta_{21} m_1 \alpha \omega - v_1 c_{11} \delta_{21} - v_2 c_{21} \delta_{22}) + 4\delta_{11} \delta_{22} m_1 m_2 \alpha \omega - \\
&\quad - \delta_{11} \delta_{22} (v_2 m_1 c_{22} + v_1 m_2 c_{11}) - c_{21} \delta_{12} (v_1 m_1 \delta_{11} + v_2 m_2 \delta_{22})] - \\
&\quad - 2\alpha \omega (\delta_{11} m_1 + \delta_{22} m_2) + c_{21} \delta_{12} (v_1 + v_2) + v_1 c_{11} \delta_{11} + v_2 c_{22} \delta_{22}.
\end{aligned}$$

Formulas (11) were used for calculating the dynamic compliances of a beam with the following parameters: total length  $l = 60$  cm,  $l_1 = l_2 = l_3 = 20$  cm are the lengths of the individual sections;  $J = 0.97$  cm<sup>4</sup> is the moment of inertia of the beam cross section;  $m_1 = m_2 = 3.5$  kg ( $3.57 \cdot 10^{-3}$  kg-cm<sup>-1</sup>-sec<sup>2</sup>) are the masses of the weights placed on the beam;  $v_1 = 0.0319$ ,  $v_2 = 0.041$  and  $\alpha = 0.905$ .

Figures 2 and 3 depict the variation in complex dynamic compliances  $\underline{e}_{11}$  and  $\underline{e}_{21}$  as a function of the frequency. The real component is plotted on the vertical axis, with the imaginary component on the abscissa. The frequency axis is drawn perpendicular to the real and imaginary axes. The vector of the complex dynamic compliance is drawn for each design frequency and a line (hodograph) is drawn through the ends of the vectors; it shows the manner in which the compliance varies in a system with two degrees of freedom and with friction. In view of the fact that friction was assumed to be proportional to the complex displacement, the dynamic compliances  $\underline{e}_{11}$  and  $\underline{e}_{21}$  will not be equal to the static compliance when  $f \rightarrow 0$ .

Note the most characteristic points on the graphs. The point of intersection of the complex dynamic compliance curve with the horizontal plane corresponds, in an ideal elastic system, to the resonance frequency.

The real component is  $\underline{M} = 0$  and the imaginary component is  $\underline{N} = \max$ , which proves the absence of displacement in the direction of the perturbing force. The phase angle is  $\pi/2$ . After this point the curve passes into the 2nd quadrant (it is shown in the figures by a dashed line). The curve goes from the 2nd back into the 1st quadrant in Fig. 2 when the 1st shape of the elastic curve of the beam changes to the 2nd. Also in the region of the 2nd resonance (the expression "resonance" is used

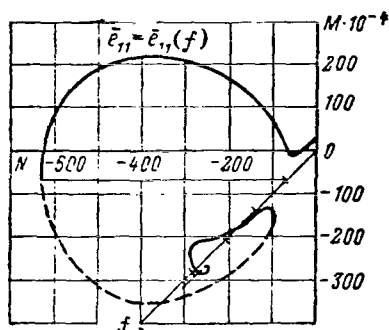


Figure 2. Graph of the Principal Complex Dynamic Compliance.

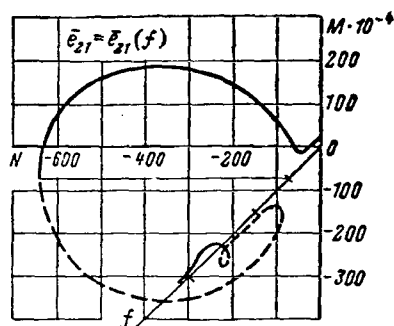


Figure 3. Graph of Auxiliary Complex Dynamic Compliance.

arbitrarily), this behavior of the curve is repeated. On further increase in the frequency, the complex dynamic compliance decreases all the time and the curve approaches the frequency axis.

The difference between curve  $\bar{e}_{21} = \bar{e}_{21}(f)$  and that described above starts in the region of the 2nd resonance, when it passes to the 3rd and 4th quadrants. This passage is also related to changes in the shape of the elastic curve of the beam.

The above equations obtained (restricted by the above described considerations) make it possible to determine the dynamic compliance in systems with several degrees of freedom at different types of friction. By its form the solution of these problems differs little from that for ordinary problems, except that the dynamic compliance turns out to be a complex quantity.

#### REFERENCES

1. Dimentberg, F.M. The method of Dynamic Stiffness with Application to Determination of Vibratory Frequencies of Systems with a Resistance. *Izv. AN SSSR, Otd. Tech. Nauk*, 110, 1948.
2. Dimentberg, F.M. Determining the Amplitudes of Forced Vibrations of a Catenary System with Resistance. In the collection: *Dinamika i prochnost' kolenchatykh valov* [Dynamics and Strength of Crankshafts]. USSR Acad. Sci. Press, 1950.
3. Sergeyev, S.I. *Dempfirovaniye mekhanicheskikh kolebaniy* [Damping of Mechanical Vibrations]. Fizmatgiz Press, 1959.
4. Sorokin, Ye.S. *K teorii vnutrennego treniya pri kolebaniyakh uprugikh sistem* [Concerning the Theory of Internal Friction Accompanying Vibrations of Elastic Systems]. Gosstroyizdat Press, 1951.
5. Strelkov, S.P. *Vvedeniye v teoriyu kolebaniy* [Introduction to the Theory of Vibrations]. GIT Press, 1951.

# FORCED VIBRATIONS OF A FREE SHAFT WITH FRICTION

Engineer Ye.A. Artemov

The term free shaft is used here to denote a rotating beam in which <sup>/56</sup> the effect of the support on the manner in which the shaft vibrates is neglected. It is assumed that the beam is coupled to its supports only by means of vibration dampers (Fig. 1). An example of such a free shaft is a rotor with sliding-contact bearings mounted at points of oscillation. Such a shaft exhibits a varying degree of necessary external concentrated damping, which depends on the kind of fluid used, as well as the dimensions of the working surfaces of the shaft and of the bearings.

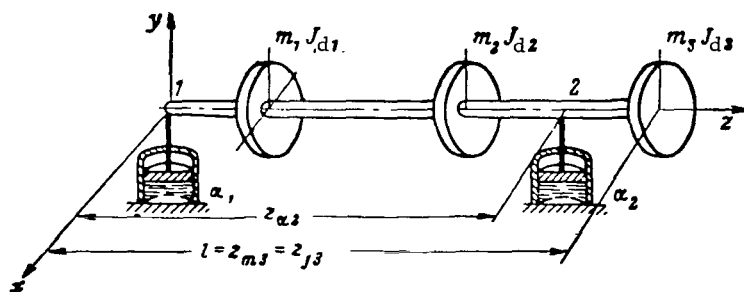


Figure 1. Schematic of a Shaft with Three Disks Coupled to Supports by Means of Vibration Dampers.

The forced vibrations of a free shaft must be calculated in determining the resonance conditions in engines with dampers using the dynamic compliance method. This paper presents an attempt to calculate the amplitudes of forced flexural vibrations of a free, rotating shaft of any shape, subjected to an arbitrary load, and equipped with  $n$  damping mounts. It is assumed that the shaft deforms linearly and that the damping mounts are hydraulic (in such mounts the friction force is assumed proportional to the frequency of vibrations). The distributed bending moments due to inertia forces in the shaft are so small that they may be neglected.

We shall solve this problem by using integral equations of forced flexural vibrations, which take into account viscous friction and are presented in [4]:

$$\left. \begin{aligned} (EJx'')'' - \omega^2 \left\{ \varrho_m Fx + \left[ \sum_1^l m_l x_l \varepsilon_{ml} \right]' - \left[ \sum_1^l J_{d1} \dot{x}_l \varepsilon_{jl} \right]'' \right\} - \\ - \omega \sum_1^l \alpha_l y_l' \varepsilon_{al} = \sum_1^l q; \end{aligned} \right|$$

$$(EJy'')'' - \omega^2 \left\{ q_m Fy + \left[ \sum_1^i m_i y_i \varepsilon_{mi} \right] - \left[ \sum_1^i J_{di}^* y_i' \varepsilon_{ji} \right] \right\} + \left. \begin{aligned} &+ \omega \sum_1^i \alpha_i x_i' \varepsilon_{ai} = 0, \end{aligned} \right\} \quad (1)$$

where  $EJ$  is the rigidity of the shaft cross section (in  $N \cdot m^2$ ),  $x$  and  $y$  are the shaft deflections in an arbitrary cross section along these axes (in  $m$ );  $\omega$  is the angular frequency of vibrations (in  $sec^{-1}$ );  $\rho_m F$  is the rotating per unit length (in  $kg/m$ );  $\underline{m}_i$  are the masses of the disks at individual sections (in  $kg$ );  $J_{di}^*$  are the reduced diameter moments of inertia of the disks (in  $kg \cdot m^2$ );  $q$  is the external distributed load per unit length (in  $N/m$ );  $\varepsilon_{ki}$  is a unit function

$$\varepsilon_{ki} = \begin{cases} 0; & z < z_{ki}; \\ 1; & z > z_{ki}; \end{cases}$$

here subscript  $k$  of  $\varepsilon$  takes on values  $\underline{m}$ ,  $\underline{p}$ ,  $\underline{j}$  and  $\underline{\alpha}$  for terms with mass  $\underline{m}$ , force  $\underline{P}$ , moment of inertia  $\underline{J}$  and friction coefficient  $\underline{\alpha}$  respectively;  $\underline{\alpha}_i$  is the viscous friction coefficient in section  $\underline{z}_i$ , and  $\underline{z}$  is an independent variable of integration.

For a free shaft, the system of equations (1) should satisfy the following boundary conditions:

$$\left. \begin{aligned} z=0 & \quad \left. \begin{aligned} EJx'' &= 0; (EJx'')' = 0; \\ EJy'' &= 0; (EJy'')' = 0; \end{aligned} \right\} \\ z=l & \quad \left. \begin{aligned} EJx'' &= 0; (EJx'')' = 0; \\ EJy'' &= 0; (EJy'')' = 0. \end{aligned} \right\} \end{aligned} \right\} \quad (2)$$

Integrating Eqs. (1) along the shaft and substituting into them conditions (2), we get

$$\left. \begin{aligned} (EJx'')' &= \omega^2 \left\{ \int_0^z q_m F x dz + \sum_1^i m_i x_i \varepsilon_{mi} - \left[ \sum_1^i J_{di}^* x_i' \varepsilon_{ji} \right] \right\} + \\ &+ \omega \sum_1^i \alpha_i y_i \varepsilon_{ai} + \sum_1^i P_i \varepsilon_{pi} + C_{ix} = 0; \end{aligned} \right\}$$

$$(EJy'')' = \omega^2 \left\{ \int_0^z Q_m F y dz + \sum_1^l m_i y_i \varepsilon_{mi} - \left[ \sum_1^l J_{di}^* y_i' \varepsilon_{ji} \right]' - \right. \\ \left. - \omega \sum_1^l \alpha_i x_i \varepsilon_{ai} + C_{1y} \right\} = 0. \quad (3)$$

The above system of equations describes by means of unit function  $\varepsilon_{ki}$  the analytic expression for the shearing force in any section of the shaft. When  $z = 0$ , constants  $C_{1x}$  and  $C_{1y}$  are also zero.

Integrating Eqs. (3) once more, we get

$$EJx'' = \omega^2 \left\{ \int_0^z dz \left[ \int_0^z Q_m F x dz + \sum_1^l m_i x_i \varepsilon_{mi} \right] - \sum_1^l J_{di}^* x_i' \varepsilon_{ji} \right\} + \\ + \omega \int_0^z \sum_1^l \alpha_i y_i \varepsilon_{ai} dz + \int_0^z \sum_1^l P_i \varepsilon_{pi} dz + C_{2x}; \\ EJy'' = \omega^2 \left\{ \int_0^z dz \left[ \int_0^z Q_m F y dz + \sum_1^l m_i y_i \varepsilon_{mi} \right] - \sum_1^l J_{di}^* y_i' \varepsilon_{ji} \right\} - \\ - \omega \int_0^z \sum_1^l \alpha_i x_i \varepsilon_{ai} dz + C_{2y}. \quad (4)$$

Substituting the conditions of the unit function for  $z = 0$  into Eqs. (4), we find that  $C_{2x} = C_{2y} = 0$ .

For convenience in subsequent manipulations, we represent Eqs. (4) as

$$\left. \begin{aligned} x'' &= \omega^2 M_x + \omega M_{ay} + M_p; \\ y'' &= \omega^2 M_y - \omega M_{ax}, \end{aligned} \right\} \quad (5)$$

where  $\underline{M_x}$  and  $\underline{M_y}$  are the expressions in the figured braces of the first and second equations of system (4), divided by EJ, i.e.,

$$M_{ax} = \frac{1}{EJ} \int_0^z \sum_1^l \alpha_i x_i \varepsilon_{ai} dz; \\ M_{ay} = \frac{1}{EJ} \int_0^z \sum_1^l \alpha_i y_i \varepsilon_{ai} dz; \quad /59$$

$$M_p = \frac{1}{EJ} \int_0^z \sum_1^l P_l \varepsilon_{pl} dz.$$

Integrating Eqs. (5) twice more, we obtain the starting integral equations for forced vibrations of a free shaft with viscous friction, subjected to external periodic forces  $\underline{P}$ :

$$\left. \begin{aligned} x' &= \omega^2 M'_x + \omega M'_{ay} + M'_p + x'(0); \\ y' &= \omega^2 M'_y - \omega M'_{ax} + y'(0) \end{aligned} \right\} \quad (6)$$

and

$$\left. \begin{aligned} x &= \omega^2 M_x + \omega M_{ay} + M_p + x'(0)z + x(0); \\ y &= \omega^2 M_y - \omega M_{ax} + y'(0)z + y(0). \end{aligned} \right\} \quad (7)$$

The unknown constants of integration  $x'(0)$ ,  $\underline{x}(0)$ ,  $\underline{y}'(0)$  and  $\underline{y}(0)$  will be found from the equations of reciprocity of work, which will be derived for our problem.

We shall set up the reciprocity equation for loads arising on free vibrations and for external loads, assuming that the viscous friction force accompanying the rotation of the system is an external force from the point of view of the dynamic equilibrium. It is obvious that in a problem incorporating friction, the equation of reciprocity of work will reduce to two equations of work in the  $\underline{x}$  and  $\underline{y}$  planes [1, 4].

The loads in free vibration are:

Force Loads [Forces]

$$\begin{aligned} P_{cx} &= \omega_{ck}^2 \left( \int_0^l \varrho_m F x_{ck} dz + \sum_1^l m_l x_{cki} \right); \\ P_{cy} &+ \omega_{ck}^2 \left( \int_0^l \varrho_m F y_{ck} dz + \sum_1^l m_l y_{cki} \right) \end{aligned}$$

Moment Loads [Moments]

$$M_{cx} = \omega^2 \sum_1^l J_d^* i x'_{cki}; \quad M_{cy} = \omega^2 \sum_1^l J_d^* i y'_{cki}.$$

Loads in forced vibrations are:

/60

Force Loads

$$P_x = \omega^2 \left( \int_0^l \varrho_m F x dz + \sum_1^l m_l x_l \right) + \omega \sum_1^l a_l y_l + \sum_1^l P_l;$$

$$P_y = \omega^2 \left( \int_0^l \rho_m F y dz + \sum_1^i m_i y_i \right) - \omega \sum_1^i a_i x_i;$$

#### Moments Loads

$$M_x = \omega^2 \sum_1^i J_{d_i}^* x_i'; \quad M_y = \omega^2 \sum_1^i J_{d_i}^* y_i'.$$

The equations of reciprocity of work for intrinsic loads  $\underline{P}_c$  and  $\underline{M}_c$  and for their corresponding intrinsic deflections  $\underline{x}_{ck}$  and  $\underline{y}_{ck}$  and angles of rotation  $\underline{x}'_{ck}$  and  $\underline{y}'_{ck}$ , as well as for external loads  $\underline{P}$  and  $\underline{M}$  and their corresponding deflections  $\underline{x}$  and  $\underline{y}$  and angles of rotation  $\underline{x}'$  and  $\underline{y}'$  in forced vibrations with friction will be, on the basis of the theorem of reciprocity of work (the derivation of equations for systems without friction is considered in detail in [2]):

$$\left. \begin{aligned} (\omega_{ck}^2 - \omega^2) \left[ \int_0^l \rho_m F x_{ck} x dz + \sum_1^i m_i x_{cki} x_i + \sum_1^i J_{d_i}^* x'_{cki} x_i' \right] &= \\ &= \sum_1^i P_i x_{cki} + \omega \sum_1^i a_i y_i x_{cki}; \\ (\omega_{ck}^2 - \omega^2) \left[ \int_0^l \rho_m F y_{ck} y dz + \sum_1^i m_i y_{cki} y_i + \sum_1^i J_{d_i}^* y'_{cki} y_i' \right] &= \\ &= -\omega \sum_1^i a_i x_i y_{cki}, \end{aligned} \right\} \quad (8)$$

where  $\underline{k} = 0, 1, 2, \dots$  is the ordinal number of the mode and frequency of natural vibrations.

It is characteristic of a free system that it is impossible to obtain a converging process on simple iteration even in the case of  $\omega < \omega_{c1}$ .

This is due to the fact that the first elastic mode of the system is preceded by zero modes, which first must be removed, i.e., it is necessary to find those orthogonality conditions which would eliminate the effect of the zero-mode components.

A free shaft has four zero modes of vibration, corresponding to its four degrees of freedom as a rigid, inelastic body, namely: displacement in space relative to itself in the  $\underline{x}$  and  $\underline{y}$  directions and rotation in space about the center of the mass about directions parallel to these axes. Analytically, the zero modes of vibrations of a free shaft can be written as

$$\left. \begin{aligned} x_{c01} &= -x_c; & x'_{c01} &= 0; \\ y_{c01} &= -y_c; & y'_{c01} &= 0. \end{aligned} \right\} \quad (9)$$

$$\left. \begin{aligned} x_{c02} &= -(z_c - z)x'_c; & x'_{c02} &= x'_c; \\ y_{c02} &= -(z_c - z)y'_c; & y'_{c02} &= y'_c. \end{aligned} \right\} \quad (10)$$

where  $\underline{x}_c$ ,  $\underline{y}_c$  and  $\underline{z}_c$  are the coordinates of the shaft's center of mass.

Substituting Eqs. (9) and (10) into Eq. (8) and making use of the fact that  $\omega_{c01}$  and  $\omega_{c02}$  are equal to zero, we obtain conditions analogous to the orthogonality condition

$$\left. \begin{aligned} \omega^2 \left( \int_0^l \rho_m F x dz + \sum_1^i m_i x_i \right) + \omega \sum_1^i a_i y_i + \sum_1^i P_i &= 0; \\ \omega^2 \left( \int_0^l \rho_m F y dz + \sum_1^i m_i y_i \right) - \omega \sum_1^i a_i x_i &= 0; \\ \omega^2 \left( \int_0^l \rho_m F x z dz + \sum_1^i m_i x_i z_i + \sum_1^i J_{d_i}^* x_i' \right) + \omega \sum_1^i a_i y_i z_i + \\ &+ \sum_1^i P_i z_i = 0; \\ \omega^2 \left( \int_0^l \rho_m F y z dz + \sum_1^i m_i y_i z_i + \sum_1^i J_{d_i}^* y_i' \right) - \omega \sum_1^i a_i x_i z_i &= 0. \end{aligned} \right\} \quad (11)$$

We now substitute Eqs. (6) and (7) (one after another) into the above expressions. Now, if we disregard friction forces in these expressions (they are small compared to other quantities) then the design equations will simplify and reduce to

$$\left. \begin{aligned} \omega^4 a_x + \omega^3 a_{xy} + \omega^2 a_p + \sum_1^i P_i + \omega^2 x'(0) n + \omega^2 x(0) m &= 0; \\ \omega^4 b_x + \omega^3 b_{xy} + \omega^2 b_p + \sum_1^i P_i z_i + \omega^2 x'(0) q + \omega^2 x(0) n &= 0; \end{aligned} \right\} \quad (12)$$

$$\left. \begin{aligned} \omega^4 a_y - \omega^3 a_{xy} + \omega^2 y'(0) n + \omega^2 y(0) m &= 0; \\ \omega^4 b_y - \omega^3 b_{xy} + \omega^2 y'(0) q + \omega^2 y(0) n &= 0, \end{aligned} \right\} \quad (13)$$

where

$$\begin{aligned}
a_x &= \int_0^l \varrho_m F M_x dz + \sum_1^l m_l M_{xl}; & a_y &= \int_0^l \varrho_m F M_y dz + \sum_1^l m_l M_{yl}; \\
b_x &= \int_0^l \varrho_m F M_x z dz + \sum_1^l m_l M_{xl} z_l + \sum_1^l J_{dl}^* M'_{xl}; \\
b_y &= \int_0^l \varrho_m F M_y z dz + \sum_1^l m_l M_{yl} z_l + \sum_1^l J_{dl}^* M'_{yl}; \\
a_{ax} &= \int_0^l F M_{ax} dz + \sum_1^l m_l M_{axl}; & a_{ay} &= \int_0^l \varrho_m F M_{ay} dz + \sum_1^l m_l M_{ayl}; \\
b_{ax} &= \int_0^l \varrho_m F M_{ax} z dz + \sum_1^l m_l M_{axl} z_l + \sum_1^l J_{dl}^* M'_{axl}; \\
b_{ay} &= \int_0^l \varrho_m F M_{ay} z dz + \sum_1^l m_l M_{ayl} z_l + \sum_1^l J_{dl}^* M'_{ayl}; - \\
a_p &= \int_0^l \varrho_m F M_p dz + \sum_1^l m_l M_{pl}; & b_p &= \int_0^l \varrho_m F M_p z dz + \\
& & & + \sum_1^l m_l M_{pl} z_l + \sum_1^l J_{dl}^* M'_{pl}; \\
q &= \int_0^l \varrho_m F z^2 dz + \sum_1^l m_l z_l^2 + \sum_1^l J_{dl}^* z_l; \\
n &= \int_0^l \varrho_m F z dz + \sum_1^l m_l z_l; \\
m &= \int_0^l \varrho_m F dz + \sum_1^l m_l.
\end{aligned} \tag{14}$$

From Eqs. (12) we find

$$\begin{aligned}
x'(0) &= \frac{\omega^2 (b_x m - a_x n)}{n^2 + mq} + \frac{\omega (b_{ay} m - a_{ay} n)}{n^2 - mq} + \\
&+ \frac{\left( b_p + \frac{\sum_1^l p_l z_l}{\omega^2} \right) m - \left( a_p + \frac{\sum_1^l p_l}{\omega^2} \right) n}{n^2 - mq};
\end{aligned}$$

$$x(0) = \frac{\omega^2(a_x q - b_x n)}{n^2 - m q} + \frac{\omega(a_{ay} q - b_{ay} n)}{n^2 - m q} +$$

$$+ \frac{\left( \frac{\sum_1^i P_l}{a_p + \frac{1}{\omega^2}} \right) q - \left( \frac{\sum_1^i P_l z_l}{b_p + \frac{1}{\omega^2}} \right) n}{n^2 - m q},$$

while from Eqs. (13) we get

$$y'(0) = \frac{\omega^2(b_y m - a_y n) + \omega(a_{ax} n - b_{ax} m)}{n^2 - m q};$$

$$y(0) = \frac{\omega^2(a_y q - b_y n) + \omega(b_{ax} n - a_{ax} q)}{n^2 - m q}.$$

Substituting values of  $\underline{x}'(0)$ ,  $\underline{x}(0)$ ,  $\underline{y}'(0)$ ,  $\underline{y}(0)$  thus obtained into Eqs. (6) and (7), we find

$$\left. \begin{aligned} x' &= \omega^2 \left[ M'_x + \frac{b_x m - a_x n}{n^2 - m q} \right] + \omega \left[ M'_{ay} + \frac{b_{ay} m - a_{ay} n}{n^2 - m q} \right] + \\ &+ \left[ M'_p + \frac{\left( \frac{\sum_1^i P_l z_l}{b_p + \frac{1}{\omega^2}} \right) m - \left( \frac{\sum_1^i P_l}{a_p + \frac{1}{\omega^2}} \right) n}{n^2 - m q} \right] \\ y' &= \omega^2 \left[ M'_y - \frac{b_y m - a_y n}{n^2 - m q} \right] - \omega \left[ M'_{ax} - \frac{b_{ax} m - a_{ax} n}{n^2 - m q} \right]; \end{aligned} \right\} \quad (15)$$

$$\left. \begin{aligned} x &= \omega^2 \left[ M_x + \frac{b_x m - a_x n}{n^2 - m q} z + \frac{a_x q - b_x n}{n^2 - m q} \right] + \\ &+ \omega \left[ M_{ay} + \frac{b_{ay} m - a_{ay} n}{n^2 - m q} z + \frac{a_{ay} q - b_{ay} n}{n^2 - m q} \right] + \\ &+ \left[ M_p + \frac{\left( \frac{\sum_1^i P_l z_l}{b_p + \frac{1}{\omega^2}} \right) m - \left( \frac{\sum_1^i P_l}{a_p + \frac{1}{\omega^2}} \right) n}{n^2 - m q} \right] z + \\ &+ \frac{\left( \frac{\sum_1^i P_l}{a_p + \frac{1}{\omega^2}} \right) q - \left( \frac{\sum_1^i P_l z_l}{b_p + \frac{1}{\omega^2}} \right) n}{n^2 - m q}; \\ y &= \omega^2 \left[ M_y + \frac{b_y m - a_y n}{n^2 - m q} z + \frac{a_y q - b_y n}{n^2 - m q} \right] - \\ &- \omega \left[ M_{ax} - \frac{b_{ax} m - a_{ax} n}{n^2 - m q} z + \frac{a_{ax} q - b_{ax} n}{n^2 - m q} \right]. \end{aligned} \right\} \quad (16)$$

These are precisely the design integral equations of forced flexural vibrations of a free rotating shaft of arbitrary profile subjected to

forces  $\sum_{i=1}^n \underline{P}_i$ , taking into account viscous friction and with zero modes

eliminated.

In the case when the perturbing force is  $\underline{P} = 1$  N, Eqs. (16) become the equations of dynamic compliance.

In abbreviated form, Eqs. (15) and (16) can be represented as

$$\left. \begin{aligned} x' &= \omega^2 K'_x + \omega K'_{ay} + K'_p; \\ y' &= \omega^2 K'_y - \omega K'_{ax}; \end{aligned} \right\} \quad (17)$$

$$\left. \begin{aligned} x &= \omega^2 K_x + \omega K_{ay} + K_p; \\ y &= \omega^2 K_y - \omega K_{ax}, \end{aligned} \right\} \quad (18)$$

where  $\underline{K}_x$ ,  $\underline{K}'_x$  and  $\underline{K}_{ax}$  are the integral operators which are defined by terms

in brackets in Eqs. (15) and (16), respectively.

Let us now analyze each of the terms in Eqs. (18):

1. When  $\underline{P} = 0$  and  $\alpha = 0$ , we have free vibrations. Then  $\underline{x} = \underline{y} =$

$= \omega^2 \underline{K}_x = \omega^2 \underline{K}_y$  (if the shaft stiffness is isotropic) represent the amplitudes of free vibrations.

2. When  $\omega = \omega_c$  and  $\alpha \neq 0$ ,  $\underline{x}$  and  $\underline{y}$  are the vibrational amplitudes at resonance in the presence of friction.

3. When  $\omega = 0$ ,  $\underline{x} = \underline{K}_p$ ; its physical meaning is the "static" deflection of the system when acted upon by the maximum external force, the magnitude of which does not depend on the elastic curve of the free vibrations.

Terms  $\omega \underline{K}_{ax}$  and  $\omega \underline{K}_{ay}$  give the amplitudes of vibrations due to viscous friction.

#### SOLUTION OF EQUATIONS OF VIBRATION WITH FRICTION

We shall solve this problem by direct integration of the equations of forced vibrations, using the method of successive approximations.

Equations (18) are a system of two parametric, inhomogeneous, integral equations. It should be remembered that the following are assumed as known when solving these equations: natural frequency of the system  $\omega_c$ , imbalance

$\Delta$  (perturbing force  $\underline{P} = \Delta \omega^2 / g$ ) and viscous friction coefficient  $\alpha$ .

The formulas for vibration of a free shaft which are thus obtained can be used to construct a converging process for successive approximation for  $\omega < \omega_{\underline{c}1}$ . If one uses conformal iteration, then these formulas will yield a converging process for  $\omega < \omega_{\underline{c}1}$ . When  $\omega > \omega_{\underline{c}1}$  use can be made of the iteration method suggested in [2] for the problem without friction.

We now consider the methods for solving the equations.

#### A. Operation at Preresonance Conditions

Simple iteration. We construct the ordinary process of successive approximations from the formula /65

$$\left. \begin{aligned} x_{i+1} &= \omega^2 K_{x1} + \omega K_{ay1} + K_p; \\ y_{i+1} &= \omega^2 K_{y1} - \omega K_{ax1} \quad (i=0, 1, 2, \dots) \end{aligned} \right\} \quad (19)$$

It may be assumed for selecting the starting function that

$$x = x_0; \quad y = 0$$

or

$$x = y = x_0,$$

where  $x_0$  is the static deflection due to the external force, i.e.,  $\frac{K}{p}$ .

Conformal iteration. The process of successive approximations in this case is constructed according to the formula

$$\left. \begin{aligned} x_i &= C_{i-1} \omega^2 K_{x_{i-1}} + D_{i-1} \omega K_{ay_{i-1}} + K_p; \\ y_i &= D_{i-1} \omega^2 K_{y_{i-1}} - C_{i-1} \omega K_{ax_{i-1}}, \end{aligned} \right\} \quad (20)$$

where  $\frac{C}{i-1}$  and  $\frac{D}{i-1}$  are some coefficients which improve the convergence of the  $i$ th approximation, and which are determined from the assumption that the next approximation

$$\left. \begin{aligned} x_{i+1} &= C_i \omega^2 K_{x1} + D_i \omega K_{ay1} + K_p; \\ y_{i+1} &= D_i \omega^2 K_{y1} - C_i \omega K_{ax1} \end{aligned} \right\} \quad (21)$$

coincides with the preceding, i.e.,

$$\left. \begin{aligned} x_{i+1} &= C_i x_i; \\ y_{i+1} &= D_i y_i \end{aligned} \right\} \quad (22)$$

or

$$\begin{aligned} C_i x_i &= C_i \omega^2 K_{xi} + D_i \omega K_{ayi} + K_p; \\ D_i y_i &= D_i \omega^2 K_{yi} - C_i \omega K_{axi}. \end{aligned}$$

Whence

$$\left. \begin{aligned} C_i &= \frac{K_p (y_i - \omega^2 K_{yi})}{(x_i - \omega^2 K_{xi})(y_i - \omega^2 K_{yi}) + \omega^2 K_{axi} K_{ayi}}; \\ D_i &= \frac{-K_p \omega K_{axi}}{(x_i - \omega^2 K_{xi})(y_i - \omega^2 K_{yi}) + \omega^2 K_{axi} K_{ayi}}. \end{aligned} \right\} \quad (23)$$

Coefficients  $\underline{C_i}$  and  $\underline{D_i}$  are assumed to be constant over the entire range of integration and, consequently, Eqs. (23) hold for the shaft section  $\underline{z} = \underline{z}_{\max}$ , where the deflection functions are at maximum. Usually this is the same section over which the functions are normed, so that the values of  $\underline{C_i}$  and  $\underline{D_i}$  are determined from Eqs. (23) for  $\underline{z} = \underline{z}_{\max}$ . After this, successive approximations can be obtained from Eqs. (20) without difficulties.

It is clear from Eqs. (22) that the quality of the approximation can be estimated from coefficients  $\underline{C_i}$  and  $\underline{D_i}$ . The faster they approach unity, the better the convergence of process.

#### B. Operation at Resonance Conditions

In this case conformal iteration can be used.

In resonance,  $\omega = \omega_{\underline{c}}$ , but

$$\omega_c = \frac{x}{K_x} \Big|_{z_{\max}} = \frac{y}{K_y} \Big|_{z_{\max}}.$$

Substituting this expression into Eq. (23), we get

$$\left. \begin{aligned} C_i &= 0 \\ D_i &= \frac{-K_p}{\omega K_{ayi}} \Big|_{z_{\max}} \end{aligned} \right\} \quad (24)$$

Accordingly, Eqs. (20) will take on the form

$$\left. \begin{aligned} x_{i+1} &= \frac{-K_p}{\omega K_{ayi}} \Big|_{z_{\max}} \cdot \omega K_{ayi} + K_p; \\ y_{i+1} &= \frac{-K_p}{\omega K_{ayi}} \Big|_{z_{\max}} \omega^2 K_{yi}. \end{aligned} \right\} \quad (25)$$

### C. Operation Beyond Resonance Conditions

We shall use the method suggested by A.F. Gurov [2] for the problem not involving friction. The essence of this method is the fact that the fast-increasing components due to inertia forces, which appear due to the inexactitude and approximate nature of the calculations, are eliminated by using the condition of reciprocity of works; to use this condition, it is necessary to first determine several free modes and frequencies of vibrations.

Thus, in the case being considered the perturbation frequency  $\omega$  lies between two natural frequencies, i.e.,

$$\omega_{c1} < \omega < \omega_{c2}.$$

We use iteration in the form

$$\left. \begin{aligned} x_{i+1} &= \omega^2 K_{xi}^* + \omega K_{yi}^* + K_p; \\ y_{i+1} &= \omega^2 K_{yi}^* - \omega K_{xi}^*, \end{aligned} \right\} \quad (26)$$

where  $K_{\underline{x}}^*$ ,  $K_{\underline{y}}^*$ ,  $K_{\alpha\underline{x}}^*$  and  $K_{\alpha\underline{y}}^*$  are integral operators of the starting "corrected" functions of deflections at forced vibrations. This function will be determined from

$$\left. \begin{aligned} x_i^* &= x_i + C_{xi} x_{ci}; \\ y_i^* &= y_i + C_{yi} y_{ci}, \end{aligned} \right\} \quad (27)$$

where  $\underline{x}_i$ ,  $\underline{y}_i$  are the starting functions;

$\underline{x}_{c1}$ ,  $\underline{y}_{c1}$  are functions of modes of natural vibrations or eigenfunctions (when the shaft rigidity is isotropic,  $\underline{x}_{c1} = \underline{y}_{c1}$ ), and

$\underline{C}_{x1i}$ ,  $\underline{C}_{y1i}$  are the coefficients of the condition of reciprocity of work in planes  $\underline{x}$  and  $\underline{y}$ , respectively.

The operation which is defined by Eqs. (26) frees the desired vibration mode of errors and of terms which appear due to inexactitude of the calculations done in the process of successive approximations.

The unknown  $\underline{C}_{x1}$  and  $\underline{C}_{y1}$  will be found from conditions of reciprocity of work, expressed by Eqs. (8) in the form

$$\left( \omega_{c1}^2 - \omega^2 \right) \left[ \int_0^l \rho_m F x_{c1} x \, dz + \sum_1^i m_l x_{c1l} x_l + \sum_1^i J_{dl}^* x'_{c1l} x'_l \right] = \left[ \sum_1^i P_l x_{c1l} - \omega \sum_1^i \alpha_l y_l x_{c1l} \right]$$

$$(\omega_{c1}^2 - \omega^2) \left[ \int_0^l \varrho_m F y_{c1} dz + \sum_1^l m_l y_{c1l} y_l + \sum_1^l J_{d1}^* y'_{c1l} y'_l \right] = \left[ \begin{aligned} &= -\omega \sum_1^l \alpha_l x_l y_{c1l}. \end{aligned} \right] \quad (28)$$

We multiply Eqs. (27) by  $\frac{x}{c_1}$  or  $\frac{y}{c_1}$  and integrate the result thus obtained over the entire shaft; then adding similar terms, we get

$$\left. \begin{aligned} & \int_0^l \varrho_m F x_i^* x_{c1} dz + \sum_1^l m_l x_i^* x_{c1l} + \sum_1^l J_{d1}^* x_i^* x'_{c1l} = \int_0^l \varrho_m F x_l x_{c1} dz + \\ & + \sum_1^l m_l x_l x_{c1l} + \sum_1^l J_{d1}^* x'_l x'_{c1l} + \\ & + C_{x1l} \left( \int_0^l \varrho_m F x_{c1}^2 dz + \sum_1^l m_l x_{c1l}^2 + \sum_1^l J_{d1}^* x_{c1l}^2 \right); \\ & \int_0^l \varrho_m F y_i^* y_{c1} dz + \sum_1^l m_l y_i^* y_{c1l} + \sum_1^l J_{d1}^* y_i^* y'_{c1l} = \int_0^l \varrho_m F y_l y_{c1} dz + \\ & + \sum_1^l m_l y_l y_{c1l} + \sum_1^l J_{d1}^* y'_l y'_{c1l} + \\ & + C_{y1l} \left( \int_0^l \varrho_m F y_{c1}^2 dz + \sum_1^l m_l y_{c1l}^2 + \sum_1^l J_{d1}^* y_{c1l}^2 \right). \end{aligned} \right\} \quad (29)$$

From this, using Eq. (28), and denoting for compactness

$$\int_0^l \varrho_m F x_{c1}^2 dz + \sum_1^l m_l y_{c1l}^2 + \sum_1^l J_{d1}^* x_{c1l}^2 = \Pi_{x1} = \Pi_{y1} = \Pi_1,$$

we find

$$\left. \begin{aligned} C_{x1l} &= \frac{\sum_1^l P_l x_{c1l} + \omega \sum_1^l \alpha_l y_l x_{c1l}}{(\omega_{c1}^2 - \omega^2) \Pi_1} - \\ & - \frac{\int_0^l \varrho_m F x x_{c1} dz + \sum_1^l m_l x_l x_{c1l} + \sum_1^l J_{d1}^* x'_l x'_{c1l}}{\Pi_1}; \\ C_{y1l} &= \frac{-\omega \sum_1^l \alpha_l x_l y_{c1l}}{(\omega_{c1}^2 - \omega^2) \Pi_1} - \\ & - \frac{\int_0^l \varrho_m F y y_{c1} dz + \sum_1^l m_l y_l y_{c1l} + \sum_1^l J_{d1}^* y'_l y'_{c1l}}{\Pi_1}, \end{aligned} \right\} \quad (30)$$

but, as follows from [2] and [3], the numerators in the second terms of Eqs. (30) are orthogonality coefficients.

Then Eqs. (30) take on the form

$$\left. \begin{aligned} C_{x1l} &= \frac{\sum_1^l P_l x_{c1l} + \omega \sum_1^l a_l y_l x_{c1}}{(\omega_{c1}^2 - \omega^2) \Pi_1} - \frac{C_{x1l}}{\Pi_1}; \\ C_{y1l} &= -\frac{\omega \sum_1^l a_l x_l y_{c1l}}{(\omega_{c1}^2 - \omega^2) \Pi_1} - \frac{C_{y1l}}{\Pi_1}. \end{aligned} \right\} \quad (31)$$

From this we finally get equations for determining the unknown coefficients:

$$\left. \begin{aligned} C_{x1l} &= \frac{\sum_1^l P_l x_{c1l} + \omega \sum_1^l a_l y_l x_{c1}}{(\omega_{c1}^2 - \omega^2) (\Pi_1 + 1)}; \\ C_{y1l} &= -\frac{\omega \sum_1^l a_l x_l y_{c1l}}{(\omega_{c1}^2 - \omega^2) (\Pi_1 + 1)}. \end{aligned} \right\} \quad (32)$$

After determining  $\underline{x}_{\underline{i}+1}$  and  $\underline{y}_{\underline{i}+1}$  from Eqs. (26) in the first /69 approximation, the operation is repeated, i.e., we find  $\underline{x}_{\underline{i}+2}$ ,  $\underline{y}_{\underline{i}+2}$ , . . . ,  $\underline{x}_{\underline{n}}$ ,  $\underline{y}_{\underline{n}}$  until two successive approximations will yield sufficiently close results.

After determining  $\underline{x}_{\underline{n}}$  and  $\underline{y}_{\underline{n}}$ , the total amplitude of vibrations of the system is determined as the modulo of the complex number  $\underline{x}_{\underline{n}} + i\underline{y}_{\underline{n}}$

$$u = \sqrt{x_n^2 + y_n^2}, \quad (33)$$

and the phase angle (angle between the line of action of the force and the displacement of the system) will be

$$\varphi = \arctan \frac{y_n}{x_n}. \quad (34)$$

Example. Find the amplitudes of vibrations produced by a perturbing force  $\underline{P} = 1$  at the second disk (i.e., the dynamic compliance) of a free shaft shown in Fig. 1, if it is known that

$$\begin{array}{ll}
 l = 0.4 \text{ m}; & J_2 = 86 \cdot 10^{-8} \text{ m}^4; \\
 d_1 = 0.03 \text{ m}; & m_1 = m_2 = 3 \text{ kg}; \\
 d_2 = 0.04 \text{ m}; & m_3 = 5.5 \text{ kg}; \\
 \rho_m = 7.9 \cdot 10^3 \text{ kg/m}^3; & J_{d1} = 0.0038 \text{ kg-m}^2; \\
 E = 0.204 \cdot 10^{12} \text{ N/m}^2; & J_{d2} = 0.00746 \text{ kg-m}^2; \\
 a_1 = a_2 = 30 \text{ N-sec/m}; & J_{d3} = 0.00392 \text{ kg-m}^2; \\
 J_1 = 31.9 \cdot 10^{-8} \text{ m}^4; & \omega_{c1} = 3171 \text{ sec}^{-1};
 \end{array}$$

For the sake of brevity we shall confine one calculation to the resonance conditions, i.e., to the case of  $\omega = 3171 \text{ sec}^{-1}$ . The calculations shall use Eqs. (25). Their sequence, shown in the table, is analogous to the usual integral methods for solving vibration problems (see examples in [2] and [3]).

1. In lines 1-15 of the table are entered and calculated the geometric and mass parameters of the shaft.

Multiplier  $l/20$  of line 5, obtained from integration by the trapezoid formula for a shaft broken up into ten equal segments, is entered in the column "multiplier."

In order to calculate the values of  $\underline{m}$ ,  $\underline{n}$  and  $\underline{q}$  their components must have identical multipliers. To achieve this, multipliers  $l/20$  and

$\rho \underline{l}^2(l/20)$  are entered into the "multiplier" column of lines 6 and 16 and accordingly the "function" of these lines is multiplied by their reciprocals, i.e.,  $20/l = 0.5$  and  $20/\rho \underline{l}^3 = 39.5$

2. In lines 16-36 are determined values of  $\underline{K}_p$  and  $\underline{K}'_p$ . Coefficient 791 in line 28 is the reciprocal of  $\rho \underline{l}^2(l/20)^2$ . Similarly in line 32 coefficient 0.392 is the quantity  $(l/20)^3 10^{-6}/E$ , factored out from the "multiplier" of line 31. The same operation was performed in line 35. Lines 1-36 are constant for all the approximations.

3. In the first approximation  $\underline{y}_0$  was approximated by  $\underline{K}_p$ , and  $\underline{K}_{ay}$ ,  $\underline{K}_{y1}$  and  $\underline{D}_1$  were determined; the  $\underline{y}_1$  thus obtained served as the basis for the second approximation, etc. All the reiterated approximations start with line 37. For compactness in calculations, we do not consider approximations 1 through 3 and consider in detail the fourth approximation obtained on the basis of  $\underline{y}_3$  (and, accordingly,  $\underline{y}'_3$ ), which are given in lines 83 and 84, which yields satisfactory results ( $\underline{D}_4$  is close to unity).

TABLE

Ordinal number	Function	Multiplying factor	$z=0$	0,1	0,2	0,3	0,4	0,5	0,6	0,7	0,8	0,9	1,0
1	$c_m F$	$c_m$	3,93	4,72	5,5	5,5	5,5	5,5	5,5	5,5	5,5	5,5	5,5
2	$EJ$	$I$	3,19	5,46	8,6	8,6	8,6	8,6	8,6	8,6	8,6	8,6	8,6
3	$m$	$c_m$			387				710				387
4	$J_z$	$I$			0,038				0,0746				0,0392
5	$\int (1) dz$	$c_m (I/20)$	0	8,15	18,87	29,87	40,87	51,87	62,87	73,87	84,87	95,87	106,87
6	$m \cdot 0,5$	$c_m (I/20)$			193,5				3,55				193,5
7	$(1) \cdot z$	$c_m I$	0	0,472	11	1,65	2,2	2,75	3,3	3,85	4,4	4,95	5,5
8	$\int (7) dz$	$c_m I (I/20)$	0	0,472	2,04	4,8	8,64	13,6	19,64	26,79	35,04	44,4	54,84
9	$mz \cdot 0,5$	$c_m I (I/20)$			38,7				213				193,5
10	$z^2$	$I^2$	0	0,01	0,04	0,09	0,16	0,25	0,36	0,49	0,64	0,81	1
11	$(1) \cdot (10)$	$c_m I^2$	0	0,0472	0,22	0,495	0,88	1,375	1,98	2,69	3,52	4,45	5,5
12	$(3) \cdot (10) \cdot mz^2$	$c_m I^2$			15,5				2,56				387
13	$\int (11) dz$	$c_m I^2 (I/20)$	0	0,0472	0,314	1,029	2,404	4,659	8,014	12,68	18,89	26,86	36,81
14	$(9) \cdot z$	$c_m I^2 (I/20)$			7,74				127,8				193,5
15	$J_d \cdot 39,5$	$c_m I^2 (I/20)$			1,501				2,547				1,548
16	$P$	$P$							1,0				
17	$\sum_1 P$	$P$	0	0	0	0	0	0	1,0 0	1,0	1,0	1,0	1,0
18	$\int (17) dz = M_p$	$P (I/20)$	0	0	0	0	0	0	0	2,0	4,0	6,0	8,0
19	$(18)/(2)$	$P/E (I/20)$	0	0	0	0	0	0	0	0,2325	0,4651	0,6977	0,9302
20	$\int (19) dz = K_p$	$(P/E) (I/20)^2$	0	0	0	0	0	0	0	0,2325	0,9301	2,093	3,721
21	$\int (20) dz = K_p$	$(P/E) (I/20)^3$	0	0	0	0	0	0	0	0,2325	1,3951	4,4182	10,232
22	$(1) \cdot (21)$	$c_m P/E (I/20)^3$	0	0	0	0	0	0	0	1,2787	7,6731	24,3	56,276
23	$\int (22) dz$	$c_m P/E (I/20)^4 = P A_0$	0	0	0	0	0	0	0	1,2787	10,231	42,204	122,78
24	$(6) \cdot (21)$	$P A_0$			0				0				1979,9
25	$(7) \cdot (21)$	$c_m I A/E (I/20)^3$	0	0	0	0	0	0	0	0,89513	6,1384	21,8701	56,276
26	$\int (25) dz$	$P A_0 I$	0	0	0	0	0	0	0	0,89513	7,9287	35,937	114,08
27	$(9) \cdot (21)$	$P A_0 I$			0				0				1979,9
28	$(4) \cdot 791$	$c_m (I/20)^2 I$			30,058				59,009				31,007
29	$(28) \cdot (20)$	$P P_0 I$			0				0				115,38

Commas represent decimal points.

TABLE (cont.)

Ordinal number	Function	Multiplying factor	$z=0$	0,1	0,2	0,3	0,4	0,5	0,6	0,7	0,8	0,9	1,0
30	$K_p'(0) \cdot z$	$(Q_m/E) (l/20)^3$	0	-116	-2,32	-3,48	-4,64	-5,8	-6,96	-8,12	-9,28	-10,44	-11,6
31	$(21) + (30) + K_p(0) = K_p$	$(Q_m/E) (l/20)^3$	2,46	1,3	0,14	-1,02	-218	-3,34	-4,5	-5,4275	-5,4249	-3,5618	1,092
32	$K_p(31) \cdot 0,3 \cdot 92$	$P \cdot 10^{-5}$	0,96432	0,5096	0,0549	-0,3998	-0,8546	-1,3093	-1,764	-2,1276	-2,1266	-1,3062	0,4281
33	$K_p = (31)/(32)_{z=0,9}$	$P \cdot 10^{-5} (-2,1266) = A_1$	-0,4535	-0,2396	-0,02582	0,188	0,4019	0,6157	0,8295	1,0004	1,0	0,6565	-0,2013
34	$(20) + K_p(0)/20$	$(Q_m/E) (l/20)^2$			-0,58				-0,58				3,141
35	$(34) \cdot 0,196$	$P \cdot 10^{-5}$			-0,11368				-0,11368				0,61564
36	$K_p' = (35)/(32)_{z=0,8}$	$A_1$			0,05346				0,05346				-0,2895
37	$\alpha K_p = \alpha y_0$	$\alpha A_1$	-0,4535										
38	$\Sigma \alpha y_0 = \Sigma(37)$	$\alpha A_1$											
39	$\int (38) dz$	$\alpha A \cdot l/20$											
83	$y_1$	$1_1$	181,04	181,04	181,04	13,85	-35,9	-71,57	-84,4	-60,27	-29,64	24,62	84,84
84	$y'$	$A_1$			-13,81				0,176				15,18
Fourth approximation													
37	$\alpha y_1$	$\alpha A_1$	181,04	0	0	0	0	0	0	0	-29,847	0	
38	$\Sigma \alpha y_1 = \Sigma \alpha y_1$	$\alpha \cdot 1_1$	181,04	181,04	181,04	181,04	181,04	181,04	181,04	181,04	151,19	151,19	151,19
39	$\int (38) dz$	$\alpha A_1 \cdot (l/20)$	0	362,08	724,16	1086,2	1448,3	1810,4	2172,5	2534,6	2896,6	3199,0	3501,4
40	$(39)/(2)$	$(\alpha A_1/E) (l/20)$	0	66,32	132,64	166,3	168,4	210,51	252,61	294,72	336,81	371,97	407,13
41	$\int (40) dz$	$(\alpha A_1/E) (l/20)^2$	0	66,32	216,84	427,34	722,04	1101	1564,1	2111,4	2742,9	3451,7	4230,8
42	$\int (41) dz$	$(\alpha A_1/E) (l/20)^3$	0	66,32	349,48	993,66	2143,0	3966,1	6681,2	10307	15161	21355	29038
43	$(1) \cdot (42)$	$(\alpha A_1 Q_m/E) (l/20)^3$	0	313,03	1522,1	5465,1	117,87	21814	36472	56689	83386	117453	159709
44	$\int (43) dz$	$\alpha A_0 A_1$	0	313,03	2548,2	9935,4	27187	60788	119174	212335	352410	553249	830411
45	$(6) \cdot (42)$	$\alpha A_0 A$			57,24				2354076				5618851
46	$(43) \cdot z$	$(\alpha A_1 Q_m/E) (l/20)^3 l$	0	31,303	384,42	1639,5	4714,8	10907	21888	39682	66709	105708	159709
47	$\int (46) dz$	$\alpha A_1 A_0 l$	0	31,303	447,03	2470,9	8825,2	24447	57237	118802	225193	397610	663027
48	$(45) \cdot z$	$\alpha A_1 A_0 l$			13525				1412446				5618853
49	$(28) \cdot (41)$	$\alpha A_1 A_0 l$			6517,8				92296				131184
50	$K_{xy}'(0) \cdot z$	$(A_1 \alpha/E) (l/20)^3$	0	-3445,6	-6891,2	-10337	-13782	-17228	-20674	-24119	-27565	-31010	-34456
51	$(42) + (50) + K(0) = K_{xy}$	$(A_1 \alpha/E) (l/20)^3$	9845,6	6466,3	3303,9	508,26	-1793,4	-3416,3	-4197,2	-3966,4	-2558,4	190,6	4428
52	$(51) \cdot 0,0373 \cdot 10^{-2} = \omega K_{xy}$	$A_1$	3,672	2,412	1,232	0,187	-0,669	-1,274	-1,566	-1,479	-0,954	0,0711	1,652
53	$(41) + \frac{K_{xy}'(0)}{20} = K_{xy}'$	$(\alpha A_1/E) (l/20)^2$			-1505,96				-158,7				2508,0
54	$(53) \cdot 0,01865 \cdot 10^{-2} = \omega K_{xy}'$	$A_1$			-0,281				-0,0296				0,468
55	$(1) \cdot y_1$	$Q_m A_1$	711,49	588,02	378,35	76,208	-197,5	-393,64	-464,27	-381,02	-164,16	135,45	466,61
56	$\int (55) dz$	$Q_m A_1 (l/20)$	0	1299,5	2265,9	2720,4	2599,2	2008	1150,1	304,81	-240,37	-269,08	332,98
57	$(6) \cdot y_1$	$Q_m A_1 (l/20)$			13311				-29966				16416

TABLE (cont.)

Ordinal number	Function	Multiplying factor	z=0	0,1	0,2	0,3	0,4	0,5	0,6	0,7	0,8	0,9	1,0
58	$\Sigma(57)$	$Q_m A_1 (1/20)$	0	0	13311 0	13311	13311	13311	—16655 13311	—16655	—16655	—16555	—239 —16655
59	$(56) + (58)$	$Q_m A_1 (1/20)$	0	1299,5	15577 2295,9	16031	15910	15319	—15505 14461	—16350	—16415	—16386	93,98 —16322
60	$\int (59) dx$	$Q_m A_1 (1/20)^2$	0	1299,5	4864,9	36473	68414	99644	129133	97568	64803	32002	—706,0
61	$40(28) \cdot u_3$	$Q_m A_1 (1/20)^2$			—16004				415,44				18828
62	$\Sigma(61)$	$Q_m A_1 (1/20)^2$	0	0	—16564 0	—16004	—16604	—16604	—16159 —16004	—16189	—16189	—16189	2639 —16189
63	$(60) + (62)$	$Q_m A_1 (1/20)^2$	0	1299,5	—11739 4864,9	16031	51810	83679	113234 113819	81379	48644	15813	1933 —16295
64	$(63)/(2)$	$(Q_m A_1/E)(1/20)^2$	0	238,0	—1325 565,68	2319,3	60244	9655,6	13166 13118	9462,6	5652,7	18387	224,76 —1664,5
65	$\int (64) dx$	$(Q_m A_1/E)(1/20)^3$	0	238,0	1041,7	1667,0	10322	26002	48775	71404	86519	94011	93885
66	$\int (65) dx$	$A_1 A_0$	0	238,0	1517,7	4546,4	16855	53179	127956	248135	406058	586588	774484
67	$(1) \cdot (66)$	$Q_m A_1 A_0$	0	1123,4	8347,4	25005	92703	292485	703758	1364743	2233319	3226234	4259662
68	$\int (67) dx$	$Q_m A_1 A_0 (1/20)$	0	1123,4	10504	47947	161655	546843	1543086	3611587	7206649	12669202	20155098
69	$(6) \cdot (66)$	$Q_m A_1 A_0 (1/20)$			243675				45424380				149862654
70	$(67) \cdot z$	$Q_m A_1 A_0 z$	0	112,34	1669,5	7501,5	37081	146243	422255	955320	1786655	2903611	1256662
71	$\int (70) dx$	$Q_m A_1 A_0 z (1/20)$	0	11234	1894,2	11065	55648	238972	807470	2185045	4927020	9617286	16780559
72	$(69) \cdot z$	$Q_m A_1 A_0 z (1/20)$			58735				27254628				149862654
73	$(28) \cdot (65)$	$Q_m A_1 A_0 z (1/20)$			31311				2878164				2911092
74	$K'_y(0) \cdot z$	$A_1 A_0$	0	—93403,3	—186807	—280210	—373613	—467017	—560420	—653823	—747226	—840630	—934033
75	$(65) + (74) + K'_y(0) = K_y$	$A_1 A_0$	296031	202866	110742	20367	—60727	—117807	—136433	—109657	—45137	—41989	136482
76	$(75) \cdot 623,4 \cdot 10^{-6} = K_y \omega^2$	$A_1$	184,55	126,47	69,037	12,7	—37,86	—73,44	—85,05	—68,36	28,138	26,177	85,083
77	$(65) + K'_y(0)/20 = K'_y$	$(Q_m A_1/E)(1/20)^3$			—45660				2073				47183
78	$(77) \cdot 311,5 \cdot 10^{-6} = K'_y \omega^2$	$A_1$			—14,223				0,646				14,698
79	$D_3(52)$	$A_1$	3,849	2,528	1,291	0,196	—0,701	—1,335	—1,641	—1,55	—1,0	0,0745	1,742
80	$(79) + (33) = x_3$	$A_1$	3,396	2,288	1,265	0,384	—0,299	—0,719	—0,812	—0,55	0	0,731	1,521
81	$D_3 \cdot (54)$	$A_1$			—0,295				—0,03103				2,491
82	$(81) + (36) = x'_4$	$A_1$			—0,242				—0,02243				0,2015
83	$D_4 \cdot (76) = y_3$	$A_1$	193,45	132,57	72,365	13,312	—39,695	—76,98	—89,149	—71,655	—29,494	27,44	89,184
84	$D_4 \cdot (78) = y'_4$	$A_1$			—14,91				0,677				15,406
85	$ x_1 ^2 =  80 ^2$	$A_1^2$	11,533	5,235	1,6002	0,1475	—0,0894	—0,517	—0,6593	—0,3025	0	0,5144	2,314
86	$ y_1 ^2 =  83 ^2$	$A_1^2$	37423	17575	5236,7	177,21	—1575,7	—5925,7	—7947,5	—5134,4	—869,9	752,95	7053,8
87	$ 85  +  87 $	$A_1^2$	37434,5	175892	5238,3	177,36	—157579	—5926,4	—3948,2	—5134,7	—869,9	753,48	7056,1
88	$\sqrt{87}$	$A_1$	193,48	132,59	72,38	13,32	—39,7	—76,99	—89,15	—71,651	—29,5	27,45	89,19
89	$(88) \cdot A_1 = u$	$10^{-6}$	—4114,5	—2819,7	—1539,2	—283,26	—844,26	+1637,3	—1895,9	+1523,7	+627,35	—543,75	—1896,7
90	$\arctan(84)/(80)$	$\arctan$	56,964	57,941	57,205	34,666	132,75	107,061	99,78	130,28	∞	37,517	58,252
91	$\varphi$	1	89°	89°01'	80°	88°21'	89°34'	89°28'	89°29'	89°33	90°	88°28'	89°1'

$$m = (5)_{z-1} + \sum_1^3 (6) = 848,8$$

$$n = (8)_{z-1} + \sum_1^3 (9) = 500$$

$$q = (13)_{z-1} + \sum_1^3 (14) - \sum_1^3 (16) = 359,9$$

$$n^2 - mq = -55483$$

$$A_0 = \frac{qm}{E} \left( \frac{l}{20} \right)^4 = \frac{7,9 \cdot 10^{-6}}{2,04 \cdot 10^6} \left( \frac{40}{20} \right)^4 = 62 \cdot 10^{-12} \text{ Кг. м/Н}$$

$$a_p = (23)_{z-1} + \sum_1^1 (24) = 128,78 + 1979,9 = 210268$$

$$b_p = (26)_{z-1} + \sum_1^1 (27) - \sum_1^1 (29) = 114,08 + 1979,9 - 115,38 = 1978,6$$

$$\frac{\left( b_p + \frac{z_p}{A_0 \omega^2} \right) m - \left( a_p + \frac{1}{A_0 \omega^2} \right) n}{n^2 - mq} = K'_p(0)$$

$$K'_p(0) = \frac{\frac{0,6}{(1978,6 + 62 \cdot 10^{-12} \cdot 31712)} - 848,8 - \left( 2102,68 + \frac{1}{62 \cdot 10^{-12} \cdot 31712} \right)}{-55483} = -11,6$$

$$K_p(0) = \frac{\left( a_p + \frac{1}{A_0 \omega^2} \right) q - \left( b_p + \frac{z_p}{A_0 \omega^2} \right) n}{n^2 - mq} =$$

$$= \frac{\left( 2102,68 + \frac{1}{62 \cdot 10^{-12} \cdot 31712} \right) \cdot 359,9 - \left( 1978,6 + \frac{0,6}{62 \cdot 10^{-12} \cdot 31712} \right) 500}{55483} = 2,46$$

$$a_{ay} = (44)_{z-1} + \sum_1^3 (45) = 830411 + 8040553 = 8870964$$

$$b_{ay} = (47)_{z-1} + \sum_1^3 (48) - \sum_1^3 (49) = 663027 + 7044824 = 229998 = 7477853$$

$$a_{ay} = (44)_{z-1} + \sum_1^3 (45) = 830411 + 8040553 = 8870964$$

$$b_{ay} = (47)_{z-1} + \sum_1^3 (48) - \sum_1^3 (49) = 663027 + 7044824 - 229998 = 7477853$$

$$K'_{ay}(0) = \frac{b_{ay}m - a_{ay}n}{n^2 - mq} = \frac{7477853 \cdot 848,8 - 8870964 \cdot 500}{-55483} = -34456$$

$$K_{ay}(0) = \frac{a_{ay}q - b_{ay}n}{n^2 - mq} = \frac{8870964 \cdot 359,9 - 7477853 \cdot 500}{-55483} = 9845,6$$

$$K'_{ay}(0)/20 = -1722,8$$

$$a = (68)_{z-1} + \sum_1^3 (69) = 20155098 + 195580709 = 215735807$$

$$b = (71)_{z-1} + \sum_1^3 (72) - \sum_1^3 (73) = 16780559 + 177176017 - 5820567 = 188136009$$

$$K'_y(0) = \frac{b_y m - a_y n}{n^2 - mq} = \frac{188136009 \cdot 848,8 - 215735807 \cdot 500}{-55483} = -934033$$

$$K_y(0) = \frac{a_y q - b_y n}{n^2 - mq} = \frac{215735807 \cdot 359,9 - 188136009 \cdot 500}{-55483} = 296031$$

$$K'_y(0)/20 = -46702$$

$$D_4 = - \frac{(33)}{(52)} \Big|_{z=0,8} = - \frac{1}{(-0,954)} = 1,0482$$

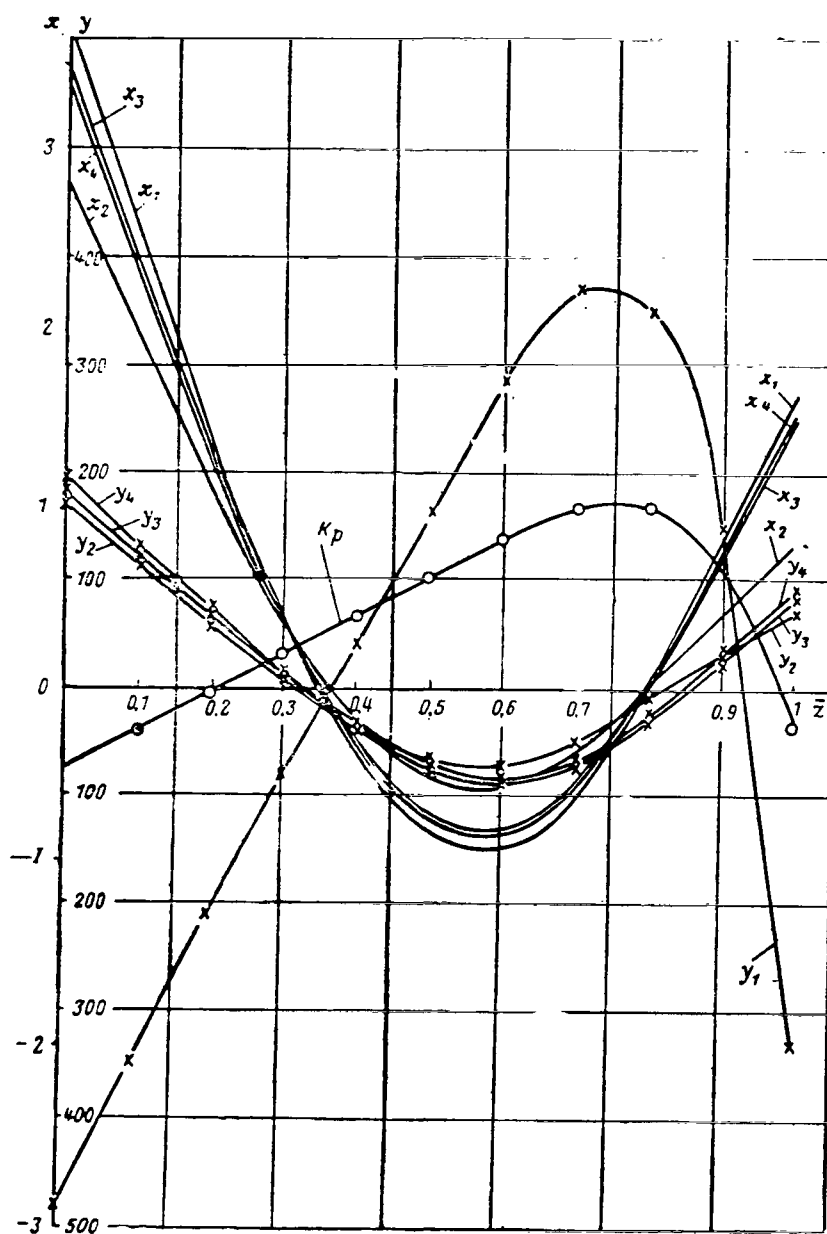


Fig. 2. Modes of the Elastic Curves of a Shaft in Successive Approximations.

In lines 37 through 54 we determine the operators  $\omega \underline{K}_{\alpha y}$  and  $\omega \underline{K}'_{\alpha y}$ . /71  
 Constants  $\underline{a}_{\alpha y}$ ,  $\underline{b}_{\alpha y}$ ,  $\underline{K}'_{\alpha y}(0)$  and  $\underline{K}_{\alpha y}(0)$  are to the left of the columns  
 of the table.

Coefficients  $0.0373 \cdot 10^{-2}$  and  $0.01865 \cdot 10^{-2}$  in lines 52 and 54 are  $(\alpha / \underline{E})$  expressions  $(l / 20)^3$  and  $(\alpha / \underline{E}) (l / 20)^2$ , factored out from the respective "multipliers" of lines 51 and 53 and multiplied by  $\omega = 3171$ .

Since  $\underline{K}'_{\alpha \underline{y}}(0)$ , the multiplier of which is  $(\alpha \underline{A}_1 20 / \underline{E})(l / 20)^2$ , is added to the multiplier  $(\alpha \underline{A}_1 / \underline{E})(l / 20)^2$  in line 41, it is multiplied by  $1/20$ .

4. In lines 55-78 we determine, by analogy with the preceding,  $\omega^2 \underline{K}_{\underline{y}}$  and  $\omega^2 \underline{K}'_{\underline{y}}$ . Coefficient  $623.4 \cdot 10^{-6}$  of line 76 is the expression  $\underline{A}_0 = (\rho \underline{m} / \underline{E})(l / 20)^3$  factored out from the "multiplier" of line 75, and multiplied by 3171; coefficient  $311.5 \cdot 10^{-6}$  of line 78 is the expression  $(\rho \underline{m} / \underline{E})(l / 20)^3$  from the "multiplier" of line 77 multiplied by  $\omega^2$ .

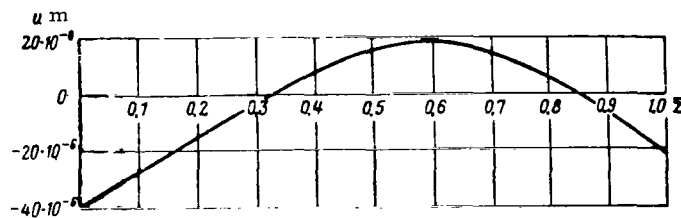


Fig. 3. Deflections of a Rotating System.

The coefficient of conformal iteration  $\underline{D}$  is determined from Eq. (24) over the normed section of the shaft  $\underline{z} = 0.8$ .

5. In lines 79-84 we determine  $\underline{x}_4$  and  $\underline{y}_4$  (as well as  $\underline{x}'_4$  and  $\underline{y}'_4$ ) from Eqs. (25). Figure 2 shows the elastic curves of the shaft in the successive approximations, where it can be seen that these curves are practically identical in the third and fourth approximations.

6. In lines 85 through 91 we determine, from Eqs. (33) and (34), the total deflections of the shaft and the phase angles.

The deflections of a rotating system produced by periodic force  $\underline{P} = 1$  are shown graphically in Fig. 3.

Calculations for the preresonance and beyond-resonance conditions are performed in approximately the same manner. In the first case they are calculated using Eqs. (23) and in the second, using Eqs. (27).

#### SUMMARY

An integral method was developed for calculating the vibrations of a free shaft, taking into account viscous friction.

The formulas thus obtained can be used to calculate the amplitude-frequency characteristic of a rotating shaft, taking into account the distribution of masses and the effect of gyroscopic moments of the disks. In the numerical example presented, the system has two damping devices, but the method developed can also be used for a system with a large number of damping devices.

#### REFERENCES

1. Belyayev, N.M. Soprotivleniye materialov [Strength of Materials]. GITL Press, 1953.
2. Gurov, A.F. Izgibnyye kolebaniya detaley i uzlov aviatsionnykh gazoturbinnykh dvigateley [Flexural Vibrations of Parts and Sub-assemblies of Aircraft Gas-Turbine Engines]. Oborongiz Press, 1959.
3. Tikhonov, A.N. and Samarskiy, A.A. Uravneniya matematicheskoy fiziki [Equations of Mathematical Physics]. Gostekhizdat Press, 1953.
4. Chan-che-Wen. Izgibnyye kolebaniya vrashchayushchegosya rotora na uprugo-demp fernoy opore [Flexural Vibrations of a Rotating Rotor on a Hydraulic Damping Mounting]. Trudy MAI, Issue, 136. Oborongiz Press, 1961.

## SELF-INDUCED VIBRATIONS OF AXIAL-COMPRESSOR BLADES

Candidate of Technical Sciences I.M. Movshovich

Stages of modern axial compressors, which have a large capacity, /73 are subjected to high loads and operate over a wide range of reduced rpm pass, when operating under nondesign conditions, through a region where the blade profiles are streamlined under large angles of attack. Under these conditions self-induced (natural) vibrations arise in some of the stages. Experimental studies of natural vibrations performed when adjusting gas turbine engines have brought to light many features characteristic of this phenomenon.

When natural vibrations ensue, one or several blades start to vibrate first and then the vibrations extend to the entire blading stage. Steady-state flexural natural vibrations then exist simultaneously in all the blades of the stage. All the blades of the stage vibrate with the same frequency but with different phases. Here one can observe an appreciable scatter of vibration stresses in individual blades of a given blading stage.

Different blading stages of the same design start to vibrate at different flow pressures at the compressor intake. This pressure is called the initial pressure. The initial pressure inducing natural vibrations is a particular property of the given blading set. The scatter in these pressures may be as high as 200-300%. When the pressure is increased above the initial, the amplitude of natural vibrations increases rapidly to dangerous levels. Hence an engine certified for service should not have natural vibrations in the operating rpm range.

### THE AMPLITUDE-FREQUENCY EQUATION

Due to the unavoidable dimensional deviations inherent in any manufacturing process, the natural frequencies of torsional vibrations of blades have a scatter of as much as 5-10%; however, as was noted above, in self-induced vibrations each blade does not vibrate with its own natural frequency, but rather with a frequency common to the entire blading stage. The appearance of this common frequency is due to interaction between the vibrating blades, hence mathematical description of natural vibrations of blades in a cascade requires consideration of a system with many degrees of freedom. /74 In the general case this will be a system of nonlinear equations, containing as many independent variables and, consequently, as many equations, as there are blades in the cascade. Solution of such a system of equations, although not difficult in principle, requires extremely cumbersome calculations and can be obtained only on computers. The problem is made more complicated by the fact that the aerodynamic and mechanical interaction of the blades vibrating in a cascade has not been sufficiently well investigated. Hence, in order to construct its first approximation, it is advantageous to consider the motion of each blade separately, by replacing the effect of neighboring blades by an external periodic force, the frequency of which is equal to the frequency of vibrations of the entire blading. In this manner the problem reduces to forced vibrations of a self-excited system with one degree of freedom.

We shall assume the simplest scheme of purely flexural vibrations and we shall consider the vibrations of a profile which has the reduced mass of the entire blade and the aerodynamic characteristics of its peripheral cross section. We shall also make use of the "steady-state hypothesis" for aerodynamic forces on the vibrating profile. Under these conditions the equation of motion for the profile has the form

$$m \frac{d^2 z}{dt^2} + \gamma z + P_{fr} - P_a = F \cos \omega_0 t, \quad (1)$$

where  $P_{fr} = \alpha z^2 \frac{dz}{dt}$  is the mechanical damping force in the material and in the blade root;

$P_a = \frac{1}{2} k_g M^2 \rho S [C_R(i) - C_R(i_0)]$  is the aerodynamic force;

$F \cos \omega_0 t$  is an external periodic force and

$C_R(i) = C_R(i_0) + \left( \frac{\partial C_R}{\partial i} \right)_0 \Delta i + \frac{1}{6} \left( \frac{\partial^3 C_R}{\partial i^3} \right)_0 \Delta i^3 + \dots$  is a force factor.

We introduce the notation:

$$\begin{aligned} \omega_i^2 &= \frac{\gamma}{m}; \quad \omega = \frac{\omega_l}{\omega_0}; \quad \tau = \omega_0 t; \\ C_1 &= \frac{1}{2} k_g M^2 \rho S \frac{\omega_0}{\omega} \left( \frac{\partial C_R}{\partial i} \right)_0; \quad C_3 = \frac{1}{12} k_g M^2 \rho S \left( \frac{\omega_0}{\omega} \right)^3 \left( \frac{\partial^3 C_R}{\partial i^3} \right)_0, \\ \frac{\omega^2}{\gamma} F &= \mu \lambda_0; \quad \omega^2 = 1 + \mu a; \quad -\frac{\omega^2}{\gamma} C_1 = \mu, \end{aligned}$$

where  $a$  is the mismatch between the frequency of the external force and the natural frequency and  $\lambda_0$  is the reduced amplitude of the external

force. Then we will get the following nonlinear differential equation

$$\ddot{z} + z = \mu \left[ \lambda_0 \cos \tau - a z + \frac{a}{C_1} z^2 \dot{z} + \frac{C_3}{C_1} \dot{z}^3 + \dot{z} \right]. \quad (2)$$

An estimate of parameter  $\mu$  for an ordinary compressor stage yields  $\mu = 0.05$ , which means that the problem can be solved as a quasilinear problem. /75

Periodic solutions of this equation were first considered by Van-der-Pol, after whom this equation has been named. A detailed study of periodic solutions of the Van-der-Pol equation was presented by A.A. Andronov and A.A. Vitt [1]. They have determined the range of "capture" of the natural frequency of the system by the frequency of the external force and the range of combined vibrations, when the natural frequency of the system and the frequency of the applied force exist side by side, and they have mapped out the stability boundaries for both ranges. The

parameter which denotes transition from one range to another is the limiting frequency mismatch  $\underline{a}_{\text{lim}}$ . In the case of moderate frequency

mismatch, the frequency is "captured"; when the mismatch increases, combined vibrations arise.

#### Case of Small Frequency Mismatch

We shall first consider steady-state vibrations with small frequency mismatch and we shall, consequently, seek the periodic solutions of Eq. (2) with an external force period of  $2\pi$  in the form

$$z = z_0 + \mu z_1 + \mu^2 z_2 + \dots$$

When  $\mu = 0$ , we get the linear generating equation

$$\ddot{z}_0 + z_0 = 0, \quad (3)$$

the general solution of which has the form

$$z_0 = M_0 \sin \tau + N_0 \cos \tau. \quad (4)$$

$\underline{M}_0$  and  $\underline{N}_0$  will be found from the assumption that the second approximation

$$z = z_0 + \mu z_1 \quad (5)$$

is also periodic. Substituting solution (5) into Eq. (2), and equating the coefficients of terms incorporating  $\mu$  to the first power, we will get

$$\ddot{z}_1 + z_1 = \lambda_0 \cos \tau - a z_0 + \frac{a}{C_1} z_0^2 \dot{z}_0 + \dot{z}_0 + \frac{C_3}{C_1} \dot{z}_0^3. \quad (6)$$

Substituting the above expression into Eq. (4), we get

$$\begin{aligned} \ddot{z}_1 + z_1 = & \left[ \lambda_0 - a N_0 + M_0 + \frac{1}{4} \frac{a}{C_1} M_0^3 + \frac{1}{4} \frac{a}{C_1} M_0 N_0^2 + \right. \\ & + \frac{3}{4} \frac{C_3}{C_1} M_0 N_0^2 + \frac{3}{4} \frac{C_3}{C_1} M_0^3 \left. \right] \cos \tau + \left[ -a M_0 - N_0 - \frac{1}{4} \frac{a}{C_1} M_0^2 N_0 - \right. \\ & - \frac{1}{4} \frac{a}{C_1} N_0^3 - \frac{3}{4} \frac{C_3}{C_1} M_0^2 N_0 - \frac{3}{4} \frac{C_3}{C_1} N_0^3 \left. \right] \sin \tau + F_1 \cos 2\tau + \\ & + F_2 \sin 2\tau + F_3 \cos 3\tau + F_4 \sin 3\tau + F_5, \end{aligned} \quad (7)$$

where  $\underline{F}_1$ ,  $\underline{F}_2$ ,  $\underline{F}_3$ ,  $\underline{F}_4$  and  $\underline{F}_5$  are polynomials in  $\underline{M}_0$  and  $\underline{N}_0$ , which are /76  
time-independent. In order that  $\underline{z}_1$  obtained from Eq. (7) be periodic, the coefficients of  $\cos \tau$  and  $\sin \tau$  must be zero:

$$\left\{ \begin{array}{l} P(M_0, N_0) = \lambda_0 - aN_0 + M_0 + \frac{1}{4} \frac{a}{C_1} M_0^3 + \frac{1}{4} \frac{a}{C_1} M_0 N_0^2 + \\ \quad + \frac{3}{4} \frac{C_3}{C_1} M_0 N_0^2 + \frac{3}{4} \frac{C_3}{C_1} M_0^3 = 0; \\ Q(M_0, N_0) = -aM_0 - N_0 - \frac{1}{4} \frac{a}{C_1} M_0^2 N_0 - \frac{1}{4} \frac{a}{C_1} N_0^3 - \\ \quad - \frac{3}{4} \frac{C_3}{C_1} M_0^2 N_0 - \frac{3}{4} \frac{C_3}{C_1} N_0^3 = 0 \end{array} \right\} \quad (8)$$

We denote

$$\left. \begin{array}{l} M_0 = A \sin \varphi; \\ N_0 = A \cos \varphi, \end{array} \right\} \quad (9)$$

then  $A$  is the amplitude of vibrations from the first approximation and  $\varphi$  is the phase difference between the external force and the displacement of the vibrating blade.

Then the solution of system (8) will have the form

$$\begin{aligned} k\lambda_0^2 &= kA^2 \left[ a^2 + \left( 1 - \frac{kA^2}{4} \right)^2 \right]; \\ \tan \varphi &= - \frac{1 - \frac{kA^2}{4}}{a}, \end{aligned} \quad (10)$$

where  $\underline{k} = -(\underline{\alpha}/\underline{C}_1 + 3\underline{C}_3/\underline{C}_1)$ . The above solution is the amplitude-

frequency equation of induced vibrations in a self-excited system.

The Lyapunov stability conditions for periodic solutions of Eq. (2) yield the following inequalities [1]:

$$-\frac{\partial P}{\partial M_0} + \frac{\partial Q}{\partial N_0} \leq 0; \quad (11)$$

$$\frac{\partial(P, Q)}{\partial(M_0, N_0)} = \begin{vmatrix} \frac{\partial P}{\partial M_0} & \frac{\partial Q}{\partial M_0} \\ \frac{\partial P}{\partial N_0} & \frac{\partial Q}{\partial N_0} \end{vmatrix} < 0, \quad (12)$$

which in terms of  $A$  and  $\varphi$  give, respectively,

$$kA^2 \geq 2 \quad (13)$$

and

$$\frac{3}{16} k^2 A^4 - kA^2 + a^2 + 1 > 0. \quad (14)$$

The last two expressions yield conditions for the existence of stable /77  
periodic solutions, i.e., conditions under which it is possible for a  
self-excited system to vibrate with the frequency of the external force  
which "captures" the natural frequency of the system.

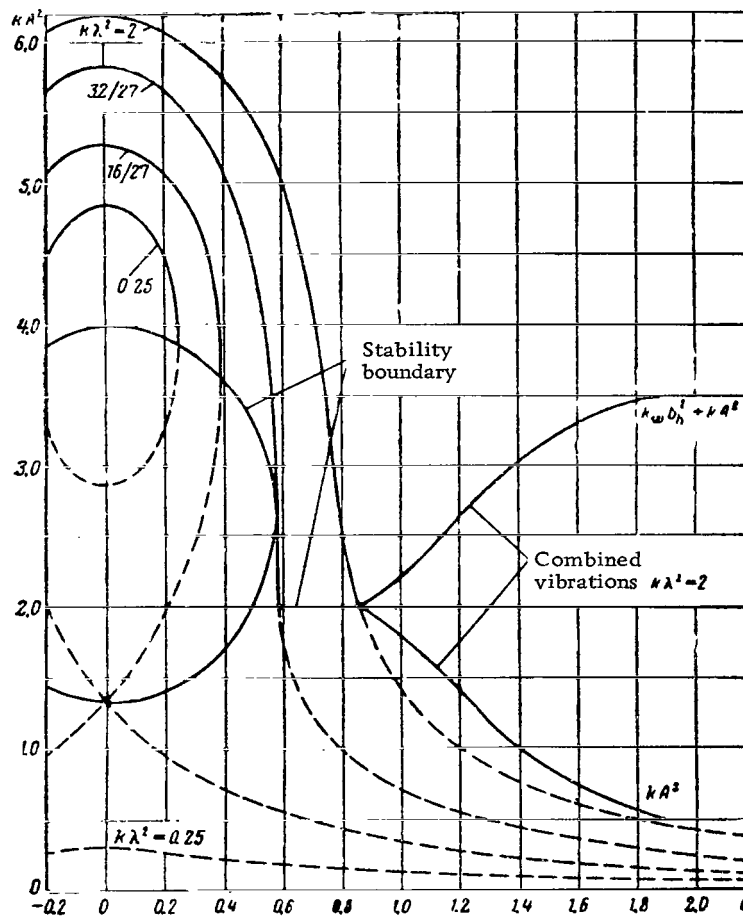


Fig. 1. Amplitude-frequency Curves for Compressor  
Blades.

Figure 1 depicts amplitude-frequency curves corresponding to periodic  
solution (10). They also show the stability boundaries corresponding to  
conditions (13) and (14). It can be seen that for any magnitude of the  
external force  $k\lambda^2$ , it is possible to find a frequency mismatch such that /78  
Eq. (13) will be violated. This is precisely the limiting frequency mis-  
match. When the frequency mismatch is higher than the limiting, combined  
vibrations set in.

### Case of Large Frequency Mismatch

We write Eq. (1) in the form

$$\ddot{z} + z\omega^2 + \frac{\omega^2}{x} az^2\dot{z} + \frac{\omega^2}{x} C_1\dot{z} + \frac{\omega^2}{x} C_3\dot{z}^3 = F \frac{\omega^2}{x} \cos \tau; \quad (15)$$

the notation here is that previously used.

Following Stoker's presentation [3], we shall seek the solution for combined vibrations in the form

$$z = b_f \cos \omega \tau + A \cos(\tau - \varphi); \quad (16)$$

here  $\underline{b_f}$  is the amplitude of vibrations at the natural frequency,

measured in the new time scale.

Substituting Eq. (16) into Eq. (15) and equating the coefficients of  $\sin \omega \tau$ ,  $\cos \omega \tau$ ,  $\sin \tau$  and  $\cos \tau$  in the right and left-hand sides of equations, we will get, after simple transformations:

$$k\lambda_0^2 = kA^2 \left[ a^2 + \left( 1 - \frac{2k_\omega b_f^2 + kA^2}{4} \right)^2 \right]; \quad (17)$$

$$k_\omega b_f^2 + 2kA^2 = 4; \quad (18)$$

$$\tan \varphi = - \frac{1 - \frac{2k_\omega b_f^2 + kA^2}{4}}{a} \quad (19)$$

The only new notation here is

$$k_\omega = - \left( \frac{a}{C_1} + 3 \frac{C_3}{C_1} \omega^2 \right).$$

Conditions (17) and (19), together with Eq. (18), yield

$$k\lambda_0^2 = kA^2 \left[ a^2 + \left( 1 - \frac{3kA^2}{4} \right)^2 \right] \quad (20)$$

and

$$\tan \varphi = - \frac{1 - \frac{3kA^2}{4}}{a}. \quad (21)$$

Equations (20) and (21) are the amplitude-frequency equations of combined vibrations written in terms of the amplitude of these vibrations which have the frequency of the external force. Combined vibrations must satisfy Eq. (18), for which reason it is also possible to write similar equations for the amplitude of vibrations which have the frequency of free vibrations. /79

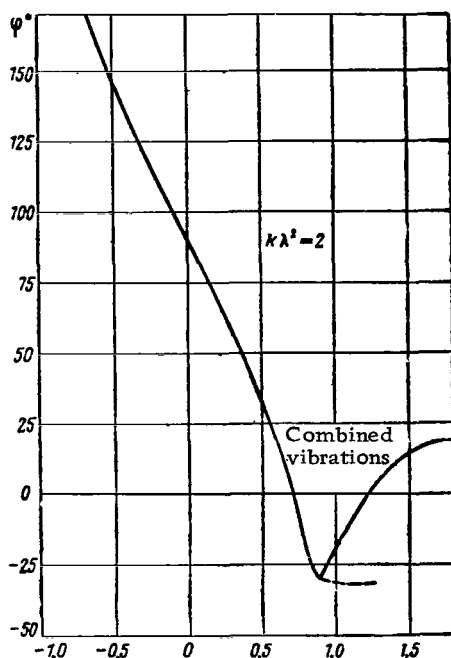


Fig. 2. Phase Differences between Vibrating Blades.

well as the combined amplitudes  $\underline{kA}^2 + \frac{k_b}{\omega - f}$

Studies of stability of combined vibrations yield the stability condition

$$kA^2 \leq 2. \quad (22)$$

The amplitude-frequency curves and phase shifts as a function of frequency mismatch are shown in Figs. 1 and 2, respectively. These curves make it possible to explain the scatter in vibration stresses and the phase shifts between vibrating blades which are observed in practice. If we assume that  $\mu = 0.05$ , then a scatter of natural frequencies within the limits of  $\pm 2.5\%$  corresponds to a frequency mismatch of  $\underline{a} = \pm 1$ , while a scatter of  $\pm 5\%$  corresponds to  $\underline{a} = \pm 2$ , i.e., it reaches a value which gives an appreciable scatter of the amplitude of vibrations and phase difference between the blades.

For the case of combined vibrations ( $\underline{kA}^2 \leq 2$ ), Fig. 1 shows amplitudes of vibrations with the frequency of the external force, as

#### ENERGY RELATIONSHIPS

We shall first consider the case of less than limiting frequency mismatch, and, using the approximate expression for the displacement of the blade as a function of time

$$z_0 = A \cos(\tau - \varphi),$$

we shall determine the work done by aerodynamic forces  $\underline{R}_a$  and the damping forces  $\underline{R}_{fr}$  in one vibration period, namely

$$R_a = -C_1 \pi A^2 \left( 1 + \frac{3}{4} \frac{C_3}{C_1} A^2 \right), \quad (23)$$

$$R_{fr} = -\frac{\pi a A^4}{4}. \quad (24)$$

By adding we get

/80

$$R = R_a + R_{fr} = -\pi C_1 A^2 \left(1 - \frac{k A^2}{4}\right). \quad (25)$$

The work of the external force applied to the blade is

$$R_{ext} = \pi A F \sin \varphi. \quad (26)$$

Expressing  $\sin \varphi$  in terms of  $\tan \varphi$  and using Eqs. (10), we get the following expression for the work performed by the external force

$$R_{ext} = \pi C_1 A^2 \left(1 - \frac{k A^2}{4}\right).$$

As should have been expected, the total work of all the forces under steady-state condition is zero, i.e.,

$$R_{ext} + R_a + R_{fr} = 0. \quad (27)$$

It follows from the above equation and from Eq. (25) that blades vibrating with amplitude

$$A = A_v = \sqrt{\frac{4}{k}}$$

operate, as it were, under equilibrium conditions, i.e., the work of the external force on these blades is zero. It can be determined from Eq. (10) which blades will have the so-called critical frequency mismatch

$$a_{cr} = \pm \sqrt{\lambda_0^2 \frac{k}{4}}. \quad (28)$$

Blades with frequency mismatch smaller than  $\underline{a_{cr}}$  have an amplitude greater than  $\underline{A_v}$  and consequently the total work of the aerodynamic and friction forces will be negative, i.e., the work of the friction forces exceeds the work of aerodynamic forces. In order to maintain vibrations in these blades, work must be supplied by an external periodic force. Analysis of phase shifts for blades with below-critical frequency mismatch shows that work from an external force is actually supplied to them. These blades will serve as "dampers" of their blading stage.

Blades with frequency mismatch greater than  $|\underline{a_{cr}}|$  have an amplitude smaller than  $\underline{A_v}$  and the total work of the aerodynamic and friction

forces will be positive, i.e., work of aerodynamic forces exceeds the work of friction forces, while the work of the external force is negative; consequently, the blades themselves supply work to the external force. In other words, they are the sources of the external force. The external force serves for transmitting the excess work of aerodynamic forces from these blades to the "damper" blades. These blades will be called "exciters."

It can be seen from Fig. 1 that the limiting frequency mismatch will always be greater than the critical; hence blades subjected to combined vibrations will also be exciter-type blades, but due to the fact that they vibrate with two frequencies, their energetics will be different.

The equation of motion for a blade with a frequency mismatch higher than the limiting, i.e.,

$$z_0 = b_f \cos \omega \tau + A \cos(\tau - \varphi), \quad (29)$$

will be used for determining the work of the aerodynamic and friction forces. The above expression describes, in the general case, when  $\omega$  is not commensurable with unity, an almost periodic motion, hence the work will be determined as an average from the following expressions

$$R_a = \lim_{\tau \rightarrow \infty} \frac{1}{\tau} \int_0^{\tau} P_a \dot{z}_0 d\tau; \quad (30)$$

$$R_{fr} = \lim_{\tau \rightarrow \infty} \frac{1}{\tau} \int_0^{\tau} P_{fr} \dot{z}_0 d\tau, \quad (31)$$

from which we get

$$R_a = -\frac{C_1}{2} \left[ \omega^2 b_f^2 + A^2 + \frac{C_3}{C_1} \left( \frac{3}{4} \omega^4 b_f^4 + 3\omega^2 b_f^2 A^2 + \frac{3}{4} A^4 \right) \right], \quad (32)$$

$$R_{fr} = -\frac{\alpha}{8} (\omega^2 b_f^4 + 2A^2 b_f^2 \omega^2 + 2A^2 b_f^2 + A^4). \quad (33)$$

Adding terms and using Eq. (18) will give the total work of the aerodynamic and damping [frictional] forces

$$R = R_a + R_{fr} = -\frac{C_1}{2} A^2 \left[ 1 - \frac{kA^2 + 2k_\omega b_f^2}{4} \right] = \frac{C_1}{2} A^2 \left( 1 + \frac{3kA^2}{4} \right). \quad (34)$$

For convenience, we shall refer the work in Eqs. (23)-(25) to a unit of time. Then

$$R_a = -\frac{C_1}{2} A^2 \left( 1 + \frac{3}{4} \frac{C_3}{C_1} A^2 \right) \quad (35)$$

$$R_{fr} = -\frac{a}{8} A^4; \quad (36)$$

$$R = R_a + R_{fr} = -\frac{C_1}{2} A^2 \left(1 - \frac{kA^2}{4}\right). \quad (37)$$

Since the natural frequencies of a blading set are random, then the initial pressure for self-induced vibrations, which depends on the ratio between the number of the damping and exciting blades, can have an appreciable scatter.

The blading set as a whole is not subject to any external forces, /82 for which reason we should also have the condition

$$\sum_i^n (R_a + R_{fr}) = 0. \quad (38)$$

We introduce still another assumption, namely, that an identical external periodic force acts on all the blades of the set, irrespective of their position in the disk. This in itself suffices for determining the initial self-induction pressure.

Using Eqs. (34), (37) and (38) and breaking up the blading set into groups with the same frequency mismatch relative to the common frequency of the set, we will get the following condition for absence of a periodic force in the set as a whole:

$$\sum_i^p m_i A_i^2 \left(1 - \frac{kA_i^2}{4}\right) + \sum_s^q n_s A_s^2 \left(1 + \frac{3}{4} kA_s^2\right) = 0, \quad (39)$$

where subscript i pertains to a blade with a lower-than-limiting frequency mismatch, m<sub>i</sub> is the number of blades in each group, and p is the

number of groups of such blades; correspondingly, s, n<sub>s</sub> and q will be

the subscript, number of blades in a group and number of groups for blades with a higher-than-limiting frequency mismatch. On the basis of our assumption that the external forces within the set are identical for all the blades, we will get as many equations such as Eqs. (40) and (41) as there are groups of blades:

$$k\dot{\gamma}_0^2 = kA_i^2 \left[ a_i^2 + \left(1 - \frac{kA_i^2}{4}\right)^2 \right] \quad (i=1, 2 \dots p); \quad (40)$$

$$k\dot{\gamma}_0^2 = kA_s^2 \left[ a_s^2 + \left(1 - \frac{3kA_s^2}{4}\right)^2 \right] \quad (s=1, 2 \dots q). \quad (41)$$

From the above two equations, together with Eq. (39), it is possible to determine  $\frac{kA^2}{2}$  for each group of blades and thus also the amplitude;

and if one also uses Eqs. (10) and (19), then it is possible to obtain the phase differences between the blades. The quantity  $k$  is a function of the pressure of self-induced vibrations, i.e., solution of Eqs. (39)-(41) also yields the initial self-induction pressure.

The initial pressure which is obtained by solving the above system of equations depends on the frequency of the entire set on which all the calculations were based. The frequency which will ensure a minimum initial self-induction pressure, i.e., minimum vibration stability of the set, will be precisely the frequency of vibrations of the blading. In the preliminary calculations we have for convenience assumed a common frequency which is equal to the arithmetic mean frequency of the blading set.

Calculations, which are not presented here due to space limitations, were performed for two arbitrarily assembled sets of blades. It was assumed for simplicity that each blading set consisted from three blade groups: wheel No. 1 held 18 blades with natural frequency of 273 cps, 4 with 280 cps and 18 with a frequency of 287 cps, which makes up three frequency groups, but only two groups with respect to frequency mismatch, i.e., one group containing 4 blades with mismatch of  $a_0 = 0$  /83

and 36 blades with mismatch  $a_1 = \pm 1$  (the sign of the separation does not affect the amplitude, i.e., the energetics of the blade). Wheel No. 2 contains 16 blades with frequency of 273 cps, 8 blades with 280 cps and 16 blades with a natural frequency of 287 cps, i.e.,  $m_0 = 8$  and

$a_0 = 0$  and  $m_1 = 32$  and  $a_1 = \pm 1$ , respectively.

Calculations for an ordinary, serially produced stage yields an initial pressure  $p_{in}$  of 700 mm Hg for the first wheel and  $p_{in}$  of 1260 mm of Hg for the second. If we imagine a set consisting of blades with the same natural frequencies, then  $p_{in} = 600$  mm of Hg.

## CONCLUSIONS

The assumed scheme for calculating self-induced vibrations in the presence of an external periodic force makes it possible to explain the scatter in vibration stresses in blades of the same blading set and the phase differences between the blades. Scatters in the initial pressure which are observed for sets of the same design are also explained in this manner.

The above analysis can also serve as a basis for practical conclusions, namely that if blades are matched up on the basis of their natural frequencies, then it is possible to tune all the blading sets to the upper level with respect to the initial pressure. The promise of this approach for elimination of self-induced vibrations is the fact that it does not require any substantial modification of design.

The above analysis has its shortcomings. Firstly, we have examined only a profile rather than a blade, secondly, consideration was given only to translational motion of the profile, while twisting of the latter was not considered. For these reasons the results which were obtained can be used only for comparison purposes, i.e., for clarifying the qualitative aspect of the problem.

#### REFERENCES

1. Andronov, A.A. and Vitt, A.A. Concerning the Mathematical Theory of "Capture." Zh. Prikl. Fiz., No. 4, 1930.
2. Malkin, I.G. Nekotoryye zadachi teorii nelineynykh kolebaniy [Some Problems of the Theory of Nonlinear Vibrations]. Gostekhizdat Press, 1956.
3. Stoker, J.J. Nonlinear Vibrations in Electrical and Mechanical Systems. Interscience, N.Y., 1950.

COMPUTATION OF VIBRATIONS OF VARIABLE-THICKNESS DISKS  
BY THE RITZ METHOD

Engineer A.V. Karpov

Vibrations of gas turbine engine components are attributable to many factors related to the processes which take place in these machines. Hence, designing a reliable unit with an extended service life requires one to study the possible vibrations of individual elements, as well as the engine system as a whole. /84

A large number of studies were performed (by A. Stodola, R.W. Southwell, A.V. Levin, A.D. Kovalenko, V.Ya. Natanzon, I.A. Birger, D.V. Khronin) on vibrations of turbomachine disks.

The importance and complexity of these calculations require further development and refinement of existing methods, in particular those based on the Lagrange and Hamilton principles. Variational methods for solving these problems are effective (from the point of view of reducing the volume of computations) in the case when consideration is given to the effect of the individual structural elements of the disk (rim, body, radial ribs) on the frequencies and modes of its vibrations; here some approaches make it possible to obtain formulas convenient for this kind of calculations, since the geometric parameters of the above elements are contained in them in the general form.

The present paper considers a variational method for designing variable-thickness disks with a rim and radial ribs. The suggested methods for solving the problem of vibrations of intricately-shaped disks can in principle be simplified and used for solving of other problems of disk vibrations.

FREE VIBRATIONS OF AN INTRICATELY-SHAPED NONROTATING DISK

According to Hamilton's principle, an elastic system which is in motion actually undergoes during a time interval  $t_0 - t_1$  displacements which are proportional to the extremum of the action integral  $J$ , where

$$J = \int_{t_0}^{t_1} (\bar{E} - K) dt, \quad (1)$$

where  $\bar{E}$  is the potential energy of the elastic system and  $K$  is its kinetic energy.

For the case of natural vibrations of a circular plate,  $\bar{E}$  is expressed as /85

$$\begin{aligned} \mathfrak{A} = & \frac{1}{2} \int_{r_0}^r \int_0^{2\pi} D \left( \left( \frac{\partial^2 W}{\partial r^2} + \frac{1}{r} \frac{\partial W}{\partial r} + \frac{1}{r^2} \frac{\partial^2 W}{\partial \theta^2} \right)^2 - \right. \\ & \left. - 2(1-\mu) \left[ \frac{\partial^2 W}{\partial r^2} \left( \frac{1}{r^2} \frac{\partial^2 W}{\partial \theta^2} + \frac{1}{r} \frac{\partial W}{\partial r} \right) - \left( \frac{1}{r} \frac{\partial^2 W}{\partial r \partial \theta} - \frac{1}{r^2} \frac{\partial W}{\partial \theta} \right)^2 \right] \right) r d\theta dr. \end{aligned} \quad (2)$$

Accordingly,  $\underline{K}$  is expressed as

$$K = \frac{\rho}{2} \int_{r_0}^r \int_0^{2\pi} h \left( \frac{\partial W}{\partial t} \right)^2 r d\theta dr, \quad (3)$$

where  $\underline{r}_0$  is the free radius of the inner circle of the disk,  $\underline{r}_{out}$  is its outside radius,  $\underline{D}$  is the cylindrical rigidity, variable over the radius;  $\underline{W}$  is the deflection of the middle plane;  $\mu$  is Poisson's ratio,  $\underline{r}$  and  $\theta$  are polar coordinates,  $\underline{h}$  is the thickness of the disk (which is variable along the radius), and  $\rho$  is the density of the disk material. The deflection  $\underline{W}$  will be represented in the form

$$W = u(r) \cos n \theta \cdot \cos pt, \quad (4)$$

where  $\underline{p}$  is the circular frequency of vibrations and  $\underline{n}$  is the number of nodal diameters.

Following Ritz, we seek the solution of Eq. (1) in the form

$$u = \sum_{l=1}^n a_l \varphi_l. \quad (5)$$

where  $\underline{a}_l$  are the sought coefficients and  $\underline{\varphi}_l$  is a suitable function

which satisfies, as a minimum, the geometric boundary conditions.

Since, according to Hamilton's principle, functional  $\underline{J}$  possesses extremal properties, then  $\delta \underline{J} = 0$ , or

$$\frac{\partial J}{\partial a_k} = 0. \quad (6)$$

We introduce the notation

$$\begin{aligned} \frac{\partial}{\partial a_k} \left( \frac{\partial^2 u}{\partial r^2} \right) &= \varphi_{krr}; \\ \frac{\partial}{\partial a_k} \left( \frac{\partial u}{\partial r} \right) &= \varphi_{kr}; \\ \frac{\partial}{\partial a_k} (u) &= \varphi_k. \end{aligned} \quad (7)$$

Substituting Eqs. (2)-(4) into Eq. (1), and using Eqs. (5)-(7), we get /86

$$\begin{aligned} & \int_{r_0}^r D \left\{ \left( \sum_{i=1}^n a_i \tilde{\varphi}_{ir} + \frac{1}{r} \sum_{i=1}^n a_i \tilde{\varphi}_{ir} - \frac{n^2}{r^2} \sum_{i=1}^n a_i \varphi_i \right) \times \right. \\ & \times \left( \varphi_{kr} + \frac{1}{r} \varphi_{kr} - \frac{n^2}{r^2} \varphi_k \right) (1 - \nu) \left[ \sum_{i=1}^n a_i \tilde{\varphi}_{ir} \left( \frac{1}{r} \varphi_{kr} - \frac{n^2}{r^2} \varphi_k \right) + \right. \\ & + \left( \frac{1}{r} \sum_{i=1}^n a_i \tilde{\varphi}_{ir} - \frac{n^2}{r^2} \sum_{i=1}^n a_i \varphi_i \right) \varphi_{kr} - n^2 \left( \frac{1}{r^2} \sum_{i=1}^n a_i \varphi_i - \right. \\ & \left. \left. - \frac{1}{r} \sum_{i=1}^n a_i \tilde{\varphi}_{ir} \right) \left( \frac{1}{r^2} \varphi_k - \frac{1}{r} \varphi_{kr} \right) \right] \Bigg\} r dr - \\ & - \rho p^2 \int_{r_0}^r h \left( \sum_{i=1}^n a_i \varphi_i \right) \varphi_k r dr = 0. \end{aligned} \quad (8)$$

The above expression is a system of homogeneous equations which has nonzero solutions in the case when the determinant made up of coefficients of  $\underline{a}_i$  is equal to zero. From this follows a frequency equation,

which serves for determining the natural frequency.

For intricately-shaped disks,  $\underline{D}$  and  $\underline{h}$  which are terms in Eqs. (8) are functions of radius  $\underline{r}_1$  and the usual method for solving the fre-

quency equation consists in integrating it by sections; here it is assumed that the rate of increase of the disk thickness along the radius is constant.

In real disks the number of such sections is large, requiring a correspondingly large amount of intermediate calculations. It is of interest to solve Eqs. (8) by a method which uses functions approximating the variable thickness of the disk (taking into account the rim and the radial ribs) in the range of radius variations  $\underline{r}_0$  to  $\underline{r}_{out}$ . For example,

for a disk with a linearly-variable body thickness one can use a combination of the following functions

$$\text{I. } \underline{h} = \underline{b} - \underline{k} \underline{r}$$

$$\text{II. } h = \sqrt[m]{\frac{r}{a}}, \text{ - where } \underline{m} \text{ is an odd number;}$$

$$\text{III. } h = e^{-\frac{1}{r^{\underline{m}_1}}} \text{ - where } \underline{m}_1 \text{ is an even number.}$$

Graphs of these functions with appropriate shift of the coordinate origin are represented in Fig. 1. The real thickness of the disk can be obtained with an accuracy sufficient for engineering calculations by adding up the abscissas of functions (I), (II) and (III) along the radius. /87

It should be noted that in 1928 Pichler proposed, for use in calculations related to the deflection of circular plates of variable thickness (without the rim and radial ribs), the exponential function

$y = e^{-\frac{\beta x^2}{6}}$  as an approximating relationship. Pichler pointed out that by appropriately selecting coefficient  $\beta$ , it is possible to describe a wide class of variable-thickness plates.

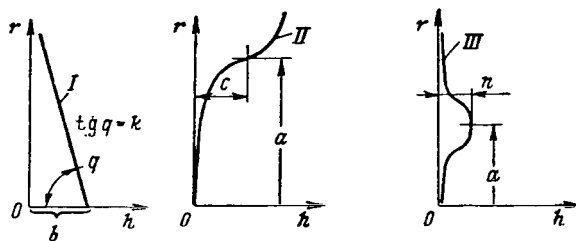


Fig. 1. Graphs of Functions Approximating the Variable Thickness of a Disk with a Rim and Radial Ribs.

Example. Let us find in the general form the frequency equation of a disk of linearly-varying thickness with a rim, the disk central bore radius being  $r_0$  (Fig. 2).

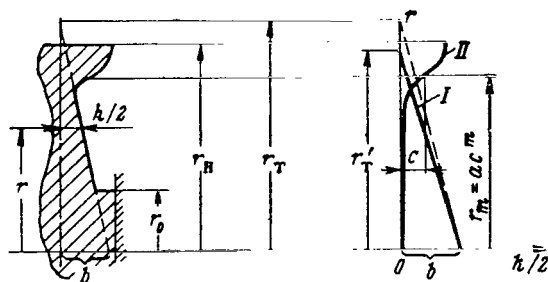


Fig. 2. Schematic Diagram of a Disk with Bore Radius  $r_0$ .

In this case functions (I) and (II) have the form

$$(h/2)_I = b - kr;$$

$$(h/2)_{II} = c + \sqrt[m]{\frac{r + aC^m}{a}}.$$

Quantity D has the form

/88

$$D = \frac{Eh^3}{12(1-\mu^2)} = 0,67 \frac{E \left( l - kr + \sqrt[m]{\frac{r - ac^m}{a}} \right)^3}{(1-\mu^2)} \quad (9)$$

where

$$l = b + c.$$

We select

$$\zeta_i = (r - r_0)^{i+1}; \quad u = \sum_{i=1}^n a_i (r - r_0)^{i+1}. \quad (10)$$

As is shown by calculations, this selection of the function for deflection of the middle surface gives, in many cases encountered in practice, the circular frequency p (5-10% for i = 1 and 3-5% for i = 2) with an accuracy sufficient for engineering purposes. We assume further that the disk profile is sufficiently well approximated by a third-order parabola (disks with smooth transition from the disk body to the rim when the ratio of the average disk thickness to the rim thickness is more than 1/3). Then, restricting ourselves to i = 1 and assuming  $\mu = 0.3$ , we get

$$\begin{aligned} & \frac{0,67 E}{1-\mu^2} \int_{r_0}^H \left( l - kr + \sqrt[3]{\frac{r - ac^3}{a}} \right)^3 [(4 - n^2)^2 - (5,6 - 4,2n^2) - \\ & - \frac{r_0}{r} (10,4 - 14,4n^2 + 4n^4) + \frac{r_0^2}{r^2} (4 - 16n^2 + 6n^4) + \\ & + \frac{r_0^3}{r^3} (4n^2 - 4n^4) + \frac{r_0^4}{r^4} (4n^4 + 1,4n^2) ] r dr - \\ & - 2\rho p^2 \int_{r_0}^H \left( l - kr + \sqrt[3]{\frac{r - ac^3}{a}} \right) (r - r_0)^4 r dr = 0. \end{aligned} \quad (11)$$

The above expression can be used to calculate in the first approximation the circular frequency p for a different number n of nodal diameters for a number of disks with different geometric parameters l, k, a and c.

#### SUMMARY

1. A method was presented for vibration design of intricately-shaped disks by the Ritz method, using functions approximating the actual thickness of the disk.

2. Functions for approximating the thickness of intricately-shaped disks were given.

3. The method presented is suitable for disks with a rim and radial rib thickness conforming to the concept of a thin plate.

#### REFERENCES

1. Birger, I.A. Variatsionnyye metody v stoitel'noy mekhanike turbomashin [Variational Methods in Structural Mechanics of Turbomachines]. Oborongiz Press, 1959.
2. Timoshenko, S.P. Plates and Shells. McGraw-Hill Book Company, 1958.

# THE HYDROSTATIC BEARING AS A SOURCE OF VIBRATIONS

Candidate of Technical Sciences, G.A. Ivanov

Figure 1 depicts schematically a hydrostatic bearing with communicating chambers /89  
 and the assumed diagram of pressure distribution over its length. It is assumed that the bearing uses an incompressible viscous fluid and that the flow in all the elements of the bearing is laminar. It is also assumed that the stream constriction coefficient  $\epsilon_{str} = 1$  and the sum of pressure losses  $\xi_{in}$  at the duct inlet and  $\xi_{out}$  at its outlet is appreciably smaller than the pressure lost in the duct in friction, i.e.,

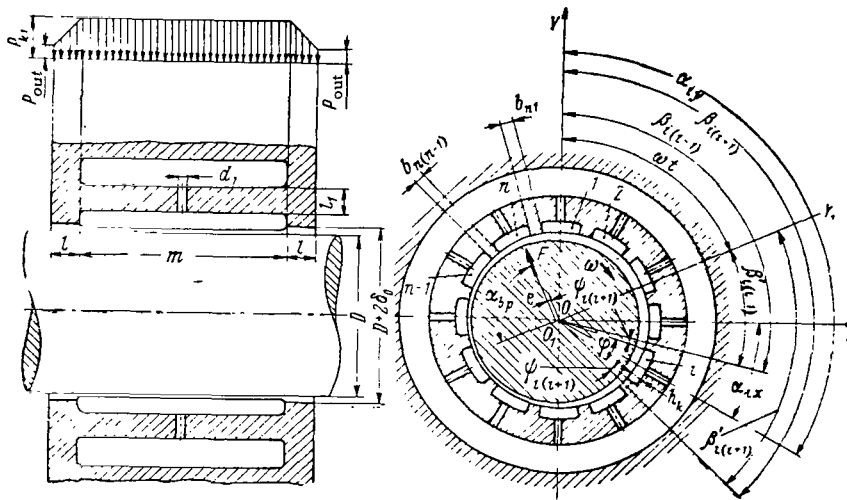


Fig. 1. Schematic drawing of a hydrostatic bearing with communicating chambers.

$$\xi_{in} + \xi_{out} \ll \xi_{fr}. \quad (1)$$

We assume that

$$\delta \ll D, \quad (2)$$

where  $\delta$  is the size of the clearance and  $D$  is the shaft diameter. This permits us to assume that the flow of the fluid in all the clearances between the connecting web of the bearing race and the shaft is equivalent to the fluid flow in a flat slot. The hydrodynamic effect which is produced at the connecting webs is disregarded.

It is assumed that the bearing acts as the so-called rotating load, the angular velocity  $\omega'$  of which is in general not the same as the angular velocity of the shaft. For a rotating load the volume of fluid bounded by the  $i$ th chamber is variable.

We select a stationary coordinate system  $\underline{XOY}$  (Fig. 1) and a moving axis  $\underline{OY}_1$ . This axis passes through center  $\underline{O}$  of the rim and through center  $\underline{O}_1$  of the shaft which is displaced relative to the rim.

We now write the flow-rate balance equation for the  $i$ th chamber in the form [sic]

$$\begin{aligned} a_{i(i-1)}\overline{H}_{k(i-1)} + a_{ii}\overline{H}_{ki} + a_{i(i+1)}\overline{H}_{k(i+1)} = \\ = 1 + a_{bpi} - \frac{dV_i}{dt} B_1 \Phi, \end{aligned} \quad (3)$$

where

$$\begin{aligned} a_{i(i-1)} &= -3,4\Phi K K_{i(i-1)}; \\ a_{ii} &= 1 + 3,4\Phi [K_{ie} + K(K_{i(i-1)} + K_{i(i+1)})]; \\ a_{i(i+1)} &= -3,4\Phi K K_{i(i+1)}; \\ \overline{H}_{k(i-1)} &= \frac{H_{k(i-1)}}{H_{in}}; \quad \overline{H}_{ki} = \frac{H_{ki}}{H_{in}}; \quad \overline{H}_{k(i+1)} = \frac{H_{k(i+1)}}{H_{in}}; \\ a_{bpi} &= -10,2 \frac{m\varepsilon\omega l\mu\Phi}{\gamma H_{in} \delta_0^2} (\cos \beta'_{i(i+1)} - \cos \beta'_{i(i-1)}); \\ \frac{dV_i}{dt} &= -0,5(m+2l)\delta_0 D \varepsilon \omega' (\cos \beta'_{i(i+1)} - \cos \beta'_{i(i-1)}); \\ B_1 &= \frac{128\mu l}{\pi \gamma H_{in} D \delta_0^3}; \quad \Phi = \frac{D l_1 \delta_0^3}{l d_1^4}; \quad K = \frac{m}{D} \frac{l}{b}; \\ K_{i(i-1)} &= (1 + \varepsilon \cos \beta_{i(i-1)})^3; \\ K_{ie} &= \beta'_{i(i+1)} - \beta'_{i(i-1)} + 3\varepsilon (\sin \beta'_{i(i+1)} - \sin \beta'_{i(i-1)}) + \\ &+ 1,5\varepsilon^2 [\beta'_{i(i+1)} - \beta'_{i(i-1)} + 0,5 (\sin 2\beta'_{i(i+1)} - \sin 2\beta'_{i(i-1)})] + \\ &+ 0,25\varepsilon^3 \left[ 3 (\sin \beta'_{i(i+1)} - \sin \beta'_{i(i-1)}) + \frac{1}{3} (\sin 3\beta'_{i(i+1)} - \sin 3\beta'_{i(i-1)}) \right]; \\ K_{i(i+1)} &= (1 + \varepsilon \cos \beta_{i(i+1)})^3; \\ \beta'_{i(i-1)} &= \beta_{i(i-1)} - \omega' t; \quad \beta'_{i(i+1)} = \beta_{i(i+1)} - \omega' t; \\ \beta_{i(i-1)} &= \alpha_{iy} - \frac{\varphi}{2} - \psi_{i(i-1)}; \quad \psi_{i(i-1)} = \arcsin \frac{b_{i(i-1)}}{D}; \\ \beta_{i(i+1)} &= \alpha_{iy} + \frac{\varphi}{2} + \psi_{i(i+1)}; \quad \psi_{i(i+1)} = \arcsin \frac{b_{i(i+1)}}{D}. \end{aligned} \quad /91$$

For a multichamber bearing a system of equations analogous to Eq. (3) is set up for each chamber.

The carrying capacity of the bearing is found from

$$F = (P_{in} - P_{out})(m + l)D\theta, \quad (4)$$

where  $P_{in}$  is the fluid pressure at the bearing's inlet,  $P_{out}$  is the same at the bearing's outlet;  $m$  is the length of the bearing's chamber,  $l$  is the length of the annular connecting web;  $D$  is the shaft diameter and  $\theta$  is the load factor of the bearing.

$$\begin{aligned} \theta &= \sqrt{\theta_x^2 + \theta_y^2}; \\ \theta_x &= \sum_{i=1}^{i=n} \bar{H}_{ki} \cos \alpha_{ix} \sin(\varphi_i + \psi_{i(i+1)} + \psi_{i(i-1)}); \\ \theta_y &= \sum_{i=1}^{i=n} \bar{H}_{ki} \cos \alpha_{iy} \sin(\varphi_i + \psi_{i(i+1)} + \psi_{i(i-1)}), \end{aligned} \quad (5)$$

where  $n$  is the number of chambers.

The angle between the direction of the load and the direction in which the shaft is displaced

$$\alpha_{bp} = \arctan \frac{\theta_x}{\theta_y} \quad (6)$$

The rate of flow through the bearing

$$Q = \frac{\pi \gamma d_1^4}{128 \mu l_1} H_{in} \left( n - \sum_{i=1}^{i=n} \bar{H}_{ki} \right) \quad (7)$$

We start the analysis of the load carrying bearing with a three-chamber bearing with the relative dimensions

$$\frac{m}{D} = 1; \quad \frac{b}{D} = 0,2; \quad \frac{b}{\delta_0} = 100; \quad \frac{l}{\delta_0} = 100,$$

where  $\delta_0$  is the size of the radial gap, which is determined with the shaft situated concentrically with respect to the [bearing's] rim.

For the bearing under consideration we assume that  $b$ , the width of the connecting web is constant for all the chambers. It is assumed that the shaft diameter is  $D = 50$  mm, the angular velocity of the shaft and the load is  $\omega = \omega' = 400 \text{ sec}^{-1}$ . The circumferential rotational speed in this case comes out to  $v = 100 \text{ m/sec}$ .

Compressor oil with density of  $882 \text{ Kg/m}^3$ ,  $\mu = 95.7 \cdot 10^{-2} \text{ N-sec/m}^2$  is selected as the working fluid. The pressure drop over the bearing  $\Delta P = P_{in}$

$$-P_{out} = 962 \text{ N/m}^2.$$

Figure 2 shows curves of the load factor  $\theta$  as a function of the relative eccentricity  $\epsilon$  for a three-chamber bearing with the above relative dimensions. It follows from the figure that for the same  $\epsilon$  the magnitude of  $\theta$  varies as a function of two limiting instantaneous directions of the rotating load, i.e., toward the "center of chamber" and toward the "connecting web."

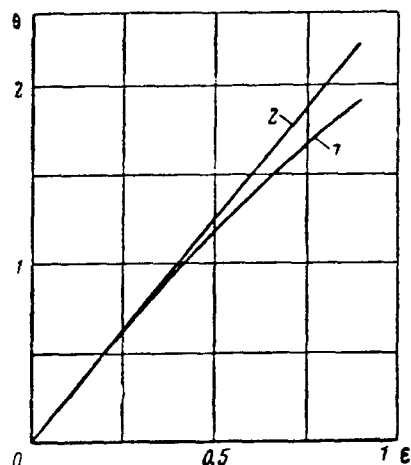


Fig. 2. Load Factor as a Function of the Relative Eccentricity. 1) Direction of Displacement toward the "Connecting Web"; 2) Direction of Displacement toward the "Center of Chamber."

This means that due to differences in the carrying capacity of the lubricating layer a source of vibrations exists in the bearing. Thus, when  $\theta = 1$ , the amplitude of vibrations involving displacement of the center of the journal in the bearing is 0.002 mm, while when  $\theta = 1.8$  this amplitude is 0.01 mm. Then this analysis was applied to a five-chamber bearing with relative dimensions  $\underline{m}/\underline{D} = 1$ ,  $\underline{b}/\underline{D} = 0.2$ ,  $\underline{b}/\delta_0 = 100$ ,  $1/\delta_0 = 100$ . Here it was assumed

that the shaft diameter is  $\underline{D} = 50$  mm and the angular speed of the shaft and the load is  $\omega = \omega' = 4000 \text{ sec}^{-1}$ . The previously described compressor oil was again selected as the working fluid.

Calculations have shown that a five-chamber bearing has the same load carrying capacity for any direction of the rotating load's vector. This means that changing from a three- to a five-chamber bearing makes it possible to eliminate undesirable vibrations of the shaft which are due to differences in the carrying capacity of the lubricating layer.

#### REFERENCES

1. Cameron, A. Theory of Lubrication in Engineering. [Transl. from Engl.] Mashgiz Press, 1962.
2. Raimondi, Albert A. and Boyd, John. Investigation of Hydrostatic Sliding-Contact Bearings with Diaphragm and Capillary Compensations. Collection; "Mashinostroyeniye", Vol 7, IL Press, 1957.
3. Rozenberg, Yu.A. and Vinogradova, I.Z. Smazka mekhanizmov i mashin [Lubrication of Mechanisms and Machines]. Gostoptekhizdat Press, 1960.
4. Frenkel', N.Z. Gidravlika [Hydraulics]. Gosenergoizdat Press, 1956.
5. Shaw, M.C. and Macks, E.F. Analysis and Lubrication of Bearings, New York, 1949.

# STABILITY OF THREE-LAYER CYLINDRICAL SHELLS BEYOND THE ELASTIC LIMIT

Candidate of Technical Sciences V.V.Serdyukov

The present paper examines the stability of cylindrical shells /94  
consisting of two outer layers interconnected by a filler and sub-  
jected to a normal pressure and axial force when the stresses in the  
bearing layers exceed the proportional limit. It is assumed that the  
thickness of the bearing layers and their temperatures are different  
and that they may be made from different materials.

The stability of three-layer cylindrical shells beyond the elastic  
limit was considered previously in [1] and [4], etc.; however, in all  
the cases known to the author the study was limited to the case of  
bearing layers of the same thickness and temperature. These conditions,  
as a rule, do not apply to elements of modern aircraft, which has made  
the present investigation necessary.

This study is based on:

- 1) the theory of plastic deformations;
- 2) principle of "continuing loading";
- 3) theory of shells with large radii of curvature; and the follow-  
ing additional assumptions:

a) the bearing layers take up forces in their plane and deflect\*\*  
(the Kirchhoff-Love hypothesis holds for them);

b) the filler take up shearing /95  
forces only, so that the normal of  
the entire section remains straight;

c) the total thickness of the  
shell is small as compared with its  
radius.

We shall consider an infinitesimal element of the shell, separated by two planes passing through the axis of the cylinder and two parallel circles (Fig. 1).

It will be assumed that in the bearing layers of the shell act internal forces  $T'_1, T''_1, S', S'', T'_2,$

$T''_2$  and moments  $M'_1, M''_1, H', H''.$

$M'_2, M''_2$ , the variations of which in each layer (in the absence of external twisting moments), can be represented on the basis of the theory of plastic strain.

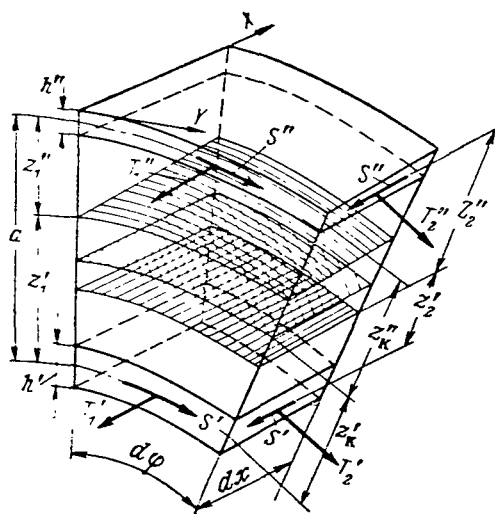


Fig. 1. Element of a Three-layer Cylindrical Shell.

\*\*Transl. Note: The Russian sentence makes no sense.

$$\left. \begin{aligned} \delta T_1^i &= b_{11}^i \delta \varepsilon_1^i + b_{12}^i \delta \varepsilon_2^i; \quad \delta S^i = b_{33}^i \delta \gamma_{12}^i; \quad \delta T_2^i = b_{12}^i \delta \varepsilon_1^i + b_{22}^i \delta \varepsilon_2^i; \\ \delta M_1^i &= -d_{11}^i \delta \chi_1^i - d_{12}^i \delta \chi_2^i; \quad \delta H^i = -d_{33}^i \delta \chi_{12}^i; \\ \delta M_2^i &= -d_{12}^i \delta \chi_1^i - d_{22}^i \delta \chi_2^i, \end{aligned} \right\} \quad (1)$$

where  $\delta \varepsilon_1^i$ ,  $\delta \varepsilon_2^i$ ,  $\delta \gamma_{12}^i$ ,  $\delta \chi_1^i$ ,  $\delta \chi_2^i$ ,  $\delta \chi_{12}^i$ —are variations of the tensile and shearing strain, variations in curvature and twisting of the middle surfaces on the bearing layers [2]\*.

$$\begin{aligned} b_{11}^i &= \frac{12}{h^{i2}} d_{11}^i = B^i \left( 1 - \frac{3}{4} K^i \sigma_{x0}^{i2} \right); \\ b_{12}^i &= \frac{12}{h^{i2}} d_{12}^i = \frac{1}{2} B^i \left( 1 - \frac{3}{2} K^i \sigma_{x0}^i \sigma_{y0}^i \right); \\ b_{22}^i &= \frac{12}{h^{i2}} d_{22}^i = B^i \left( 1 - \frac{3}{4} K^i \sigma_{y0}^{i2} \right); \\ b_{33}^i &= \frac{6}{h^{i2}} d_{33}^i = \frac{1}{4} B^i; \end{aligned}$$

here

$$\begin{aligned} B^i &= \frac{4}{3} E_c h^i; \quad K^i = 1 - (E_t^i / E_c^i); \\ \sigma_{x0}^i &= \sigma_x^i / \sigma_e^i; \quad \sigma_{y0}^i = \sigma_y^i / \sigma_e^i, \end{aligned}$$

where  $\underline{h}^i$  is the thickness of the corresponding bearing layer,  $\frac{E^i}{t}$  is the tangent modulus;  $\frac{E^i}{c}$  is the secant modulus;  $\sigma_{x0}^i$  and  $\sigma_{y0}^i$  are normal stresses in the subcritical state and  $\sigma_e^i$  is the generalized stress.

We shall consider pure bending of an isolated element in planes perpendicular to axes  $\underline{X}$  and  $\underline{Y}$ . If the variations of forces  $\frac{T_1^i}{1}$  and  $\frac{T_2^i}{2}$  are denoted respectively by  $\delta \frac{T_1^i}{1f1}$  and  $\delta \frac{T_2^i}{2f1}$ , then we will have, from the equilibrium conditions, /96

$$\left. \begin{aligned} \delta T_{1f1}^i + \delta T_{1f1}^* &= 0; \\ \delta T_{2f1}^i + \delta T_{2f1}^* &= 0 \end{aligned} \right\} \quad (2)$$

or, on the basis of Eqs. (1)

\*Subscript  $\underline{i}$  replaces one or two primes and defines the ratio of parameters to the inner or outer bearing layer of the shell, respectively.

$$\left. \begin{aligned} b_{11}' \delta \varepsilon_{1f1}' + b_{12}' \delta \varepsilon_{2f1}' + b_{11}'' \delta \varepsilon_{1f1}'' + b_{12}'' \delta \varepsilon_{2f1}'' &= 0; \\ b_{12}' \delta \varepsilon_{1f1}' + b_{22}' \delta \varepsilon_{2f1}' + b_{12}'' \delta \varepsilon_{1f1}'' + b_{22}'' \delta \varepsilon_{2f1}'' &= 0, \end{aligned} \right\} \quad (3)$$

where

$$\delta \varepsilon_{1f1}', \delta \varepsilon_{2f1}', \delta \varepsilon_{1f1}'', \delta \varepsilon_{2f1}'' - \text{are variations}$$

of the corresponding strain in the bearing layers in pure bending.

On the basis of the assumption that the common normal remains straight we have

$$\left. \begin{aligned} \delta \varepsilon_{1f1}' &= z_1' \chi_1; & \delta \varepsilon_{1f1}'' &= -z_1'' \chi_1; \\ \delta \varepsilon_{2f1}' &= z_2' \chi_2; & \delta \varepsilon_{2f1}'' &= -z_2'' \chi_2, \end{aligned} \right\} \quad (4)$$

where  $z_1'$ ,  $z_1''$ ,  $z_2'$  and  $z_2''$  are distances to the corresponding neutral surfaces (see Fig. 1),  $\chi_1$  and  $\chi_2$  are changes in the curvatures of the neutral surfaces of the shell.

On the basis of assumptions of this paper (retention of a straight common normal and the theory of shells with large radii of curvatures) we can write

$$\left. \begin{aligned} \chi_1 &= \chi_1' = \chi_1'' = w_{xx}; \\ \chi_2 &= \chi_2' = \chi_2'' = w_{yy}, \end{aligned} \right\} \quad (5)$$

where  $w$  is the radial displacement of the neutral surface (subscripts  $x$  and  $y$  denote differentiation with respect to the corresponding coordinate).

Substituting Eq. (4) into Eqs. (3) with reference to Eqs. (5), we will get expressions for the positions of the neutral bending surfaces in the form

$$\left. \begin{aligned} z_1 &= a \frac{A_1 w_{xx} + B_1 w_{yy}}{C w_{xx}}; & z_1'' &= a \frac{E_1 w_{xx} - B_1 w_{yy}}{C w_{xx}}; \\ z_2' &= a \frac{A_2 w_{xx} + B_2 w_{yy}}{C w_{yy}}; & z_2'' &= a \frac{E_2 w_{yy} - A_2 w_{xx}}{C w_{yy}}, \end{aligned} \right\} \quad (6)$$

where  $a$  is the distance between the middle surfaces of the bearing layers;

$$\begin{aligned} A_1 &= b_{11}'(b_{22}' + b_{22}'') - b_{12}'(b_{12}' + b_{12}''); \\ A_2 &= b_{12}'(b_{11}' + b_{11}'') - b_{11}'(b_{12}' + b_{12}''); \\ B_1 &= b_{12}'(b_{22}' + b_{22}'') - b_{22}'(b_{12}' + b_{12}''); \\ B_2 &= b_{22}'(b_{11}' + b_{11}'') - b_{12}'(b_{12}' + b_{12}''); \end{aligned}$$

$$C = (b'_{11} + b''_{11})(b'_{22} + b''_{22}) - (b'_{12} + b''_{12})^2;$$

$$E_1 = C - A_1; \quad E_2 = C - B_2.$$

The position of the neutral surface on torsion ( $\underline{z}'_{\underline{t}}$  and  $\underline{z}''_{\underline{t}}$ ) will be obtained by considering the twisting of the isolated element and equating the sum of variations of forces  $\underline{S}$  to zero (we denote them by  $\underline{S}_{\underline{t}}$ )

$$\delta S'_t + \delta S''_t = 0 \quad (7)$$

or, having reference to Eqs. (1)

$$b'_{33}\delta\gamma'_t + b''_{33}\delta\gamma''_t = 0. \quad (8)$$

The variations of the shearing strain of bearing layers,  $\gamma'_{\underline{t}}$  and  $\gamma''_{\underline{t}}$  on the basis of the hypothesis of a straight common normal are

$$\left. \begin{aligned} \delta\gamma'_t &= -2z'_t\chi_{12}; \\ \delta\gamma''_t &= 2z''_t\chi_{12}. \end{aligned} \right\} \quad (9)$$

On the basis of the assumptions made the relative twist of the neutral surface  $\chi_{12}$  can be represented in the form

$$\chi_{12} = \chi'_{12} = \chi''_{12} = w_{xy}. \quad (10)$$

On the basis of the above expression and Eqs. (8) and (9) we get

$$z'_t = a \frac{b''_{33}}{b'_{33} + b''_{33}}; \quad (11)$$

$$z''_t = a \frac{b'_{33}}{b'_{33} + b''_{33}}$$

Thus, in the general case and on the assumptions made all the three neutral surfaces are at different distances from the middle surfaces of the bearing layers of the shell; here the position of the neutral surface of twist depends on the stressed state of the bearing layers, while the position of the neutral shearing surfaces, in addition, also depends on the manner in which the shell is deformed. /98

The stability equations for a cylindrical shell with large radius of curvature have the form

$$\left. \begin{aligned} (\delta T_1)_x + (\delta S)_y &= 0; \\ (\delta S)_x + (\delta T_2)_y &= 0; \\ \frac{1}{R}\delta T_2 + (\delta M_1)_{xx} + 2(\delta H)_{xz} + (\delta M_2)_{yy} + T_1^0 w_{xx} + T_2^0 w_{yy} &= 0, \end{aligned} \right\} \quad (12)$$

where  $\underline{T}_1^0$  and  $\underline{T}_2^0$  are forces corresponding to the subcritical state.

We now apply these equations to our problem; the variations of forces and moments will denote those total values of forces and moments in the entire cross section of the shell which can be expressed in the form

$$\left. \begin{aligned} \delta T_1 &= \sum_{i=1}^2 \delta T_1^i; \\ \delta T_2 &= \sum_{i=1}^2 \delta T_2^i; \\ \delta S &= \sum_{i=1}^2 \delta S^i; \\ \delta M_1 &= -\delta T_1' z_1' + \delta T_1'' z_1'' - \sum_{i=1}^2 (d_{11}^i \delta \chi_1^i - d_{12}^i \delta \chi_2^i); \\ \delta M_2 &= -\delta T_2' z_2' + \delta T_2'' z_2'' - \sum_{i=1}^2 (d_{12}^i \delta \chi_1^i - d_{22}^i \delta \chi_2^i); \\ \delta H &= -\delta S' z_k' + \delta S'' z_k'' - \sum_{i=1}^2 d_{33}^i \delta \chi_{12}^i. \end{aligned} \right\} \quad (13)$$

Substituting the force and moment variations given by Eq. (13) into stability equations (12), and using Eqs. (1), (5) and (10) while bearing in mind that the variations of tensile and shearing strains of the middle surfaces of the bearing layers have the form

$$\delta \varepsilon_1^i = u_x^i; \quad \delta \varepsilon_2^i = v_y^i - \frac{w}{R}; \quad \delta \gamma_{12}^i = u_y^i + v_x^i, \quad (14)$$

where  $\underline{u}^i$  and  $\underline{v}^i$  are the displacements of the middle surfaces of the bearing layers along axes  $\underline{X}$  and  $\underline{Y}$ , respectively, we get

/99

$$\begin{aligned} & b_{11}' u_{xx}' + b_{11}'' u_{xx}'' + (b_{12}' + b_{33}') v_{xy}' + (b_{12}'' + b_{33}'') v_{xy}'' + b_{33}' u_{yy}' + b_{33}'' u_{yy}'' - \\ & - (b_{12}' + b_{12}'') \frac{w_x}{R} = 0; \\ & (b_{33}' + b_{12}') u_{xy}' + (b_{33}'' + b_{12}'') u_{xy}'' + b_{33}' v_{xx}' + b_{33}'' v_{xx}'' + b_{22}' v_{yy}' + b_{22}'' v_{yy}'' - \\ & - (b_{22}' + b_{22}'') \frac{w_y}{R} = 0; \\ & b_{12}' \frac{u_x'}{R} + b_{12}'' \frac{u_x''}{R} + b_{22}' \frac{v_y'}{R} + b_{22}'' \frac{v_y''}{R} - b_{11}' z_1' u_{xxx}' + b_{11}'' z_1'' u_{xxx}'' - \end{aligned}$$

$$\begin{aligned}
& -b'_{12}z'_1v'_{xxy} + b''_{12}z''_1v''_{xxy} - 2b'_{33}z'_1u'_{xyy} + 2b''_{33}z''_1u''_{xyy} - 2b'_{33}z'_1v'_{xxy} + \\
& + 2b''_{33}z''_1v''_{xxy} - b'_{12}z'_1u'_{xyy} + b''_{12}z''_1u''_{xyy} - b'_{22}z'_2v'_{yyy} + \\
& + b''_{22}z''_2v''_{yyy} - (b'_{22} + b''_{22})\frac{w}{R^2} + (b'_{12}z'_1 - b''_{12}z''_1)\frac{w_{xx}}{R} + \\
& + (b'_{22}z'_2 - b''_{22}z''_2)\frac{w_{yy}}{R} - (d'_{11} + d''_{11})w_{xxx} - \\
& - 2(d'_{12} + d''_{12} + d'_{33} + d''_{33})w_{xxyy} - (d'_{22} + d''_{22})w_{yyyy} + \\
& + T_1^0w_{xx} + T_2^0w_{yy} = 0.
\end{aligned} \tag{15}$$

In addition, on the basis of the hypothesis of retention of straight common normal we have

$$\left. \begin{aligned} u' - u'' - aw_x &= 0; \\ v' - v'' - aw_y &= 0. \end{aligned} \right\} \tag{16}$$

We have thus obtained a system of five differential equations for  $\underline{u}'$ ,  $\underline{u}''$ ,  $\underline{v}'$ ,  $\underline{v}''$  and  $\underline{w}$ , the five displacements of the bearing layers which are produced when the shell bulges. We assume that these displacements can also be represented in the form

$$\left. \begin{aligned} u^i &= U^i \sin \mu \xi \sin n\varphi; \\ v^i &= V^i \cos \mu \xi \cos n\varphi; \\ w &= W \cos \mu \xi \sin n\varphi, \end{aligned} \right\} \tag{17}$$

where .

$$\xi = x/R; \quad \mu = m\pi R/l;$$

$\underline{n}$  is the number of waves which form on the surface when the shell bulges,  $\underline{m}$  is the number of half-waves along the generatrix;  $\underline{l}$  is the length of the shell,  $\underline{U}^i$ ,  $\underline{V}^i$  and  $\underline{W}$  are the amplitudes of the corresponding displacements.

$-b'_{11}\mu^2 - b'_{33}n^2$	$-b''_{11}\mu^2 - b_{33}n^2$	$(b'_{12} + b'_{33})\mu n$	$(b''_{12} + b''_{33})\mu n$	$(b'_{12} + b''_{12})\mu$
$(b'_{33} + b'_{12})\mu n$	$(b''_{33} + b''_{12})\mu n$	$-b'_{33}\mu^2 - b'_{22}n^2$	$-b''_{33}\mu^2 - b''_{22}n^2$	$-(b'_{22} + b''_{22})n$
$b'_{12}\mu +$ $+ b'_{11}\psi'_1\mu^3 +$ $+ 2b'_{33}\psi'_R\mu n^2 +$ $+ b'_{12}\psi'_2\mu n^2$	$b''_{12}\mu -$ $-b''_{11}\psi''_1\mu^3 -$ $-2b''_{33}\psi''_R\mu n^2 -$ $-b'_{12}\psi''_2\mu n^2$	$-b'_{22}n -$ $-b'_{12}\psi'_1\mu^2 n -$ $-2b'_{33}\psi'_R\mu^2 n -$ $-b'_{22}\psi'_2 n^3$	$-b''_{22}n +$ $+ b'_{12}\psi''_1\mu^2 n +$ $+ 2b''_{33}\psi''_R\mu^2 n +$ $+ b'_{22}\psi''_2 n^3$	$-b'_{22} - b''_{22} - (b'_{12}\psi'_1 - b''_{12}\psi''_1)\mu^2 -$ $-(b'_{22}\psi'_2 - b''_{22}\psi''_2)n^2 - \frac{d'_{11} + d''_{11}}{R^2}\mu^4 -$ $-2(d'_{12} + d''_{12} + d'_{33} + d''_{33})\frac{\mu^2 n^2}{R^2} -$ $-\frac{d'_{22} + d''_{22}}{R^2}n^4 - T_1^0\mu^2 - T_2^0 n^2$
1	-1	0	0	$\frac{a}{R}\mu$
0	0	1	-1	$-\frac{a}{R}n$

(18)

Substituting Eqs. (17) into Eqs. (15) and (16) and dividing out the 101 trigonometric functions, we will get a system of five linear homogeneous equations for  $\underline{U}'$ ,  $\underline{U}''$ ,  $\underline{V}'$ ,  $\underline{V}''$ , and  $\underline{W}$ , the determinant of which has the form of Eq. (18), where

$$\begin{aligned}\psi_1' &= \frac{a}{R} \frac{A_1 \mu^2 + B_1 n^2}{C \mu^2}; & \psi_1'' &= \frac{a}{R} \frac{E_1 \mu^2 - B_1 n^2}{C \mu^2}; \\ \psi_2' &= \frac{a}{R} \frac{A_2 \mu^2 + B_2 n^2}{C n^2}; & \psi_2'' &= \frac{a}{R} \frac{-A_2 \mu^2 + E_2 n^2}{C n^2}; \\ \psi_1' &= \frac{a}{R} \frac{b_{33}'}{b_{33}' + b_{33}''}; & \psi_1'' &= \frac{a}{R} \frac{b_{33}''}{b_{33}' + b_{33}''}.\end{aligned}$$

Expanding determinant (18) in the fifth-column minors and equating it to zero, we get an expression for the critical loads

$$\begin{aligned}-T_1^0 \mu^2 - T_2^0 n^2 &= (b_{12}' \psi_1' - b_{12}'' \psi_1'') \mu^2 + (b_{22}' \psi_2' - b_{22}'' \psi_2'') n^2 + \\ &+ \frac{d_{11}' + d_{11}''}{R^2} \mu^4 + \frac{2}{R^2} (d_{12}' + d_{12}'' + d_{33}' + d_{33}'') \mu^2 n^2 + \frac{d_{22}' + d_{22}''}{R^2} n^4 - \\ &- (b_{12}' + b_{12}'') \mu \frac{A_{51}}{A_{53}} - (b_{22}' + b_{22}'') \left( n \frac{A_{52}}{A_{53}} - 1 \right) + \\ &+ \frac{a}{R} \mu \frac{A_{54}}{A_{53}} + \frac{a}{R} n \frac{A_{55}}{A_{53}},\end{aligned}\tag{19}$$

where  $A_{51}$ ,  $A_{52}$ ,  $A_{53}$ ,  $A_{54}$  and  $A_{55}$  are understood to denote the corresponding minors of the fifth column of determinant (18).

Let us now consider some particular cases of practical importance for which simpler results are obtained.

a) Symmetrical bulging on axial compression.

Setting in this case in Eq. (19)  $\underline{T}^0 = 0$  and  $\underline{n} = 0$ , we get

$$-T_1^0 = \frac{1}{\mu^2} A + B + \mu^2 D,\tag{20}$$

where

$$\begin{aligned}A &= b_{22}' + b_{22}'' - \frac{(b_{12}' + b_{12}'')^2}{b_{11}' + b_{11}''}; \\ B &= b_{12}' \psi_1' - b_{12}'' \psi_1'' + (b_{11}' \psi_1' - b_{11}'' \psi_1'') \frac{b_{12}' + b_{12}''}{b_{11}' + b_{11}''} + \frac{a}{R} \frac{b_{12}' b_{11}'' - b_{12}'' b_{11}'}{b_{11}' + b_{11}''};\end{aligned}$$

$$D = \frac{a^2}{R^2} \frac{b'_{11} \bar{b}_{11}}{b'_{11} + \bar{b}_{11}} + \frac{d'_{11} + \bar{d}_{11}}{R^2};$$

here

$$\psi'_1 = \frac{a}{R} \frac{A_1}{C}; \quad \psi''_1 = \frac{a}{R} \frac{E_1}{C}.$$

Finding the minimum of Eq. (20) with respect to  $\mu$ , we will get an expression for the critical compressive force in the form

$$-T_{1cr}^0 = 2\sqrt{AD} + B. \quad (21)$$

b) Case in which  $\mu^2 \ll \underline{n}^2$  (this condition for a single-layer shell defines "medium length" shells.

In this case we disregard in Eq. (19) terms with multipliers  $\mu^2$  as being negligible as compared with terms with multipliers  $\underline{n}^2$ , and as a result we get

$$-T_{1\mu^2}^0 - T_{2n^2}^0 = F \frac{\mu^4}{n^4} + G\mu^2 + Ln^4, \quad (22)$$

where

$$\begin{aligned} F &= b'_{11} + \bar{b}_{11} - \frac{(b'_{12} + \bar{b}_{12})^2}{b'_{22} + \bar{b}_{22}}; \\ G &= b'_{12}\psi'_2 - \bar{b}_{12}\psi''_2 + \frac{a}{R} \frac{b'_{12}\bar{b}_{22} - \bar{b}_{12}b'_{22}}{b'_{22} + \bar{b}_{22}}; \\ L &= \frac{a^2}{R^2} \frac{b'_{22}\bar{b}_{22}}{b'_{22} + \bar{b}_{22}} + \frac{d'_{22} + \bar{d}_{22}}{R^2}; \end{aligned}$$

here

$$\psi'_2 = \frac{a}{R} \frac{B_2}{C}; \quad \psi''_2 = \frac{a}{R} \frac{E_2}{C}.$$

c) Stability when subjected to external pressure only and under the condition  $\mu^2 \ll \underline{n}^2$ .

Setting in Eq. (22)  $T_1^0 = 0$  and finding its minimum with respect to  $\underline{n}$ , we will get in this case a formula for the critical load in the form

$$-T_{2cr}^0 = 2\sqrt{2\pi} \frac{R}{l} \sqrt{L} \frac{4FL + G^2 + G\sqrt{G^2 + 12FL}}{(G + \sqrt{G^2 + 12FL})^{3/2}}. \quad (23)$$

The number of waves for which buckling occurs can be then determined from

$$n^4 = \pi^2 \frac{R^2}{l^2} \frac{G + \sqrt{G^2 + 12FL}}{2L}.$$

In general, stability calculations on the basis of Eqs. (19) and (22) can be performed by using the method of V.I. Feodos'yev [5] for determining the stressed stage of the shell. This is done in the following sequence.

1. We specify a number of values of total deformations  $\varepsilon_{1n}$  of the shell in the axial direction, and then for each  $\varepsilon_{1n}$  we specify a number of total deformations  $\varepsilon_{2n}$  in the circumferential direction; deducting the temperature deformations, we find the corresponding force-induced deformations of the bearing layers of the shell [5]

$$\varepsilon_1^i = \varepsilon_{1n} - \alpha^i t^i; \quad \varepsilon_2^i = \varepsilon_{2n} - \alpha^i t^i,$$

where  $\varepsilon_1^i$  and  $\varepsilon_2^i$  are the force-induced deformation of the bearing layers,

while  $\alpha^i$  and  $t^i$  are the linear expansion coefficients and average temperatures of these layers.

2. On the basis of the magnitudes of force-induced deformations obtained we determine the effective deformations of the bearing layers from [3]

$$\varepsilon_e^i = \frac{2}{\sqrt{3}} \sqrt{\varepsilon_1^{i2} + \varepsilon_2^{i2} + \varepsilon_1^i \varepsilon_2^i},$$

where  $\varepsilon_e^i$  are the effective deformations of the bearing layers.

3. From the stress-strain diagrams for the given materials and temperatures we find the corresponding effective stresses  $\sigma_e^i$ .

4. We determine the subcritical stresses in the bearing layers of the shell from [3]

$$\sigma_{x0}^i = \frac{4}{3} \frac{\sigma_e^i}{\varepsilon_e^i} \left( \varepsilon_1^i + \frac{1}{2} \varepsilon_2^i \right);$$

$$\sigma_{y0}^i = \frac{4}{3} \frac{\sigma_e^i}{\varepsilon_e^i} \left( \varepsilon_2^i + \frac{1}{2} \varepsilon_1^i \right)$$

and the circumferential and axial forces corresponding to them from

$$T_1^0 = \sum_{i=1}^2 \sigma_{x0}^i h^i; \quad T_2^0 = \sum_{i=1}^2 \sigma_{y0}^i h^i.$$

5. From stress-strain diagrams we determine for each layer its secant and tangent moduli, on the basis of which, using Eqs. (19) or

(22), we calculate the critical circumferential force  $\underline{T}_{2cr}^0$ , since then

$\underline{T}_1^0$  is defined as in paragraph 4 above.

6. We construct for each  $\underline{\epsilon}_{ln}$  a curve of  $\underline{T}_{2cr}^{0*}$  vs  $\underline{T}_2^0$ , according to paragraphs 4 and 5. The actual critical value  $\underline{T}_{2cr}^0$  will be defined at the intersection of this curve with the straight line  $\underline{T}_{2cr}^{0*} = \underline{T}_2^0$ . On the same graph, according to paragraph 4 it is possible to lay off values of  $\underline{T}_1^0$  as a function of  $\underline{T}_2^0$ ; here the  $\underline{T}_{2cr}^0$  thus obtained will have corresponding to it  $\underline{T}_{1cr}^0$ , defined by a vertical line drawn from the point of intersection of the curves of  $\underline{T}_{2cr}^{0*}$  vs  $\underline{T}_2^0$  to the intersection of the curve of  $\underline{T}_1^0$  vs  $\underline{T}_2^0$  (Fig. 2).

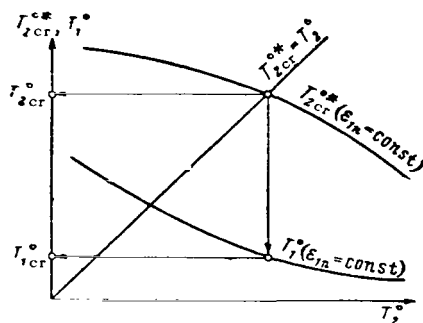


Fig. 2. For Determining the  
Critical Forces  $\underline{T}_{1cr}^0$  and  $\underline{T}_{2cr}^0$   
for  $\underline{\epsilon}_{ln} = \text{Const}$ .

7. We construct a graph of  $\underline{T}_{2cr}^0$  vs  $\underline{T}_{1cr}^0$ , from which we estimate the stability of the shell, comparing the graph with values of  $\underline{T}_2^0$  and  $\underline{T}_1^0$  which are produced by the actual loads.

For particular cases when only an axial force or external pressure is applied, there will be no differences in principle when performing calculations on the basis of Eqs. (21) or (23), and these calculations can be performed in approximately the same sequence.

#### REFERENCES

1. Grigorlyuk, E.I. The Stability of Three-Layer Plates and Shells Beyond the Elastic Limit. Izv. AN SSSR, Otd. Tekh. Nauk, No. 6, 1958.
2. Grigorlyuk, E.I. The Bulging of Thin Shells Beyond the Elastic Limit. Izv. AN SSSR, Otd. Tekh. Nauk, No. 10, 1957.
3. Il'yushin, A.A. Plastichnost' [Plasticity]. Gostekhizdat Press, 1948.
4. Kurshin, L.M. Ustoychivost' trekhsloynoy tsilindricheskoy obolochki za predelom uprugosti [Stability of a Three-Layer Cylindrical Shell Past the Elastic Limit]. Voprosy rascheta elementov aviat-sionnykh konstruktsiy [Design of Structural Elements of Aircraft]. Collection No. 2. Oborongiz Press, 1959.
5. Feodos'yev, V.I. Prochnost' kamery zhidkostnogo raketnogo dvigatelya [Strength of the [Combustion] Chamber of Rocket Engines]. Oborongiz Press, Moscow, 1957.

# THE APPLICATION OF CONFORMAL MAPPING TO PROBLEMS OF THE THEORY OF ELASTICITY

Candidate of Technical Sciences V.B. Gorlov

Many practical problems of the theory of elasticity can be solved in the final form if one knows the conformal mapping function which allows one-to-one mappings of one region onto another. Thus, for example, if the known stress paths form an isometric grid in the given region, then it is possible to obtain a solution for another region subjected to the same stress pattern if one knows the function which maps the given region onto the region for which the solution is sought. /105

However, the derivation of a conformal mapping function even for a region of the simplest geometric shape is a quite complicated task, and frequently runs into unsoluble mathematical difficulties.

The problem of deriving conformal mapping functions has intrigued many authors. All their approaches can be divided into analytic [3] and graphical [5], all quite cumbersome and, because of the great difficulties in their practical application, very rarely used.

Hence, in addition to the above methods, extensive use is made of techniques which employ various analogies for deriving mapping functions. Among these are the semiempirical methods based on the electrohydrodynamic analogy.

In 1922 Pavlovskiy [5] has suggested an effective technique for solving filtration problems based on electrohydrodynamic analogies. Later on, in 1937 this method served as a basis for the work by Bradfield, Hooker and Southwell [8] in which they have suggested an electrical simulation technique for conformal mapping, known as the method of orthogonal trajectories or potential lines. This method is based on restoring (simulating) corresponding orthogonal trajectories, i.e., potential lines and stream lines, and determining the corresponding points as points of intersection of equipotential lines. /106

In 1955 A.G. Ugodchikov [7] has applied this method, utilizing electrically conducting paper [2], to the mapping of a circle onto a given simply-connected region on the condition that the center of the circle and one of its bounding points are transformed onto given points in the given region. The advantage of this method is the fact that it allows finding the conformal mapping function in a form very convenient for applications, namely in the form of the polynomial

$$z = \omega(\zeta) = C_0\zeta + C_1\zeta^2 + \dots + C_n\zeta^n + \dots,$$

where  $C_1$  and  $C_2$  are in general complex coefficients.

Thus, for example, the function which maps a circle of unit radius onto a specified simply-connected region  $S$  which lacks corner points on contour  $L$  and which does not have axes of symmetry, has the form

$$\omega(\zeta) = \sum_{k=0}^{k=m} C_k \zeta^{k+1},$$

where  $\underline{m}$  is the number of corresponding points in conformal mapping and  $\underline{C}_{\underline{k}}$  are complex coefficients.

When the region does have an axis of symmetry, which is very frequently the case in practice, the mapping function has a somewhat different form

$$\omega(\zeta) = \sum_{k=0}^{k=m} C_k \zeta^{qk+1}, \quad (1)$$

where  $\underline{q}$  is the number of axes of symmetry and  $\underline{C}_{\underline{k}}$  are real coefficients.

The number of points  $\underline{m}$  in conformal mapping depends substantially on the complexity of the geometrical shape of contour  $\underline{L}$  of the given region  $\underline{S}$ . Thus, for an  $\underline{L}$  in the shape of an ellipse, the number of corresponding points is 8-12, while for a more complex contour, for example, a disk with dovetail slots, the number of such points in mapping is 18-25 or more, i.e., the number of corresponding points in conformal transformation increases with an increase in the complexity /107 of the geometric shape. It should be noted that increasing, i.e., increasing the number of terms in polynomial (1) is one of the methods for increasing the accuracy of conformal mapping by the electrical analog technique. However, one should be careful when increasing, since increasing it excessively may seriously reduce the accuracy of the mapping. This is due to the following: As is known, the electrically conductive paper used is anisotropic with respect to conductivity. For this reason this paper is calibrated prior to use. On the basis of this calibration it is possible to determine the shift,  $\Delta \underline{r}$  of a point belonging to a given paper cutout relative to its real position. The cutout is considered satisfactory if  $\Delta \underline{r}_{\max} < 0.01 \underline{r}_1$ , where  $\underline{r}_1$  is the radius of that point on contour  $\underline{L}$  which is furthest from the coordinate origin.

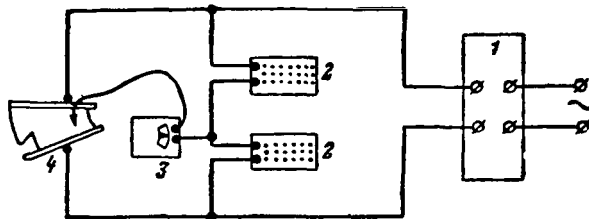


Fig. 1. Schematic of the Instrument.  
1) Rectifier; 2) Plug-in Type Resistance Box; 3) Galvanometer; 4) Model.

The maximum number of correspondence points  $\underline{m}$  should be selected so that the minimum distance  $\Delta \underline{h}_{\min}$  between two such adjacent points would be greater than  $\Delta \underline{r}_{\max}$ , i.e.,

$$\Delta h_{\min} > \Delta r_{\max}.$$

One of the means for increasing the accuracy of analog simulation consists of iterating (from 6 to 15 times, depending on the geometric complexity of contour  $\underline{L}$ ) the simulation of the specified contour  $\underline{L}$ , with subsequent averaging out of the results.

As can be seen from the above, the accuracy of electrical analog simulation of conformal mapping depends on a number of factors, which must be taken into account when using electrically conducting paper. Hence it is better to use an electrolytic bath or a metal foil as analogs of a given region. But their use is also not free of difficulties.

In order to determine the coordinates  $\underline{x}_n$  and  $\underline{y}_n$  of correspondence points  $\underline{a}_n$ , use is usually made of the EGDA-5, 51 unit, or of an instrument assembled in the manner shown in Fig. 1.

The operation of these instruments is based on an electrical analogy which consists in the fact that the orthogonal grid of rays  $\theta = \text{const}$  and circles with  $\rho = \text{const}$  (Fig. 2) of the region of the unit circle and its corresponding orthogonal grid in region  $\underline{S}$  will be a reflection of the motion of the current in the conducting medium. Hence, if a potential difference is applied in an appropriate manner to the specified region, then the current flow lines and equipotential lines form on it an orthogonal grid. Due to the uniqueness [one-to-one correspondence] of the conformal mapping, this grid will coincide with the grid of  $\theta = \text{const}$  and  $\rho = \text{const}$ , which is obtained on conformal mapping of a unit circle onto region  $\underline{S}$ .

/108

This analogy was used for constructing conformal mapping functions for an ellipse and a region which is filled by a disk with dovetail-shaped slots. Since these regions have axes of symmetry, only parts of these regions, included between axes of symmetry, were cut out from the electrically conductive paper for simulation purposes. A specified potential difference was applied to the cutout (along the sectioning lines) by means of busbars. It should be noted that a poor connection between the busbars and the cutout introduces an error into the determination of the correspondence points, which makes it necessary to manufacture the busbar in such a manner that tight contact between the cutout and busbar be ensured over the entire contact surface. In addition, in order to increase the accuracy in determining the correspondence point on the cutout, it is better to supply to the busbars a potential difference exceeding the recommended by 30-50 volts. After coordinates  $\underline{x}_n$  and  $\underline{y}_n$  of the correspondence points are determined the

known formulas [7]

$$\begin{aligned} C_0 &= \frac{1}{2m} (u_0 + u_m) + \frac{1}{m} \sum_{n=1}^{n=m-1} u_n; \\ C_m &= \frac{1}{2m} [u_0 + (-1)^m u_m] + \frac{1}{m} \sum_{n=1}^{n=m-1} (-1)^n u_n; \\ C_k &= \frac{1}{m} [u_0 + (-1)^k u_m] + \frac{2}{m} \sum_{n=1}^{n=m-1} u_n \cos \frac{\pi}{m} kn \end{aligned} \quad (2)$$

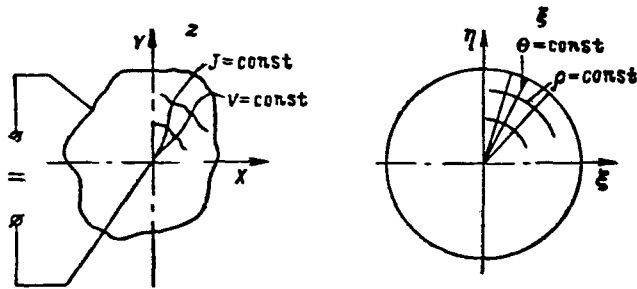


Fig. 2. The Electrical Analogy Phenomenon.

are used to determine coefficients  $\underline{C_k}$  of the conformal mapping function (1) (see Tables 1 and 2).

Table 1

Coefficients  $\underline{C_k}$  for an Ellipse

$k$	0	1	2	3	4	5	7	8	9
$C_k$	2.7822	0.4485	0.1565	0.0605	0.0330	0.0138	0.0079	0.0020	0.0014

Table 2

Coefficients  $\underline{C_k}$  for a Disk with Dovetail-Shaped Slots

$k$	0	1	2	3	4	5
$C_k$	123.22006	13.18116	8.02388	4.16576	0.55554	-1.40282

Continued

6	7	8	9	10	11	12
-2.22430	-1.66228	-0.72320	0.12524	1.00728	0.93868	0.84386

Continued

13	14	15	16	17	18	19
0.15524	-0.38642	-0.65808	-0.69270	-0.37074	0.02408	0.32936

Continued

20	21	22	23	24	25
0.59704	0.50404	0.21970	-0.00824	-0.57486	-0.18714

The conformal mapping functions obtained in this manner allow us to construct, within a given approximation, the contour  $\underline{L}'$  of a given region  $S$ . Naturally, contour  $\underline{L}'$  will differ from the given contour  $\underline{L}$  (Fig. 3). This difference is governed by the precision of the conformal mapping. As is known, any machine part is made with some tolerance describing its deviation from its required geometric shape. Hence, the criterion of the required precision of conformal mapping should be the tolerance for deviation from the geometric shape of the given machine part; a conformal mapping should be regarded as satisfactory if the scatter of points of contour  $\underline{L}'$  relative to specified contour  $\underline{L}$  lies within the manufacturing tolerance.

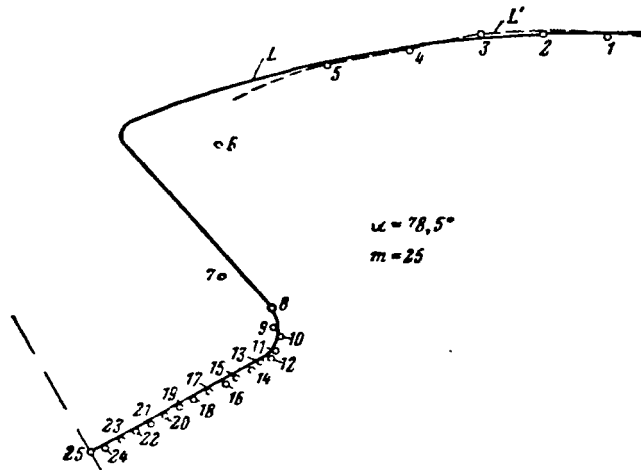


Fig. 3. Comparison of Contour  $\underline{L}'$  with Specified Contour  $\underline{L}$ .

Alongside with the method of [8], in which the coefficients of the mapping function (1) are calculated from Eqs. (2) obtained by interpolation, another approach was suggested by G.N. Polozhiy [6] who has used the Christoffel-Schwarz integral for determining the coefficients of the mapping function. The latter method also allows us to determine this function in regions with corner points. Thus the use of electrical analog simulation of conformal mapping has appreciably extended the capabilities of the mathematical tools of the theory of elasticity in solving a number of engineering problems.

The above method for determining conformal mapping functions which is suitable for simply, as well as doubly-connected regions, makes it possible to solve a wide range of problems of stresses to calculate the

stress concentration factors in machine parts of complex shape. This method was used successfully by this author for determining the stresses and stress concentration factors in a dovetail-shaped turbine-blade locking device [1].

#### REFERENCES

1. Gorlov, V.B. An Analytical Method for Determining the Stress Concentration Factors in Intricately-Shaped Components. *Izv VUZov, Aviatsionnaya Tekhnika*, No. 2, 1961.
2. Gutman, B.B. *Elektroprovodyashchaya bumaga* [Electrically-Conducting Paper]. Gosbumizdat Press, 1944.
3. Lavrent'yev, M.A. *Konformnyye otobrazheniya* [Conformal Mapping]. Gostekhizdat Press, 1946.
4. Melent'yev, P.V. *Neskol'ko novykh metodov i priyemov priblizhennykh vychisleniy* [Several New Methods and Devices of Approximate Calculations]. ONTI Press, 1937.
5. Pavlovskiy, N.N. *Teoriya dvizheniya gruntovykh vod pod gidrotekhnicheskimi sooruzheniyami i yeye osnovnyye prilozheniya* [A Theory of the Motion of Ground Waters Beneath Hydraulic Structures and Its Main Applications]. Press of Acad. Sci. USSR, 1956.
6. Polozhiy, G.N. An Effective Solution of the Problem of Conformal Mapping of Simply-Connected Regions and Determination of the Christoffel-Schwarz Constants Using the Electrohydrodynamic Analogy. *Ukr, matemat. zh.* Vol. 7, 2, 1955.
8. Bradfield, Hooker, Southwell. Conformal Transformation with the Aid of an Elastic Tank. *Proc. Royal Soc., Ser. A. Math and Phys.*, 898, 1937.

# STABILITY OF THREE-LAYER CYLINDRICAL SHELLS IN THE ELASTIC AND INELASTIC REGIONS\*

Candidate of Technical Sciences I.A. Yefimov

The stability of three-layer plates and shells was studied by many Soviet and Western scientists. However, in examining all the work on the stability of three-layer shells with a rigid filler (based primarily on the theory of shallow shells) it can be seen that the problem of their stability under combined action of several different loads has not yet been sufficiently studied.

The present paper considers the "small scale" stability beyond the elastic limit of three-layer cylindrical shells with a filler made of longitudinal and transverse corrugations (these also include three-layer shells in which the ribs of the corrugation lie along a low-pitch (helix) subjected to separate or combined action of several kinds of loads. It is assumed that a purely plastic condition exists in the bearing layers at the instant of buckling and that the filler behaves elastically. The filler is regarded as continuous and orthotropic, capable of taking up longitudinal forces and moments (the resistance of the corrugation to longitudinal forces and moments was not considered in [2]), the bearing layers are isotropic, have the same thickness and identical mechanical characteristics. The substantial difference between our work and that of [1] and [4] (which are based on the theory of shallow shells) is the fact that in considering the deformation of the filler in the circumferential direction it does not consider the fact that the shell [actually] is not shallow, which in the final count increases the accuracy of results for sufficiently long shells [2].

## We introduce the following notation

$\frac{u}{\rho}_{in}, \frac{u}{\rho}_{out}, \frac{v}{\rho}_{in}, \frac{v}{\rho}_{out}$  are the displacements of points on middle surfaces of the inside and outside bearing layer, [and the velocities of these displacements], respectively;  $\omega_{in} = \omega_{out} = \omega$ ;  $t$  is the thickness of the bearing layers;  $c$  is the thickness of the filler;  $R$  is the radius of the middle surface of the filler;  $l$  is the length of the shell;  $\xi$  is a dimensionless coordinate, measured from the edge of the shell;  $\varphi$  is an angular coordinate, measured from a specified section;  $m$  is the number of wave halves, which are formed on bulging along the generatrix;  $n$  is the number of waves forming along the circumference of the shell;  $N$  is the axial force;  $q$  is the external normal pressure, and  $G$  is the reduced shearing modulus in a plane perpendicular to the ribs of the corrugation.

Using the scheme of the deformed state assumed in deriving the equations of elastic stability [3], and following the same approach as [2], we will get a system of five equations for the five unknowns  $U, V, \omega, \alpha$ , and  $\beta$ . These equations have a structure similar to that of equations for the elastic problem

---

\*The part of the report pertaining to elastic stability of three-layer cylindrical shells under combined loads is published in [2].

$$\begin{aligned}
1) \quad & (2b_{11} + B_1)U_{xx} - 4b_{13}U_{xy} + (2b_{33} + B_3)U_{yy} - \\
& - (2b_{13} + S^0)V_{xx} + [2(b_{12} + b_{33}) + v_2B_1 + B_3 - T_2^0]V_{xy} - \\
& - 2b_{32}V_{yy} - \frac{1}{R}[(2b_{12} + v_2B_1 - T_2^0)\omega_x - 2b_{32}\omega_y] = 0; \\
2) \quad & -2b_{31}U_{xx} + [2(b_{21} + b_{33}) + v_1B_2 + B_3]U_{xy} - 2b_{23}U_{yy} + \\
& + \left[2b_{33}\left(1 + \frac{t^2}{6R^2}\right) + B_3 - \frac{D_3'}{R^2} + T_1^0\right]V_{xx} - \left[b_{23}\left(4 + \frac{t^2}{2R^2}\right) - \right. \\
& - S^0 \left. \right]V_{xy} + \left[b_{22}\left(2 + \frac{t^2}{6R^2}\right) + B_2 - \frac{D_2'}{R^2}\right]V_{yy} - \\
& - \frac{1}{R}\left\{\frac{t^2}{6}b_{31}\omega_{xxx} - \left[\frac{t^2}{6}(b_{21} + 2b_{33}) - v_1D_2' - 2D_3'\right]\omega_{xy} + \right. \\
& + \frac{t^2}{2}b_{23}\omega_{xy} - \left(\frac{t^2}{6}b_{22} - D_2'\right)\omega_{yy} - \\
& - (2b_{32} - S^0)\omega_x + (2b_{22} + B_2)\omega_y + \\
& + \frac{(c+t)^2}{2}b_{31}\alpha_{xx} - \left[\frac{(c+t)^2}{2}(b_{21} + b_{33}) + v_1D_2' + D_3'\right]\alpha_{xy} + \\
& + \frac{(c+t)^2}{2}b_{23}\alpha_{yy} - \left[\frac{(c+t)^2}{2}b_{33} + D_3'\right]\beta_{xx} + \\
& + \frac{(c+t)^2}{2}2b_{23}\beta_{xy} - \left[\frac{(c+t)^2}{2}b_{22} + D_2'\right]\beta_{yy} \left. \right\} = 0; \\
3) \quad & \frac{1}{R}\left\{(2b_{21} + v_1B_2)U_x - 2b_{23}U_y - 2(b_{23} - S^0)V_x + \right. \\
& + (2b_{22} + B_2 + T_2^0)V_y + \frac{t^2}{6}2b_{13}V_{xxx} - \left[\frac{t^2}{6}(b_{12} + 4b_{33}) - \right. \\
& - v_2D_1' - 2D_3'\left. \right]V_{xy} + \frac{t^2}{6}4b_{23}V_{xy} - \left[\frac{t^2}{6}b_{22} - D_2'\right]V_{yy} \left. \right\} - \\
& - \left[\frac{t^2}{6}b_{11} - D_1'\right]\omega_{xxx} + \frac{t^2}{6}4b_{13}\omega_{xx} - \left[\frac{t^2}{6}2(b_{12} + 2b_{33}) - \right. \\
& - v_2D_1' - v_1D_2' - 4D_3'\left. \right]\omega_{xy} + \frac{t^2}{6}4b_{23}\omega_{xy} - \left[\frac{t^2}{6}b_{22} - D_2'\right] \times \\
& \times \omega_{yy} + T_1^0\omega_{xx} + 2S^0\omega_{xy} + T_2^0\omega_{yy} - (2b_{22} + B_2)\frac{\omega}{R^2} - \\
& - \left[\frac{(c+t)^2}{2}b_{11} + D_1'\right]\alpha_{xx} + \frac{(c+t)^2}{2}3b_{13}\alpha_{xy} - \\
& - \left[\frac{(c+t)^2}{2}(b_{21} + 2b_{33}) + v_1D_2' + 2D_3'\right]\alpha_{yy} + \frac{(c+t)^2}{2} \times \\
& \times b_{23}\alpha_{yy} + \frac{(c+t)^2}{2}b_{13}\beta_{xx} - \left[\frac{(c+t)^2}{2}(b_{12} + 2b_{33}) + \right. \\
& + v_2D_1' + 2D_3'\left. \right]\beta_{xy} + \frac{(c+t)^2}{2}3b_{23}\beta_{xy} - \\
& - \left[\frac{(c+t)^2}{2}b_{22} + D_2'\right]\beta_{yy} = 0; \\
4) \quad & b_{31}\alpha_{xx} - (b_{21} + b_{33})\alpha_{xy} + b_{23}\alpha_{yy} - b_{33}\beta_{xx} - 2b_{23}\beta_{xy} - \\
& - b_{22}\beta_{yy} + \frac{2}{c(c+t)}\left\{D_2'\left[\left(\omega_{yyy} + \frac{V_{yy}}{R}\right) + v_1\omega_{xy}\right] - \right.
\end{aligned}$$

$$\begin{aligned}
& -D_2'(\beta_{\nu\nu} + \nu_1 a_{x\nu}) + D_3'(2\omega_{xx\nu} + \frac{V_{xx}}{R}) - \\
& -D_3'(\beta_{xx} + a_{x\nu}) \Big\} = \frac{2}{c} G_{23} \left[ \left( \omega + \frac{V}{R} \right) - \beta \right]; \\
5) & -b_{11}a_{xx} + 2b_{13}a_{x\nu} - b_{33}a_{\nu\nu} + b_{13}\beta_{xx} - (b_{12} + b_{33})\beta_{x\nu} + \\
& + b_{32}\beta_{\nu\nu} + \frac{2}{c(c+t)} \left\{ D_1' \left[ \omega_{xxx} + \nu_2 \left( \omega_{x\nu\nu} + \frac{V_{x\nu}}{R} \right) \right] - \right. \\
& -D_1'(a_{xx} + \nu_2\beta_{x\nu}) + D_3' \left( 2\omega_{x\nu\nu} + \frac{V_{x\nu}}{R} \right) - D_3'(\beta_{x\nu} + a_{\nu\nu}) \Big\} = \\
& = \frac{2}{c} G_{13}(\omega_x - \alpha).
\end{aligned} \tag{1}$$

The above expressions are equations of stability of a three-layer cylindrical shell with a rigid orthotropic filler, when the filler itself behaves elastically, while the bearing layers are stressed beyond the elastic limit. From this system of equations it is possible to get, as particular cases, the equation of stability of a three-layer cylindrical shell with a filler made of longitudinal as well as transverse corrugations.

We shall consider the case when this shell with a filler made of longitudinal corrugation is acted upon by an axial force and a uniform transverse pressure. Then from [2] we get that

$$S^0 = 0, \quad b_{13} = b_{31} = b_{23} = b_{32} = 0, \tag{2}$$

and from Eq. [3]

$$\alpha = \omega_x, \quad \nu_2 = 0. \tag{3}$$

Making substitution

$$x = \xi R, \quad \partial y = R \partial \varphi \tag{4}$$

and using Eqs. (2) and (3), we reduce Eqs. (1) to the form

$$\left. \begin{aligned}
1) & AU_{\xi\xi} + LU_{\varphi\varphi} + (C - t_2)V_{\xi\varphi} - (F - t_2)\omega_\xi = 0; \\
2) & CU_{\xi\varphi} + (L + a + t_1)V_{\xi\xi} + (1 + d)V_{\varphi\varphi} + \\
& + b\omega_{\xi\xi\varphi} - \omega_\varphi + d\omega_{\varphi\varphi} + h^*\beta_{\xi\xi} + l^*\beta_{\varphi\varphi} = 0; \\
3) & FU_\xi - eV_{\xi\xi\varphi} + (1 + t_2)V_\varphi - dV_{\varphi\varphi} - \\
& - f\omega_{\xi\xi\xi} + t_1\omega_{\xi\xi} - g\omega_{\xi\xi\varphi} + t_2\omega_{\varphi\varphi} - d\omega_{\varphi\varphi\varphi} - \\
& - w - k^*\beta_{\xi\xi\varphi} - l^*\beta_{\varphi\varphi} = 0; \\
4) & G_1V + \delta_1\omega_{\xi\xi\varphi} + G_1\omega_\varphi + \delta_2^*\beta_{\xi\xi} + \delta_3^*\beta_{\varphi\varphi} - G_2\beta = 0.
\end{aligned} \right\} \tag{5}$$

where

$$\begin{aligned}
A &= \frac{2b_{11} + B_1}{2b_{22}}; \quad C = \frac{b_{12} + b_{33}}{b_{22}}; \quad F = \frac{b_{12}}{b_{22}}; \\
L &= \frac{b_{33}}{b_{22}}; \quad G_1 = \frac{G_{23}R}{b_{22}}; \quad G_2 = \frac{G_{23}R^2}{b_{22}};
\end{aligned}$$

$$\begin{aligned}
a &= \frac{t^2}{6R^2} \frac{b_{33}}{2b_{22}}; \quad b = \frac{(c+t)^2}{2R^2} \frac{b_{21}+b_{33}}{2b_{22}} + \frac{t^2}{6R^2} \frac{b_{21}+b_{33}}{2b_{22}}; \quad d = \frac{t^2}{12R^2}; \\
e &= \frac{t^2}{6R^2} \frac{b_{12}+4b_{33}}{2b_{22}}; \quad f = \left[ \frac{(c+t)^2}{2} + \frac{t^2}{6} \right] \frac{b_{11}}{2b_{22}R^2} + \frac{D_1}{2b_{22}R^2}; \\
g &= \left[ \frac{(c+t)^2}{2} + \frac{t^2}{3} \right] \frac{b_{12}+2b_{33}}{2b_{22}R^2}; \quad h^* = \frac{(c+t)^2}{2R} \frac{b_{33}}{2b_{22}}; \\
k^* &= \frac{(c+t)^2}{2R} \frac{b_{12}+2b_{33}}{2b_{22}}; \quad l^* = \frac{1}{2} \frac{(c+t)^2}{2R}; \\
t_1 &= \frac{T_1^0}{2b_{22}}; \quad t_2 = \frac{T_2^0}{2b_{22}}; \\
\delta_1 &= \frac{c}{R} \frac{b_{21}+b_{33}}{2b_{22}}; \quad \delta_2^* = c \frac{b_{33}}{2b_{22}}; \quad \delta_3^* = \frac{c}{2}.
\end{aligned}$$

Assuming that the edges of the shell are freely supported, we shall assume a solution for Eqs. (5) in the form

$$\left. \begin{aligned}
U &= U_0 \cos \mu \xi \sin n\varphi; \\
V &= V_0 \sin \mu \xi \cos n\varphi; \\
\omega &= \omega_0 \sin \mu \xi \sin n\varphi; \\
\beta &= \beta_0 \sin \mu \xi \cos n\varphi,
\end{aligned} \right\} \quad (6)$$

where  $U_0$ ,  $V_0$ ,  $\omega_0$  and  $\beta_0$  are arbitrary constants, and

$$\mu = \frac{m\pi R}{l}. \quad (7)$$

Here the boundary conditions for free support of edges [3] are satisfied\*, i.e.,

$$\begin{aligned}
[\omega]_{\xi=0, l/R} &= [\omega_{,\xi}]_{\xi=0, l/R} = 0; \\
[\delta T_1]_{\xi=0, l/R} &= [V]_{\xi=0, l/R} = [\beta]_{\xi=0, l/R} = 0.
\end{aligned} \quad (8)$$

Substituting Eqs. (6) into Eqs. (5) and performing operations similar to those performed in the elastic problem [3], we will get\*\*

\*If the length of the shell is  $l > 2R$ , then the results obtained can be used also for other conditions at the edges, because these conditions then have a very small effect on the magnitude of the critical load [5].

\*\*This result (without taking into account the work performed by the corrugation to resist axial loads) was obtained in [2].

$$\begin{aligned}
& -T_1^0 \mu^2 \frac{n^2+1}{n^2-1} - T_2^0 n^2 = \\
& = \frac{b_{22}}{R^2} \frac{\frac{c}{2} \frac{t^2}{6} \frac{b_{22}}{R^2 G_{23}} n^2 + \left[ \frac{(c+t)^2}{2} + \frac{t^2}{6} \right]}{\frac{c}{2} \frac{b_{22}}{R^2 G_{23}} n^2 + 1} n^2 (n^2-1) + \\
& + \left( 2 \frac{b_{11} b_{22} - b_{12}^2}{b_{22}} + B_1 \right) \frac{\mu^4}{n^2 (n^2-1)}.
\end{aligned} \tag{9}$$

This expression can be used for determining the critical load for a three-layer cylindrical shell with a filler made of longitudinal corrugation subjected to the combined action of an axial force and a transverse pressure beyond the elastic limit.

In the case when only the normal pressure is acting, we get from Eq. (9) with reference to the fact that

$$T_1^0 = 0; \quad T_2^0 = -q_{cr} R$$

that

$$\begin{aligned}
q_{cr} = & \frac{b_{22}}{R^3} \frac{\frac{c}{2} \frac{t^2}{6} \frac{b_{22}}{R^2 G_{23}} n^2 + \left[ \frac{(c+t)^2}{2} + \frac{t^2}{6} \right]}{\frac{c}{2} \frac{b_{22}}{R^2 G_{23}} n^2 + 1} (n^2-1) + \\
& + \frac{1}{R} \left( 2 \frac{b_{11} b_{22} - b_{12}^2}{b_{22}} + B_1 \right) \frac{\mu^4}{n^4 (n^2-1)}.
\end{aligned}$$

We shall now consider a three-layer cylindrical shell with a filler made of transverse corrugation when subjected to the same loads. In this case, according to [3]

$$\dot{z} = \omega_\nu + \frac{V}{R}; \quad v_1 = 0. \tag{10}$$

Substituting as in Eq. (4) and using Eqs. (2) and (10), we reduce Eqs. (1) to the form

$$\left. \begin{aligned}
1) \quad & U_{\xi\xi} + L U_{\varphi\varphi} + (C - t_2) V_{\xi\varphi} - (F - t_2) \omega_\xi = 0; \\
2) \quad & C U_{\xi\varphi} + (L + a + t_1) V_{\xi\xi} + (A + d) V_{\varphi\varphi} + \\
& + b \omega_{\xi\varphi} - A \omega_\varphi + d \omega_{\varphi\varphi} + h^* a_{\xi\varphi} = 0; \\
3) \quad & F U_\xi - e V_{\xi\xi\varphi} + (A + t_2) V_\varphi - d V_{\varphi\varphi\varphi} - \\
& - f \omega_{\xi\xi\xi} + t_1 \omega_{\xi\xi} - g \omega_{\xi\xi\varphi\varphi} + t_2 \omega_{\varphi\varphi} - \\
& - d \omega_{\varphi\varphi\varphi\varphi} - A \omega - k^* a_{\xi\xi\xi} - l^* a_{\xi\varphi\varphi} = 0; \\
4) \quad & \delta_1 V_{\xi\varphi} + G_1 \omega_\varphi + \delta_1 \omega_{\xi\varphi\varphi} + \delta_2^* a_{\xi\xi} + \\
& + \delta_3^* a_{\varphi\varphi} - G_2 a = 0.
\end{aligned} \right\} \tag{11}$$

where

$$\begin{aligned}
A &= \frac{2b_{22} + B_2}{2b_{11}}; \quad C = \frac{b_{12} + b_{33}}{b_{11}}; \quad F = \frac{b_{12}}{b_{11}}; \\
L &= \frac{b_{33}}{b_{11}}; \quad G_1 = \frac{G_{13}R}{b_{11}}; \quad G_2 = \frac{G_{13}R^2}{b_{11}}; \\
a &= \left[ \frac{(c+t)^2}{2} + \frac{t^2}{3} \right] \frac{b_{33}}{2b_{11}R^2}; \quad b = \left[ \frac{(c+t)^2}{2} b_{33} + \right. \\
&\quad \left. + \frac{t^2}{6} (b_{21} + 2b_{33}) \right] \frac{1}{2b_{11}R^2}; \\
d &= \left[ \left[ \frac{(c+t)^2}{2} + \frac{t^2}{6} \right] b_{22} + D_2 \right] \frac{1}{2b_{11}R^2}; \\
g &= \left[ \frac{(c+t)^2}{2} + \frac{t^2}{3} \right] \frac{b_{12} + 2b_{33}}{2b_{11}R^2}; \\
e &= \left[ \frac{(c+t)^2}{2} (b_{12} + 2b_{33}) + \frac{t^2}{6} (b_{12} + 4b_{33}) \right] \frac{1}{2b_{11}R^2}; \\
f &= \frac{t^2}{12R^2}; \\
h^* &= \frac{(c+t)^2}{2R} \frac{b_{21} + b_{33}}{2b_{11}}; \quad k^* = \frac{1}{2} \frac{(c+t)^2}{2R}; \\
l^* &= \frac{(c+t)^2}{2R} \frac{b_{21} + 2b_{33}}{2b_{11}}; \\
t_1 &= \frac{T_1^0}{2b_{11}}; \quad t_2 = \frac{T_2^0}{2b_{11}}; \\
\delta_1 &= \frac{c}{R} \frac{b_{12} + b_{33}}{2b_{11}}; \quad \delta_2^* = \frac{c}{2}; \quad \delta_3^* = c \frac{b_{33}}{2b_{11}}.
\end{aligned}$$

In the case of a shell freely supported at the edges, we assume a solution of Eq. (11) in the form

$$\left. \begin{aligned}
U &= U_0 \cos \mu \xi \sin n\varphi; \\
V &= V_0 \sin \mu \xi \cos n\varphi; \\
\omega &= \omega_0 \sin \mu \xi \sin n\varphi; \\
\alpha &= \alpha_0 \cos \mu \xi \sin n\varphi,
\end{aligned} \right\} \quad (12)$$

where  $U_0$ ,  $V_0$ ,  $\omega_0$  and  $\alpha_0$  are arbitrary constants, while  $\mu$  is defined by Eq. (7). In this case conditions (8) of free support of the edges are satisfied.\*

Substituting Eq. (12) into Eq. (11) and performing the usual transformations, we get

---

\*We note, that, by virtue of Eq. (10), condition (8) follows from Eqs. (1) and (4).

$$\begin{aligned}
& -T_1^0 \mu^2 \frac{n^2 + 1}{n^2 - 1} = T_2^0 n^2 = \\
& = \frac{b_{22}}{R^2} \left[ \frac{(c+t)^2}{2} + \frac{t^2}{6} + \frac{D_2}{b_{22}} \right] n^2 (n^2 - 1) + 2 \left( b_{11} - \frac{2b_{12}^2}{2b_{22} + B_2} \right) \frac{\mu^4}{n^2 (n^2 - 1)}.
\end{aligned} \tag{13}$$

This expression can be used to determine the critical load for a three-layer cylindrical shell with a filler made of transverse corrugation subjected to a combined axial force and transverse pressure beyond the elastic limit.

Since Eqs. (9) and (13) contain coefficients  $\underline{b}_{11}$ ,  $\underline{b}_{12}$  and  $\underline{b}_{22}$  which themselves are functions of the applied loads, it is expedient to calculate the critical loads by means of successive approximations. Here integers  $\underline{m}^*$  and  $\underline{n}$  should be selected ( $\underline{m} = 1, 2, 3, \dots$ ;  $\underline{n} = 0, 2, 3, 4, \dots$ ) so as to obtain a minimum for either  $T_1^0$  or  $T_1^0$  (while the other

quantity is held constant).

When  $\underline{c} = 0$  and  $\underline{h} = 2t$  Eqs. (9) and (13) become an expression for a single-layer shell

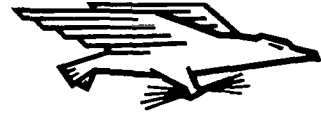
$$\begin{aligned}
& -T_1^0 \mu^2 \frac{n^2 + 1}{n^2 - 1} - T_2^0 n^2 = \\
& = \frac{h^2}{12R^2} (b_{22} n^2 (n^2 - 1)) + \frac{b_{11} b_{22} - b_{12}^2}{b_{22}} \frac{\mu^4}{n^4 (n^2 - 1)}.
\end{aligned}$$

\*Is contained in Eq. (7) for  $\mu$ .

#### REFERENCES

1. Grigorlyuk, E.I. Stability of Three-Layer Plates and Shells Beyond the Elastic Limit. Izv. AN SSSR, Otd. Tekh. Nauk, No. 6, 1958.
2. Yefimov, I.A. Stability of a Three-Layer Cylindrical Shell with a Corrugated Filler Subjected to the Combined Action of an Axial Force and External Pressure Beyond the Elastic Limit. Izv. VUZ, Aviatsionnaya tekhnika, No. 3, 1962.
3. Yefimov, I.A. Uprugaya ustoychivost' trekhsloynnykh tsilindricheskikh obolochek s zapolnitelem iz gofra pri kombinirovannykh nagruzkakh [Elastic Stability of Three-Layer Cylindrical Shells with a Corrugated Filler Subjected to Combined Loads]. Voprosy prochnosti i ustoychivosti elementov tonkostennykh konstruktsiy [Problems of Strength and Stability of Thin-Walled Structural Elements]. Collection of articles No. 2, NAI, Oborongiz Press, 1965.
4. Kurshin, L.M. Ustoychivost' trekhsloynnoy tsilindricheskoy obolochki za predelom uprugosti [Stability of a Three-Layer Cylindrical Shell Past the Elastic Limit]. Voprosy rascheta elementov aviatsionnykh konstruktsiy [Design of Structural Elements of Aircraft]. Collection of articles No. 2. Oborongiz Press, 1959.
5. Timoshenko, S.P. Theory of Elastic Stability. McGraw-Hill Book Company, N.Y.

FIRST CLASS MAIL



POSTAGE AND FEES PAID  
NATIONAL AERONAUTICS AND  
SPACE ADMINISTRATION

000 001 27 01 305 69212 00903  
AIR FORCE WEAPONS LABORATORY/AFWL/  
KIRTLAND AIR FORCE BASE, NEW MEXICO 87117

ATTN: E. L. BOWMAN, ACTING CHIEF TECH. LIB

POSTMASTER: If Undeliverable (Section 158  
Postal Manual) Do Not Return

*"The aeronautical and space activities of the United States shall be conducted so as to contribute . . . to the expansion of human knowledge of phenomena in the atmosphere and space. The Administration shall provide for the widest practicable and appropriate dissemination of information concerning its activities and the results thereof."*

—NATIONAL AERONAUTICS AND SPACE ACT OF 1958

## NASA SCIENTIFIC AND TECHNICAL PUBLICATIONS

**TECHNICAL REPORTS:** Scientific and technical information considered important, complete, and a lasting contribution to existing knowledge.

**TECHNICAL NOTES:** Information less broad in scope but nevertheless of importance as a contribution to existing knowledge.

**TECHNICAL MEMORANDUMS:** Information receiving limited distribution because of preliminary data, security classification, or other reasons.

**CONTRACTOR REPORTS:** Scientific and technical information generated under a NASA contract or grant and considered an important contribution to existing knowledge.

**TECHNICAL TRANSLATIONS:** Information published in a foreign language considered to merit NASA distribution in English.

**SPECIAL PUBLICATIONS:** Information derived from or of value to NASA activities. Publications include conference proceedings, monographs, data compilations, handbooks, sourcebooks, and special bibliographies.

**TECHNOLOGY UTILIZATION PUBLICATIONS:** Information on technology used by NASA that may be of particular interest in commercial and other non-aerospace applications. Publications include Tech Briefs, Technology Utilization Reports and Notes, and Technology Surveys.

*Details on the availability of these publications may be obtained from:*

SCIENTIFIC AND TECHNICAL INFORMATION DIVISION  
NATIONAL AERONAUTICS AND SPACE ADMINISTRATION  
Washington, D.C. 20546